Thermodynamics of Quantum Synchronization

Muhammad Taufiq Murtadho
Center for Theoretical Physics of Complex Systems, IBS School
University of Science and Technology

A thesis submitted for the degree of
Master of Science
August 2022

Master's Thesis

Thermodynamics of Quantum Synchronization

Muhammad Taufiq Murtadho

Basic Science

UNIVERSITY OF SCIENCE AND TECHNOLOGY

August 2022

Thermodynamics of Quantum Synchronization

Muhammad Taufiq Murtadho

A thesis submitted in partial fulfillment of requirements for the degree of Master of Science

August 2022

UNIVERSITY OF SCIENCE AND TECHNOLOGY
Major of: Basic Science

Supervisor: Sergej Flach
Co-supervisor: Jung-Wan Ryu

We hereby approve the Master's thesis of Muhammad Taufiq Murtadho

June 2022

Jung-Wan Ryu sign
Chairman of Thesis Committee

Sergej Flach sign
Thesis Committee Member

Dario Rosa sign
Thesis Committee Member

Juzar Thingna
Thesis Committee Member

Sai Vinjanampathy
Thesis Committee Member

UNIVERSITY OF SCIENCE AND TECHNOLOGY

Nothing in life is certain
except death, taxes, and
the second law of thermodynamics

SETH LLOYD

Acknowledgements

This thesis is more than a summary of the research I have been doing for the past year. It also concludes a 5-year period of my education in South Korea. I came to South Korea as a starry-eyed high school graduate full of hopes and aspirations. I vividly remember what it felt like. Everything seemed so new and exciting. In the span of 5 years, I have learned a tremendous amount, both personally and scientifically. I also have received a great deal of support and assistance. I would like to use this opportunity to acknowledge and express my gratitude to those who have supported me throughout this chapter of my life.

I would first like to thank my supervisor and scientific mentor, Dr. Juzar Thingna, whose patience and expertise is critical in guiding me to navigate this jungle named *research*. Thank you for trusting me as your student. Your insightful feedback has pushed me to improve my reasoning and brought my work to a higher standard. Thank you also for all the professional and personal guidance you have given me all these times.

I would like to acknowledge Prof. Sai Vinjanampathy as a collaborator in this research. Thank you for many extraordinarily fruitful discussions and invaluable feedback on this research project. Thank you also for your patient support, guidance, and kindness throughout our collaboration. It has been a great pleasure to work with you.

I also would like to thank PCS IBS for financially supporting me throughout the writing of this thesis.

In addition, I would like to thank my parents for their support and encouragement. Especially to my mom who has encouraged me to read books and be curious about the world ever since I was a child. I also would not be able to walk this path without my teachers at every stage of my education, especially those who had sparked and maintained my interest in physics and those who had taught me English. Without them, many opportunities I had been given would forever be beyond my reach.

Finally, I could not have completed this thesis without the support of my friends who provided stimulating discussions as well as happy distractions to rest my mind outside of my research. I will always remember how much kindness was given to me. I truly am lucky to have met some of the kindest and most wonderful people on earth, at this little corner of the world named Daejeon.

Abstract

Synchronization is a phenomenon where coupled limit-cycle oscillators develop stable phase relations. In classical physics, synchronization has been used to control artificial systems and enhance the performance of thermal machines. Recently, the notion of synchronization has also been extended in the quantum realm. However, most of the studies in quantum synchronization focus on how to characterize and quantify synchronization in the quantum regime. Relatively little research is done on applying quantum synchronization to quantum devices. One of the earlier works [Phys. Rev. E **101**, 020201(R)] in this direction have shown that synchronization measure bounds the steady-state power of a three-level maser heat engine. In this thesis, we investigated the effect of synchronization on a multi-level generalization of such maser in the presence of near-degeneracy and quantum interference. We showed that near-degeneracy and quantum interference give rise to two co-existing synchronization mechanisms influencing the system: entrainment and mutual coupling. We further observed that the interplay between entrainment and mutual coupling is determined by the thermodynamic functionality of the system. Specifically, they compete when the system operates as an engine and cooperate when the system operates as a refrigerator. Their competition in the engine regime causes the bound between synchronization and steady-state power to be violated. We also formulated a novel bound valid deep in the mutual coupling regime connecting synchronization measure with steady-state heat current. These results demonstrate an intimate relationship between quantum synchronization and quantum thermodynamics, in line with the paradigm of synchronization as a collective phase of matter away from equilibrium.

초록

동기화란 결합한 진동자가 안정적인 위상 관계를 가지는 것을 말한다. 고전 역학적으로 동기화는 인공적인 시스템을 컨트롤하거나 열 기계의 효율을 증가시키기 위해 사용되었다.최근 동기화의 개념은 양자의 영역까지 확장되었다. 그러나 대부분의 양자 동기화 연구에서는 양자 동기화를 어떻게 정량화하고 특성을 부여하는 것에 집중한다. 그에 반해 양자 기기에서 양자 동기화를 적용하려는 연구는 상대적으로 적다. 이러한 방향으로써의 한 선행 연구에서는[Phys. Rev. E 101, 020201(R)] 정상 상태의 3-준위 메이저(maser) 열기관에서 동기화 측정량이 정상 상태에서의 출력량을 제한한다는 것을 보였다. 우리의 논문에서는 이러한 메이저의 다 준위로의 일반화에서 스펙트럼이 거의 축퇴되어 있으며 양자 간섭이 존재할 때 동기화의 효과에 대해서 연구한다. 우리는 거의 축퇴되어 있는 성질과 양자 간섭이 연행(entrainment)과 상호 결합(mutual coupling)이라는 두 동기화의 메커니즘을 발생시킴을 보였다. 더욱이 우리는 연행과 상호 결합 간의 상호 작용이 시스템의 열역학적인 기능성에 의해 결정됨을 보았다. 특히, 이 두 효과는 시스템이 기관으로써 작동하고 있을 때는 서로 경쟁하며, 시스템이 냉각기의 역할을 하고 있을 때는 상호 협력한다. 기관에서 두 효과의 경쟁은 동기화로 인한 정상 상태에서의 출력량의 경계를 위반한다. 우리는 또한 상호 결합 영역에서 동기화 측정량과 정상 상태에서의 열 흐름을 연관 짓는 새로운 형태의 경계를 공식화하였다. 이러한 결과들은 양자 동기화와 양자 열역학이 평형 상태로부터 벗어난 물질의 상으로써의 동기화의 패러다임과 함께 긴밀한 관계를 가진다는 것을 보여준다.

Contents

List of Figures

Chapter 1

Introduction

A spontaneous emergence of order in nature has fascinated humankind since time immemorial. The phenomenon of synchronization by which interacting oscillators adjust their rhythms to move in unison [1, 2], is a captivating example of spontaneous emergence of temporal order. Synchronization as a scientific inquiry was pioneered by Christopher Huygens in the 17^{th} century. He observed that two pendulum clocks hanging from the same base tend to move together with opposing phases, a phenomenon he called as *sympathy between pendulum clocks* [3]. To this day, 350 years later, there are still on-going works in understanding a detailed physical model for the synchronization observed by Huygens [4–7]. Not only that, a multitude of other natural phenomena exhibiting synchronization have been discovered and studied. Some examples are synchronization of neurons [8–10], synchronization of flashing fireflies [11, 12], tidal-locking between planets and their moons [13], synchronization of circadian rhythms [14], and so on.

Beside describing natural phenomena, synchronization has also been proven useful to control artificial systems. Indeed, it has become an indispensable part of our everyday technology. For example, synchronization plays a crucial role in time-standardization, which is vital in many aspects of modern technology such as communication, internet, and financial sector. Precise time-standardization is typically done by synchronizing a local clock with an atomic clock located in a remote satellite using GPS technology [15]. Moreover, synchronization is also essential in the operation of modern power grid from which we receive electricity. A modern power grid connects many generators into a network which then have

to be synchronized to provide a consistent AC output [16–18]. Having mentioned these, it is important to note that synchronization is not always beneficial. It may sometimes leads to catastrophic consequences. For instance, spontaneous synchronization of neuron cells in the brain may cause chronic neurological disorders like Parkinson's disease and Alzheimer [19]. Nevertheless, all the examples mentioned thus far demonstrate that a proper understanding of synchronization can have a far-reaching consequence both in our understanding of nature as well as our technological capability.

Typically, synchronization is studied in one of two ways. The first method is by forcing target oscillators with another 'master' or reference oscillator. This type of synchronization is often called as *entrainment*, or in other context *external* synchronization. Another way is by letting the oscillators to interact and adjust their rhythms with respect to each other. In physics, this is often called as synchronization by *mutual coupling* while in engineering and related fields it is called *internal* synchronization. Yet, theoretical studies revealed that the paradigm of synchronization can be expanded to include other more exotic phenomena such as chaotic synchronization [20] and noise-induced synchronization [21]. At the first glance, chaos and synchronization might sound like an oxymoron. Especially because synchronization is a stable phenomenon - it occurs despite variation in initial condition. In contrast, the hallmark of chaos is an exponential sensitivity to initial condition. Nevertheless, Pecora and Carroll [20] have showed that two chaotic systems can synchronize, in a sense that the difference between dynamical quantities corresponding to the two chaotic systems stay constant over time. Since this discovery, chaos synchronization has been studied intensively particularly in the context of developing secure communication [22]. Noise-induced synchronization is also similarly counter-intuitive. On the one hand, synchronization can be viewed as an ordered motion. Meanwhile, noise is known to cause disorder. Yet, if the noise is correlated, it has been shown that synchronization can nonetheless occur [21]. The framework of noise-induced synchronization has been used to analyze spontaneous synchronization of thermally-sensitive neurons [23].

This thesis specifically considers *quantum* synchronization, that is synchronization in systems governed by quantum mechanics. Synchronization in the quantum realm has been intensely investigated in the recent years [24–40]. Owing to its success as a control tool for classical interacting oscillatory systems, synchronization has the potential to control the behavior of quantum systems. The control of quantum systems is desirable especially in the advent of various experimental platforms with prospects in quantum technology. There are

a variety of approaches in studying quantum synchronization in the literature. Similar to classical synchronization, quantum synchronization can be studied via entrainment [24, 25, 29] or via mutual coupling [26, 34, 41]. Chaotic [35] and noise-induced synchronization [36] have also been investigated in quantum systems. Furthermore, quantum synchronization have been studied in systems with discrete [29, 37, 41, 42] and continuous degrees of freedom [24–26, 28, 43, 44], both at the level of individual quantum system and at the mean-field level [32, 34]. More importantly, it has been demonstrated experimentally in a variety of setups such as trapped cold atoms [38], circuit QED [45], optomechanical oscillators [46], superradiant laser [32], and IBM quantum computer [31]. Despite many theoretical and experimental studies, some aspects of quantum synchronization are still unknown. For example, one big question is whether genuine quantum features such as non-commutativity and entanglement can give rise to novel effects in synchronization [26, 47–49]. It is also unclear whether synchronization can provide advantages in building quantum devices. In classical systems, there have been many reports of synchronization enhancing the performance of thermodynamic machines [50–53]. Less is known regarding the effect of synchronization in quantum thermodynamic devices such as quantum heat engines and refrigerators [54]. A preliminary study seems to indicate that there is connection between synchronization and steady-state power of quantum maser heat engine [40], a connection we will explore further in this thesis.

It might not seem obvious how can synchronization be related to heat engines and thermodynamics. One way to see the connection is through the second law of thermodynamics which dictates things in the universe to evolve to higher entropy state - state with more disorder. Yet, we observe incidents of spontaneous emergence of order like synchronization. The key to resolving this apparent contradiction is the fact that synchronization always occur in open systems [1, 2] - systems in contact with an environment. In an open system, the system's local entropy can spontaneously decrease as long as there is at least as much increase of entropy in the environment. This is precisely the principle of out-of-equilibrium systems. They are able to maintain a low entropy state by continuously increasing the entropy of the environment. Out-of-equilibrium systems are pervasive in nature and they range in size from the microscopic (such as bacteria) to the macroscopic (such as the earth's climate). Despite its pervasiveness, the thermodynamics of systems and processes far-from-equilibrium is still relatively unknown. Most of the established results in statistical physics and thermodynamics are valid for equilibrium or near-equilibrium systems. One of

the few results that has been experimentally tested to be valid for system's arbitrarily far from equilibrium is the Jarzynski equality [55], which is discovered in 1990s. This breakthrough ignited a lot of interest in investigating the thermodynamics of nanoscale systems far from equilibrium, a field nowadays known as stochastic thermodynamics [56]. Stochastic and non-equilibrium thermodynamics have been used to explore various out-of-equilibrium phenomenon, one of which is synchronization [52, 57]. Beyond stochastic thermodynamics, thermodynamics in the quantum regime has also gathered a lot of interest, especially in light of unprecedented degree of control for systems in which quantum effects become important. One of the holy grail in this field is to investigate whether quantum effects like non-commutativity, superposition, and entanglement gives rise to novel thermodynamic effects [58].

This thesis attempts to bring together two active research fields: quantum synchronization and quantum thermodynamics. The importance of this research is highlighted by the five grand challenges for basic energy science in the 21^{st} century according to a report *"Directing Matter and Energy: Five Challenges for Science and the Imagination"* published by the U.S. Department of Energy in 2007 [59]. Some of the keywords that appeared in the report are quantum control, collective phenomena, and matter far-from-equilibrium. Synchronization, both in the classical and quantum regime, is a collective phenomenon that manifests in systems away-from-equilibrium which can and has been utilized to control physical systems. Thus, investigating the thermodynamics of quantum synchronization fits well within the paradigm of the aforementioned grand energy challenges of the 21^{st} century, where, apart from academic interest, also has a great potential for applications in energy and information technology.

This thesis can potentially be useful for researchers in the field of quantum synchronization, open quantum systems, and quantum thermodynamics. But, it also includes a self-contained introduction to both classical and quantum synchronization for unfamiliar readers. The thesis is organized as follows. Chapter 1 aims to motivate research on the thermodynamics of quantum synchronization. Chapter 2 briefly reviews the foundation of classical synchronization. Chapter 3 introduces quantum synchronization by extending the concept developed in chapter 2. The author's original contribution is elaborated in chapters 4 and 5. In chapter 4, the author considers synchronization in quantum thermal machines. In chapter 5, the relationship between synchronization and the thermodynamic performance of a quantum thermal machine is explored. Lastly, the summary and future works is included in chapter 6.

Chapter 2

Classical Synchronization

2.1 Limit Cycle

Synchronization is formally defined as adjustment of frequency and/or phases of limit cycle oscillators [1]. In other words, limit cycle is a prerequisite to synchronization [60]. Limit cycle is defined as an *isolated* closed trajectory in phase-space. The phase space trajectory of a particle is a curve $(x(t), \dot{x}(t))$ where $x(t)$ is the particle's position and $\dot{x}(t)$ is its velocity. When a particle moves periodically, it forms a closed curve in phase space. However, a closed phase space trajectory alone is not sufficient for a limit cycle. Limit cycle also requires the trajectory to be isolated, meaning that a neighboring trajectory must either spiral toward or away from the limit cycle. In this thesis, we are only interested in a *stable* or *attracting* limit cycle, where any neighboring trajectories spiral towards the limit cycle.

Limit cycle is important to model a wide-class of oscillating systems known as *self-sustained oscillators* [1, 2]. In contrast to a linear or harmonic oscillator, a self-sustained oscillator has a shape, amplitude, and frequency of motion that depend only on the system's parameters and are independent from the choice of initial conditions. For this reason, a self-sustained oscillator is often called a *non-linear* oscillator owing to its non-linear equation of motion. Self-sustained oscillation is found in a range of natural phenomenon from electrical circuits [61],

pendulum clocks [62], beating of a heart [63], neurons periodic firing [64], and countless more.

The dynamics of self-sustained oscillator is dissipative. A Hamiltonian dynamics alone can not generate a stable limit cycle due to the Liouville's theorem, which asserts that Hamiltonian system must preserve phase space volume. An attractor, such as a stable limit cycle, would violate the Liouville's theorem and thus its existence is forbidden in Hamiltonian dynamics.

Having established that a limit cycle is dissipative, one might wonder how can a self-sustained oscillator maintain its motion, given that dissipation usually has a damping effect. Clearly, a source of power must continue to pump energy into the system. Crucially, the source of power must lack periodicity. Otherwise, it would include oscillations that occur simply as a response to external periodic signal. For instance, a swing which is periodically pushed by an external agent is not a self-sustained oscillator. Contrast it with a grandfather pendulum clock whose energy input is provided by a suspended weight that continues to rise as the pendulum swings. The importance of lack of periodicity in the input power is stressed on Ref. [65] where a self-sustained oscillating system is defined as an apparatus which produces a periodic process at the expense of a non-periodic energy source.

Below are some examples of limit cycles:

Example 1: Stuart-Landau Oscillator
Consider a particle moving in two-dimension (x, y). Let us denote $z = x+iy \in \mathbb{C}$. The Stuart-Landau equation is given by

$$\dot{z} = (R + i\omega - |z|^2)z, \tag{2.1}$$

with $R, \omega > 0$. Decomposing $z = re^{i\theta}$ yields separable differential equations for r and θ

$$\dot{r} = (R - r^2)r \qquad\qquad \dot{\theta} = \omega. \tag{2.2}$$

The solution for the angle θ is trivial $\theta(t) = \omega t$. Meanwhile, r has an unstable fixed point $r = 0$ and a stable fixed point $r = \sqrt{R}$. Thus, we find that $z(t) = \sqrt{R}e^{i\omega t}$ is a stable periodic solution.

The Stuart-Landau equation is originally reported in the context of turbulence and hydrodynamic stability [66]. It has also been used to describe periodic chemical reactions such as Belousov–Zhabotinsky reaction [67]. It turns out the

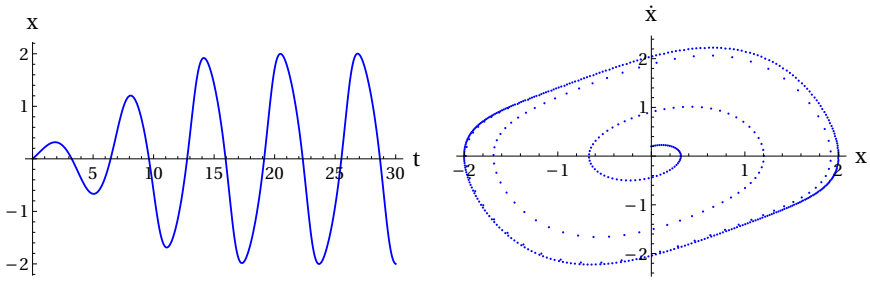

(a) x(t) (b) Van der Pol Limit Cycle

Figure 2.1: Numerical solution of van der Pol equation (2.3) with $\omega = 1, \mu = 0.5$.

Stuart-Landau form (2.1) is universal for any weakly non-linear oscillator system. The proof for the universality is given in Ref. [68].

Example 2: van der Pol Oscillator
The Van der Pol equation is given by

$$\ddot{x} + \omega^2 x + \mu(x^2 - 1)\dot{x} = 0. \tag{2.3}$$

Equation (2.3) describes a harmonic oscillator with natural frequency ω in the presence of linear damping ($-\dot{x}$) and non-linear damping ($x^2\dot{x}$). The constant $\mu \geq 0$ is a parameter that measures the strength of non-linearity. Unlike the Stuart-Landau equation, the limit cycle can not be easily obtained by analytically solving (2.3). Instead, we can solve the equation numerically as shown in Fig. 2.1. It is apparent that the limit cycle in Fig.2.1(b) is not a circle, which also means that the waveform shown in Fig.2.1(a) is not sinusoidal. The Van der Pol equation was originally used to describe the behavior of an electrical circuit consisting of an inductor, a capacitor, and a non-linear resistor [61,69]. However, its applicability is proven way beyond its original intention. For example, in biology, Van der Pol equation is used to describe an electrical model for the heart [63]. In seismology, it has been used to describe two tectonic plates at geological fault [70].

2.2 Forced Synchronization (*Entrainment*)

In this section, we are considering synchronization of a self-sustained oscillator by an external forcing. The forcing is typically induced by a larger system whose state is hardly influenced by the oscillator. For example, the circadian rhythms of cells are influenced by the periodic motion of the earth with respect to its axis, while the earth is hardly affected by the cells.

When a self-sustained oscillator with natural frequency ω is influenced by a driving of frequency Ω, the frequency of the self-sustained oscillator might latch onto the frequency of the drive. This phenomenon is also known as *entrainment*. Besides the circadian rhythms, entrainment is also relevant to many modern technological devices, e.g. standardization of radio-controlled watch [1] and injection-locking of multiple lasers [71].

At this point, it is instructive to compare the phenomenon of entrainment with that of a forced harmonic oscillator

$$m\frac{d^2x}{dt^2} + kx = F\cos\Omega t. \tag{2.4}$$

The solution to this equation is given by,

$$x(t) = \frac{F}{m(\omega^2 - \Omega^2)}\cos\Omega t + C_1\cos\omega t + C_2\sin\omega t, \tag{2.5}$$

with $\omega = \sqrt{k/m}$ is the system's natural frequency and $C_{1,2}$ are initial condition dependent constants. The solution (2.5) contains both the natural frequency ω and the driving frequency Ω. Moreover, information about the initial phase of the oscillator will get carried to the solution by the coefficients $C_{1,2}$. These two observations mark the main differences between entrainment and forced harmonic oscillators. As we will see when a self-sustained oscillator undergoes entrainment, the oscillator will oscillate only with the driving frequency Ω and the phase is always independent of the initial condition.

The amplitude of a self-sustained oscillator is stable. If the driving is not too strong, the drive can only adjust the oscillator's phases and/or frequencies. Suppose we ignore the amplitude dynamics and focus on that of the phase. In other words, we describe a self-sustained oscillator only by its phases $\dot{\theta} = \omega$. The simplest model of entrainment is given by the Adler equation [72],

$$\dot{\theta} = \omega + F\sin(\Omega t - \theta), \tag{2.6}$$

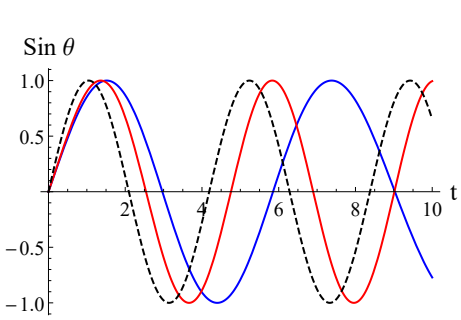

(a) $\omega = 1$, $\Omega = 1.5$, $F = 0.1$ (solid blue), $F = 0.6$ (solid red). The dashed black line is the reference signal $\sin \Omega t$.

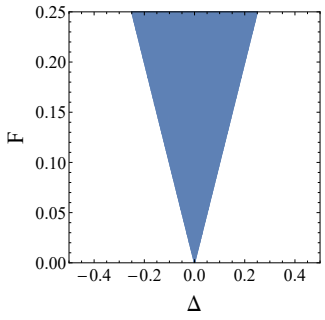

(b) Arnold tongue, shaded blue region is the entrainment region.

Figure 2.2: (a) Numerical simulation of the Adler equation. The dashed black curve is the reference driving signal, the red curve is the entrained signal and the blue curve is the drifting signal. (b) Arnold tongue structure marking $F \geq \Delta$ (dark blue) as the entrainment region of the Adler equation.

with F is the driving strength and Ω is the driving frequency. This non-linear equation can be solved by transforming to a frame rotating with the drive $\theta' = \theta - \Omega t$

$$\dot{\theta}' = \Delta - F \sin \theta', \tag{2.7}$$

with $\Delta = \omega - \Omega$ is called detuning. Equation (2.7) has two fixed points $\theta' = \arcsin(\Delta/F)$ and $\theta' = \pi - \arcsin(\Delta/F)$ given $|\Delta|/F \leq 1$. If a stable fixed point exists, then the system's observed frequency coincides with that of the drive., i.e. the system is entrained by the drive. If $|\Delta|/F > 1$, the fixed points no longer exist and thus entrainment is lost.

To check the stability of these fixed points we perform linear stability analysis [60] where we consider a slight perturbation $\theta' \to \theta' + \epsilon$ and check how the perturbation grows. Substituting this transformation to Eq. (2.7) yields

$$\dot{\epsilon} = -\epsilon F \cos \theta'. \tag{2.8}$$

If the right-hand side is evaluated at a fixed point and yields a negative value, the perturbation will decay and thus the fixed point is stable. Likewise, if the right-hand side is positive, a small perturbation grows and hence the point is unstable. By substituting the two fixed points of the Adler equation, we find that there is always one stable fixed point provided $|\Delta|/F < 1$.

The requirement $|\Delta|/F < 1$ signifies a competition between detuning and forcing strength. The forcing tends to entrain the oscillators while the detuning serves as inertia. If detuning is zero, the drive's frequency is already identical to the oscillator, but any infinitesimal forcing is enough to induce phase-locking $\theta = \Omega t$ irrespective of the initial phase of the oscillator. Contrast this with the case of a forced harmonic oscillator in which the solution always depends on the initial condition. When $\Delta > 0$, a finite force $F \geq \Delta$ must be exerted to lock the frequency of the oscillator with a finite phase-offset $\theta = \Omega t + \arcsin(\Delta/F)$. The competition can be easily seen by drawing the entrainment region on $F - \Delta$ plane. It forms a triangular region known as the *Arnold tongue* [1] (see 2.2(b)). The Arnold tongue behavior is not just a property of the Adler equation. It is found to be universal among a myriad of self-sustained oscillators under the influence of driving.

2.3 Mutual Coupling Synchronization

Another way in which synchronization may occur is by mutual coupling of multiple limit cycle oscillators. Unlike entrainment, two or more limit cycle oscillators are now allowed to influence and interact with each other. Synchronization in this regard can then be considered as an emergent collective behavior of many-body interacting limit cycle oscillators. Below, we will provide several examples of how this type of synchronization arises.

Let us couple two Stuart-Landau oscillators (2.1) via a linear coupling

$$\dot{z}_1 = (R + i\omega_1 - |z_1|^2)z_1 + k(z_2 - z_1), \tag{2.9}$$

$$\dot{z}_2 = (R + i\omega_2 - |z_2|^2)z_2 + k(z_1 - z_2). \tag{2.10}$$

Applying polar decomposition $z_j = r_j e^{i\theta_j}$ yields a system of coupled differential equations

$$\dot{r}_1 = Rr_1 - kr_1 - r_1^3 + kr_2\cos(\theta_2 - \theta_1) \tag{2.11}$$

$$\dot{r}_2 = Rr_2 - kr_2 - r_2^3 + kr_1\cos(\theta_2 - \theta_1) \tag{2.12}$$

$$\dot{\theta}_1 = \omega_1 + k\frac{r_2}{r_1}\sin(\theta_2 - \theta_1) \tag{2.13}$$

$$\dot{\theta}_2 = \omega_2 + k\frac{r_1}{r_2}\sin(\theta_2 - \theta_1). \tag{2.14}$$

Analytically solving this system of equations in general is non-trivial. Later, we will use several approximations to make this problem tractable even for more than two oscillators. For now, we can investigate the solution to (2.11)-(2.14) numerically. The solution displays three types of distinct behaviors: synchrony, asynchrony, and amplitude death [73] as shown in Fig. 2.3. Synchrony refers to the acquirement of a common frequency by the two oscillators. By contrast, the two oscillators do not achieve the same frequency in the asynchronous regime. As a consequence, their phase relation is not stable. Amplitude death is a counter-intuitive phenomenon that occurs when the amplitudes of both oscillators decay as a result of coupling [73]. In other words, the point $(z_1, z_2) = (0, 0)$ changes from an unstable fixed point in the uncoupled case to a stable fixed point in the coupled case. Such phenomena are rare and they have been identified as exceptional points in the parameter space [74]. Moreover, there is another phenomenon similar to amplitude death called oscillation death where the oscillators decay to different fixed points [73].

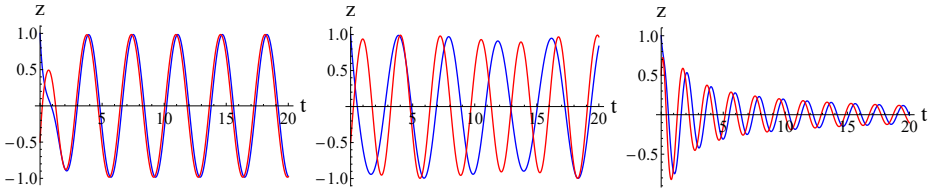

(a) $k = 1$, $\omega_1 = 1.5$, $\omega_2 = 2$ (b) $k = 0.1$, $\omega_1 = 1.5$, $\omega_2 = 2$ (c) $k = 2$, $\omega_1 = 1.5$, $\omega_2 = 5$

Figure 2.3: The behavior of coupled Stuart-Landau dimer: (a) Synchrony (b) Asynchrony (c) Amplitude Death.

The above dimer model can be easily generalized into N coupled Stuart-Landau network [73, 75, 76]

$$\dot{z}_i = (R' + i\omega_i - |z_i|^2)z_i + \sum_{j \neq i}^{N} K_{ij} z_j, \tag{2.15}$$

where $R' \equiv R - \sum_{j \neq i}^{N} K_{ij}$ is the effective limit cycle radius in the presence of mutual coupling. Equation 2.15 can be used to model synchronization of a large number of oscillators such as in the flashing of fireflies and power-grid network. Solving Eq. (2.15) analytically is difficult in general. Moreover, the qualitative behavior of a Stuart-Landau network might depend on its precise connectivity and

coupling form. For example, numerical studies have revealed a rich phenomenon such as clustering [76], chimera states [75], and oscillation death []zoin Stuart-Landau network. Nevertheless, analytical prediction is still desirable so some simplification of Eq. (2.15) is in order.

First, let us perform polar decomposition $z_i = r_i e^{i\theta_i}$ giving a coupled equation for the amplitude and the phase

$$\dot{r}_i = (R' - r_i^2) r_i + \sum_{j \neq i}^{N} K_{ij} r_j \cos(\theta_j - \theta_i) \tag{2.16}$$

$$\dot{\theta}_i = \omega_i + \sum_{j \neq i}^{N} K_{ij} \frac{r_j}{r_i} \sin(\theta_j - \theta_i). \tag{2.17}$$

Winfree [77] simplified the above equations by considering a weak coupling limit $K_{ij} \to 0$ and assuming that the amplitude dynamics quickly settle into identical limit cycles $r_i \to R$. With this approximation, we may focus our attention on solving the phase equation

$$\dot{\theta}_i = \omega_i + \sum_{j=1}^{N} K_{ij} \sin(\theta_j - \theta_i) \qquad i = 1, 2, ..., N. \tag{2.18}$$

Kuramoto [78] further simplified the problem by assuming an all-to-all coupling with equal strength $K_{ij} = K/N$ for all $i \neq j$. We finally arrive at the celebrated Kuramoto model

$$\dot{\theta}_i = \omega_i + \frac{K}{N} \sum_{j=1}^{N} \sin(\theta_j - \theta_i). \tag{2.19}$$

Another breakthrough insight of Kuramoto is to introduce an order parameter to distinguish synchronous and asynchronous states

$$r e^{i\psi} = \frac{1}{N} \sum_{j=1}^{N} e^{i\theta_j}. \tag{2.20}$$

The order parameter r quantifies the synchrony of the oscillators and ψ denotes their average phase. If all the oscillators move in the same phase, then $r \to 1$. Conversely, if the oscillators move with a random phase, then $r \to 0$. The Kuramoto model (2.19) can be re-expressed in terms of r and ψ as

$$\dot{\theta}_i = \omega_i + K r \sin(\psi - \theta_i). \tag{2.21}$$

We aim to find a long-time solution where r is stationary. Assuming such a solution exists, our task is to find the numerical values of r in the steady state. Since phase reference is arbitrary, we may set $\psi = 0$ by transforming to a co-rotating frame. In this frame, the long-time behavior of the oscillators split into two groups depending on their natural frequencies. One group is phase-locked to

$$\sin\theta_i = \omega_i/Kr \tag{2.22}$$

corresponding to the fixed point of (2.21). These are the oscillators whose natural frequencies satisfy $|\omega_r| \leq Kr$. This group will oscillate with a common frequency Ω in the steady state. Those that do not belong to this group continue to drift with their natural frequencies.

To check for self-consistency, we split the order parameter into two parts [79]

$$r = \langle e^{i\theta}\rangle_{locked} + \langle e^{i\theta}\rangle_{drift}\,, \tag{2.23}$$

with $\langle ...\rangle$ denotes population average. Let us consider the $N \to \infty$ limit where the oscillators' population can be represented by a probability density function. Let $g(\omega)d\omega$ denote the fraction of oscillators with natural frequencies between ω and $\omega + d\omega$. We assume that $g(\omega)$ is unbiased i.e. $g(\omega) = g(-\omega)$. Let $\rho(\theta,\omega)d\theta$ denotes the fraction of oscillators having natural frequency ω that lies between θ and $\theta + d\theta$. Then, the population average of $e^{i\theta}$ corresponding to the locked and drift oscillators are given by

$$\langle e^{i\theta}\rangle_{locked} = \int_{-\pi}^{\pi}\int_{-Kr}^{Kr} e^{i\theta}\rho_{locked}(\omega,\theta)g(\omega)\;d\omega\;d\theta \tag{2.24}$$

$$\langle e^{i\theta}\rangle_{drift} = \int_{-\pi}^{\pi}\int_{|\omega|>Kr} e^{i\theta}\rho_{drift}(\omega,\theta)g(\omega)\;d\omega\;d\theta. \tag{2.25}$$

Substituting the density $\rho_{locked}(\omega,\theta) = \delta(\sin\theta - \omega/Kr)$ to (2.24) yields,

$$\langle e^{i\theta}\rangle_{locked} = \int_{-Kr}^{Kr} e^{i\theta(\omega)}g(\omega)\;d\omega = \int_{-Kr}^{Kr}\cos\theta(\omega)g(\omega)\;d\omega, \tag{2.26}$$

where $\theta(\omega)$ is defined by (2.22) and for the second equality we have used the symmetric property of $g(\omega)$. The above integral can be rewritten in terms of θ by using Eq. (2.22)

$$\langle e^{i\theta}\rangle_{locked} = Kr\int_{-\pi/2}^{\pi/2}\cos^2\theta\;g(Kr\sin\theta)\;d\theta. \tag{2.27}$$

Let us now compute Eq. (2.25). Notice that we have assumed $\rho_{drift}(\omega,\theta)$ is stationary although each individual oscillator still runs with its own natural frequency. This assumption is necessary to get a fixed r in the steady state. To satisfy this constraint, the density flux $\rho_{drift}(\omega,\theta)\dot{\theta}$ at any θ must be a constant C.

$$\rho_{drift}(\omega,\theta) = \frac{C}{\dot{\theta}} = \frac{C}{\omega - Kr\sin\theta}. \tag{2.28}$$

The constant C can be found by normalization $\int_{-\pi}^{\pi} \rho_{drift}(\omega,\theta)\, d\theta = 1$

$$C\int_{-\pi}^{\pi} \frac{d\theta}{\omega - Kr\sin\theta} = \frac{2C}{\sqrt{\omega^2 - K^2r^2}} \arctan\left(\frac{\frac{Kr}{\omega} - \tan(\theta/2)}{\sqrt{1-\left(\frac{Kr}{\omega}\right)^2}} \right)\Bigg|_{-\pi}^{\pi} = 1 \tag{2.29}$$

giving

$$C = \frac{1}{2\pi}\sqrt{\omega^2 - K^2r^2}. \tag{2.30}$$

Finally, (2.25) can be computed as

$$\langle e^{i\theta}\rangle_{drift} = \frac{1}{2\pi}\int_{-\pi}^{\pi}\int_{|\omega|>Kr} e^{i\theta}\frac{\sqrt{\omega^2 - K^2r^2}}{\omega - Kr\sin\theta} g(\omega)\, d\omega\, d\theta = 0. \tag{2.31}$$

The result follows from the anti-symmetric property of the integrand under the transformation $\omega \to -\omega$ and $\theta \to \theta + \pi$. Equation (2.27) and (2.31) allow us to write the self-consistency condition (2.23) as

$$r\Big(1 - K\int_{-\pi/2}^{\pi/2} \cos^2\theta\; g(Kr\sin\theta)\, d\theta\Big) = 0. \tag{2.32}$$

Equation (2.32) has two branches of solution. The first branch is the incoherent solution $r = 0$. The second branch satisfies

$$1 = K\int_{-\pi/2}^{\pi/2} \cos^2(\theta)\; g(Kr\sin\theta)\, d\theta \tag{2.33}$$

This branch may have $r > 0$ solution for $K > K_c$ with K_c calculated by letting $r \to 0^+$ giving

$$K_c = \frac{2}{\pi g(0)}. \tag{2.34}$$

The quantity K_c is called the critical coupling above which synchrony starts to emerge.

Up to this point, we have derived the critical coupling for the Kuramoto model under two assumptions: r is constant in the steady-state and the oscillators' natural frequency distribution is symmetric $g(\omega) = g(-\omega)$. Kuramoto went further by calculating r for any $K \geq K_c$ assuming $g(\omega)$ is a Lorentzian density,

$$g(\omega) = \frac{\gamma}{\pi(\gamma^2 + \omega^2)} \tag{2.35}$$

with γ being a parameter for the distribution. Substituting this distribution to (2.33) gives,

$$1 = \frac{\gamma}{\pi K r^2} \int_{-\pi/2}^{\pi/2} \frac{\cos^2\theta}{(\gamma/Kr)^2 + \sin^2\theta} d\theta = \frac{1}{Kr^2}(\sqrt{K^2 r^2 + \gamma^2} - \gamma). \tag{2.36}$$

Rewriting in terms of $K_c = 2\gamma$,

$$r = \sqrt{1 - \frac{K_c}{K}} \qquad K \geq K_c. \tag{2.37}$$

Kuramoto's analytical results (2.34) and (2.20) were later shown to agree with numerical simulations [80].

2.4 Interplay between Entrainment and Mutual Coupling

In the previous sections, we have discussed how synchronization may arise through entrainment to an external drive or spontaneously via collective coupling. It is natural to consider what happen when both of these mechanisms co-exist. Such models are not only of theoretical interest, but might also serve as an idealization of natural phenomena. For example, mammalians have pacemaker cells which have been shown to be intrinsically oscillatory. The pacemaker cells can be thought of as biological clock that controls various organs in the body depending on the time of day. They are known to be mutually coupled although the nature of their interaction is still ambiguous. At the same time, they are entrained by day-night cycle imposed by the organisms' external environment. One could ask what happen if we modify the period or strength of the external environment, for example by artificially manipulating the light-dark cycle, as what has been done in numerous biological experiments? Or what will happen if

the natural frequencies of the pacemaker cells have been modified? Understanding the interplay between collective coupling and entrainment can help establishing a mathematical framework to answer these type of questions.

Sakaguchi pioneered the study of driven coupled phase oscillators by considering a fusion of the Kuramoto Model (2.19) and the Adler equation (2.7)

$$\dot{\theta}_i = \omega_i - \Omega + \frac{K}{N}\sum_{j=1}^{N}\sin(\theta_j - \theta_i) - F\sin\theta_i, \tag{2.38}$$

where ω_i are the natural frequencies of the oscillators, Ω is the driving frequency, K is the coupling strength, F is the driving strength, and $N > 1$ is the number of oscillators. This model is capable of exhibiting a complex behavior due to the interplay between randomness, phase preference, and frequency preference. The randomness is induced by differing intrinsic natural frequencies of the oscillators. The coupling promotes phase alignment without preferring any specific frequency. On the other hand, the drive prefers a specific frequency, namely that of the drive (Ω), while still allowing phase offset between oscillators with different natural frequencies.

Sakaguchi [81] numerically identified two types of long-time behavior of this model. He called it as *forced entrainment* and *mutual entrainment*. In the forced entrainment state, all the oscillators are phase-locked and move with the same frequency as the driving. This state has a constant Kuramoto order parameter (2.20) in the frame rotating with frequency Ω. Meanwhile, in the mutual entrainment case, a macroscopic fraction of oscillators clumped together and move with a collective frequency differ from Ω. Unfortunately, Sakaguchi was unable to resolve the detailed bifurcation analysis between forced entrainment and mutual entrainment. The full-phase diagram and stability analysis of this model was done much later by Childs and Strogatz [82].

The result by Childs and Strogatz extensively used earlier ansatz by Ott and Antonsen [83] which crucially makes use of pure sinusoidal coupling and driving. The case of non-sinusoidal driving has been studied recently by Synder, Zlotnik, and Hagberg [84]. In their paper, they construct a model where the driving and the coupling have a competing phase alignment effect. The driving pushes the phase distribution to spread over the whole circle, while the coupling attracts the

oscillators to be in phase. Specifically, the model they are considering is

$$\dot{\theta}_i = \omega_i - \Omega + \frac{K}{N}\sum_{j=1}^{N}\sin(\theta_j - \theta_i) - \frac{\theta_i}{\pi}, \tag{2.39}$$

with the driving function $F(\theta) = -\theta/\pi$ is called the *sawtooth* function. Furthermore, they choose a specific distribution of natural frequencies satisfying,

$$\omega_i - \Omega = \frac{2i}{N} - 1 \qquad i = 1, 2, ..., N. \tag{2.40}$$

In the absence of coupling $K = 0$, the steady-state has a phase-distribution given by

$$\theta_i = \Big(\frac{2i}{N} - 1\Big)\pi \qquad i = 1, 2, .., N. \tag{2.41}$$

This distribution divides the interval $(-\pi, \pi]$ into N-evenly spaced points. A straightforward calculation for the steady-state Kuramoto order parameter gives,

$$r = \frac{1}{N}\Big|\sum_{j=1}^{N} e^{i\theta_j}\Big| = \frac{1}{N}\Big|\sum_{j=1}^{N} e^{2\pi ij/N}\Big| = 0. \tag{2.42}$$

Thus, we see that based on r alone, the steady-state seems to be incoherent. Yet, this state is different from the typical Kuramoto incoherent state where each oscillator runs with its own natural frequency. Here, all the oscillators run with the same frequency Ω.

The undriven Kuramoto model with an equispace natural frequency distribution has been studied in [85]. There, the critical coupling is found to be $K_c^{und} = 4/\pi$ (*und* stands for undriven). Perhaps surprisingly, the critical coupling of the driven case is found to be two times smaller than K_c^{und} [84]. This result is counter-intuitive, given that the driving pushes the system toward an incoherent state $r \to 0$. The authors of Ref. [84] point out that their result sheds light on the role of frequency synchronization for phase alignment. In the undriven Kuramoto model, the coupling has to overcome the randomness provided by natural frequency variation. In the driven Kuramoto model given by (2.39), the driving would help tame the natural frequency variation while leaving the phases to be incoherent. Therefore, the coupling K only needs to overcome the phase variation induced by driving, which could be easier than overcoming frequency variation.

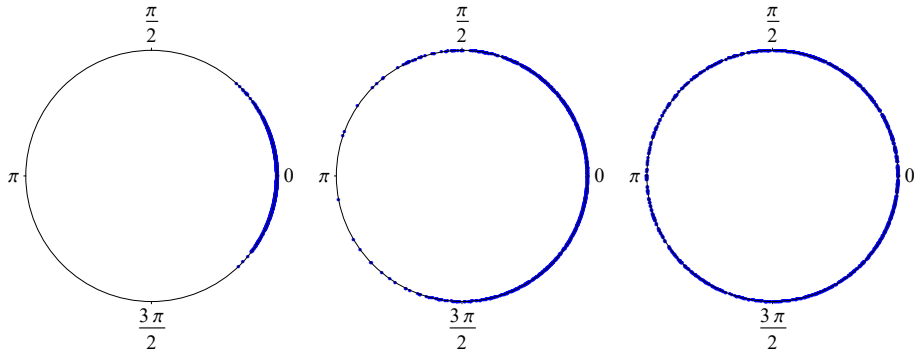

(a) t = 2 (b) t = 20 (c) t = 70

Figure 2.4: Simulation of the phase distribution of noisy oscillator (2.43) with $D = 0.2$ and 10^3 noise realization plotted on a unit circle.

2.5 Synchronization in the Presence of Noise

Oscillators in the real world are noisy, their behavior is influenced by random fluctuations coming from outside and inside the system. For example, an electrical circuit oscillator is subject to random thermal motion of electrons and ions that could influence instantaneous circuit parameters (e.g. conductance or inductance) which in turn will affect its oscillation. In this section, we will briefly develop theoretical tools to model noise and see how it affects synchronization.

Noise is modelled as a time-dependent stochastic term in the equation of motion. For instance, consider a noisy phase oscillator

$$\dot{\theta} = \omega + D\xi(t), \tag{2.43}$$

where D is the noise strength and $\xi(t)$ is a random function sampled from a normal distribution,

$$\langle \xi(t) \rangle = 0 \qquad \langle \xi(t)\xi(t') \rangle = \delta(t - t'). \tag{2.44}$$

A noise whose statistics follow (2.44) is called *Gaussian white noise*. Differential equation with stochastic terms such as Eq. (2.43) is called *stochastic differential equation* (SDE). We focus on a type of SDE known as Ito process [86] which takes the form,

$$\dot{x}(t) = f(x,t) + g(x,t)\xi(t), \tag{2.45}$$

which can be mapped into a Fokker-Planck equation [87]

$$\frac{\partial}{\partial t}P(x,t) = -\frac{\partial}{\partial x}(f(x,t)P(x,t)) + \frac{1}{2}\frac{\partial^2}{\partial x^2}(g^2(x,t)P(x,t)). \tag{2.46}$$

where $P(x,t)$ describes probability density function of obtaining x as a function of t.

In the simple noisy oscillator (Eq. (2.43)), one can further simplify the equation by defining $\theta' = \theta - \omega t$ such that the equation of motion only contains the noise term $\dot{\theta}' = D\xi(t)$. Then, the corresponding Fokker-Planck equation is identical to a diffusion equation [88]

$$\frac{\partial}{\partial t}P(\theta,t) = \frac{D^2}{2}\frac{\partial^2 P}{\partial \theta^2}, \tag{2.47}$$

where D is now associated with the diffusion constant. We look for a stationary solution with $\frac{\partial P}{\partial t} = 0$ which can be satisfied by $P(\theta) = A\theta + B$ where A and B are constants. But, the phase distribution lies on a ring and thus it must satisfy $P(\theta + 2\pi) = P(\theta)$. This can only be satisfied if $A = 0$. Furthermore, it is trivial to obtain $B = 1/2\pi$ by normalization. Finally, one concludes that the stationary solution must be uniform over the ring.

Qualitatively, the time evolution of the probability distribution can be understood as follows. Let us start from a probability distribution $\delta(\theta - \theta_0)$. Without any noise, this distribution will oscillate according to $\delta(\theta - \omega t - \theta_0)$. In the presence of noise, the distribution would broaden as it continues to rotate. Eventually, the distribution becomes uniform when the spread of the distribution spans through the whole ring. This qualitative picture is supported by numerical simulation as shown in Fig. 2.5. The evolution from a phase distribution centered at a particular value to a uniform distribution is called *phase diffusion*. So far, we have seen that a phase oscillator in the presence of noise will undergo phase diffusion toward a uniform distribution. The story is different if the noisy oscillator is forced or coupled to other oscillators. In these cases, one must take into account the effect of synchronization. Here, we will only focus to the case of entrainment in the presence of noise. Noisy interacting oscillators (e.g. noisy Kuramoto model) are discussed in other references such as Ref. [81].

Next, we consider the stochastic version of the Adler equation

$$\dot{\theta}' = \Delta - F\sin\theta' + D\xi(t). \tag{2.48}$$

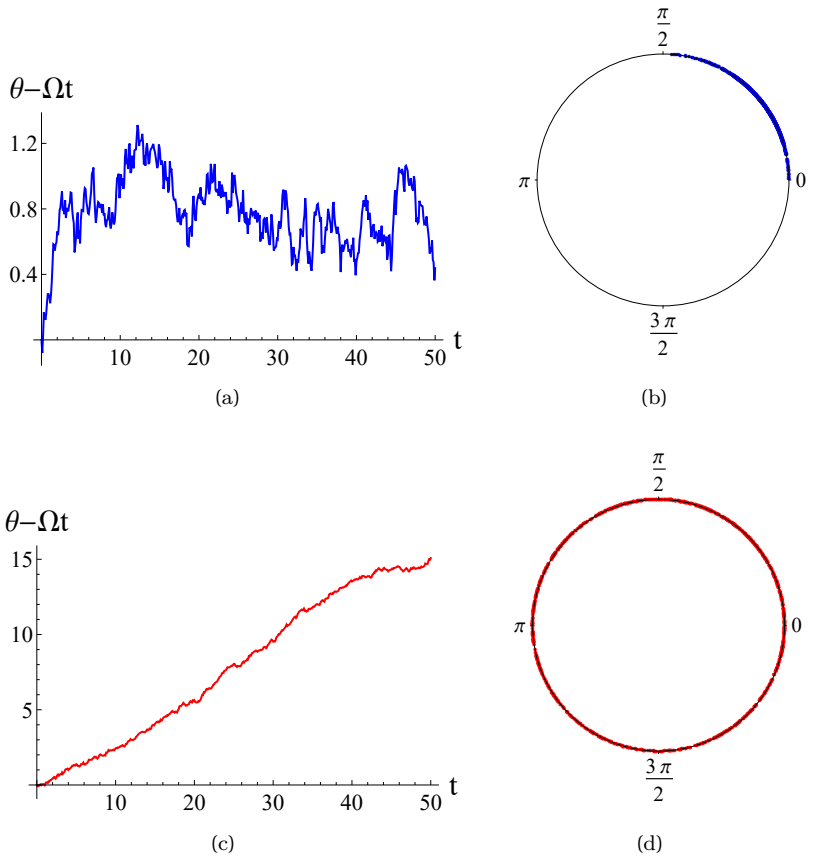

Figure 2.5: Numerical simulation of stochastic Adler equation. Time-series (a,c) and long-time phase distribution (b,d) of entrained (a,b) and drifting (c,d) noisy phase oscillator. The parameter values are $\Delta = 0.3$, $D = 0.2$, $F = 0.5$ for (a,b) and $F = 0.1$ for (c,d). The long-time phase distribution is sampled from 10^3 noise realization and $t = 1000$.

The corresponding Fokker-Planck equation is given by,

$$\frac{\partial}{\partial t}P(\theta',t) = \frac{D^2}{2}\frac{\partial^2}{\partial\theta'^2}P(\theta',t) - (\Delta - F\sin\theta')\frac{\partial}{\partial\theta'}P(\theta',t) + F\cos\theta' P(\theta',t). \quad (2.49)$$

This is a second-order non-linear partial differential equation. Finding solutions of such equations is hard in general. Instead of pursuing an analytical solution

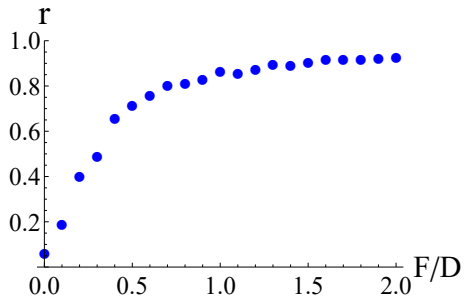

Figure 2.6: Synchronization measure r [Eq. (2.50)] vs forcing-to-noise ratio F/D ($D = 0.5$) for zero-detuning $\Delta = 0$ case in the stochastic Adler equation (2.48).

for the phase density $P(\theta', t)$, one may instead perform numerical experiments with many realizations of $\xi(t)$. The time-series and long-time phase distribution for such simulations are shown in Fig. 2.5. The oscillator can either be entrained [Fig. 2.5(a)] or drifting [Fig. 2.5(c)] with respect to the driving. If the oscillator drifts, then phase distribution in the long-time limit is uniform due to diffusion [Fig. 2.5(d)]. In contrast, for entrained dynamics, the phase distribution localizes into a finite region [Fig. 2.5(b)]. The spread of the distribution is determined by the noise strength relative to the forcing. We can quantify the strength of synchronization by calculating the complex order parameter

$$\rho = re^{i\psi} = \int_0^{2\pi} d\theta' e^{i\theta'} P(\theta', t \to \infty). \tag{2.50}$$

Equation (2.50) is nothing but the average of $e^{i\theta'}$ in the long-time limit where the norm $|\rho| = r$ measures the strength of synchronization while $\arg(\rho) = \psi$ is interpreted as the average phase. In other words, it is the continuous version of the Kuramoto order parameter introduced earlier in Eq. (2.20). It is obvious that for a uniform phase distribution, such as in the case of $F = 0$ and $\Delta/F > 1$, r is always identically zero.

In the case of a free (unforced) limit cycle oscillator undergoing phase diffusion, the order parameter ρ approaches zero by an exponential decay as shown below

$$\frac{d\rho}{dt} = \int_0^{2\pi} d\theta' \; e^{i\theta'} \frac{\partial}{\partial t} P(\theta', t) = \frac{D^2}{2} \int_0^{2\pi} d\theta' e^{i\theta'} \frac{\partial^2}{\partial \theta'^2} P(\theta', t). \tag{2.51}$$

With integration by parts, one obtains

$$\frac{d\rho}{dt} = -\frac{D^2}{2}\rho \rightarrow \rho(t) = \rho(0)\exp(-D^2 t/2). \tag{2.52}$$

Equation (2.52) implies that noise acts as an additional source of phase fluctuation which would limit the phase relation associated with synchronization. Thus, in the stochastic Adler equation, the forcing has to overcome both detuning and noise to entrain the oscillator. As opposed to the noiseless case, infinitesimal forcing is not sufficient for entrainment even when $\Delta = 0$. In Fig. 2.5, we plot the synchronization measure r as a function of F/D for $\Delta = 0$. We see that to obtain a noticeable synchronization the forcing has to be in the same order as the noise strength $F \sim D$. As we will see in the next chapter, the exponential decay of the synchronization order parameter is also observed in the quantum limit cycle [see Sec. 3.3 and Eq. (3.19)].

In this chapter, we have reviewed some important aspects of classical synchronization. In particular, we have established a limit cycle oscillator as a prerequisite for synchronization. We also discussed two ways in which synchronization is typically studied: entrainment and mutual coupling. In the last two sections, we consider an extension of the traditional synchronization model. For example, in Sec. 2.4 we consider models where both entrainment and mutual coupling co-exist. Finally, in the last section, we cover synchronization in the presence of noise. For a more comprehensive review, readers are encouraged to consult other literature on synchronization [1, 2]. Here, we only choose subtopics that will be relevant foundations before discussing synchronization in the quantum regime. This is what we will do in the next chapter.

Chapter 3

Quantum Synchronization

Quantum description of physical phenomena can often be derived by quantizing classical equations of motion. The study of quantum synchronization began by quantizing the equation of motion for a classical limit cycle. However, as emphasized before, a limit cycle is a dissipative system. Therefore, before discussing quantum synchronization, one must first understand the framework for treating dissipation in quantum systems. The first section of this chapter will briefly review the Lindblad Quantum Master Equation (QME) used to describe dissipative quantum dynamics. Then, the next section will be devoted to the quantum description of the Stuart-Landau limit cycle and its synchronization in the quantum regime. The last section will be on extending the notion of quantum synchronization to quantum systems in a finite-dimensional Hilbert space.

3.1 Dissipative Quantum Dynamics

The Schrödinger equation, which governs the dynamics of an isolated quantum system can be put into the Liouville-von Neumann form

$$\frac{d\rho}{dt} = -i[H, \rho], \tag{3.1}$$

where $\rho = \sum_n p_n |\psi_n\rangle \langle\psi_n|$ is the density operator representing the system's state and H is the Hamiltonian. For convenience, we have set the Planck constant

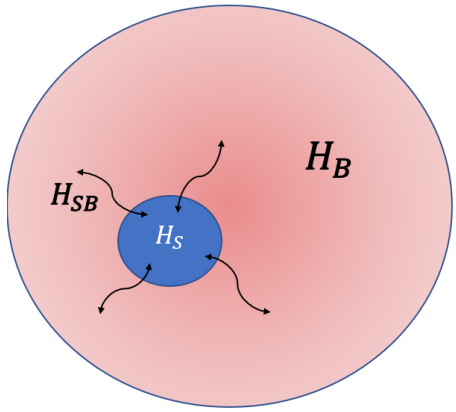

Figure 3.1: Schematic diagram of an open quantum system consisting of a quantum system (small blue circle) embedded in an environment (big red circle). The total system is governed by a Hamiltonian $H = H_S + H_B + H_{SB}$ where $H_S(H_B)$ denotes the system (environment) part and H_{SB} denotes their interaction.

$\hbar = 1$. The Hermiticity property of the Hamiltonian $H = H^\dagger$ guarantees unitary time-evolution for ρ.

However, no system is ever truly isolated from its environment. The behavior of the system interacting with its environment often can not be described by the Schrödinger equation. For start, the time evolution of such systems is not necessarily unitary since some information might leak out to the environment, leading to an irreversible time evolution of the system. In this section, we will develop the tools and frameworks to be able to describe a quantum system in a dissipative environment.

We consider a system governed by Hamiltonian H_S, embedded in an environment with Hamiltonian H_B, and they interact through interaction Hamiltonian H_{SB}. The Hamiltonian of total system (system + environment) is given by,

$$H = H_S + H_B + H_{SB} \tag{3.2}$$

We then transform it into the interaction picture with respect to $H_S + H_B$. Let $\chi(t)$ be the density operator of the total system in the interaction picture. The

Liouville-von Neumann equation is then

$$\frac{d\chi}{dt} = -i[H_{SB}(t), \chi], \tag{3.3}$$

with $H_{SB}(t) = e^{i(H_S+H_B)t} H_{SB} e^{-i(H_S+H_B)t}$. From here, we need to use the partial tracing procedure to find the equation of motion for the density operator of the system alone. We denote $\mathrm{Tr}_B\,(...)$ as the trace over the environment's Hilbert space. Then, $\rho = \mathrm{Tr}_B\,\chi$ is the reduced density operator of the system. Employing the Born-Markov approximation [89, 90], one arrives from (3.3) to the Redfield equation [91]

$$\frac{d\rho}{dt} = -\int_0^\infty d\tau\ \mathrm{Tr}_B[H_{SB}(t), [H_{SB}(t-\tau), \rho(t) \otimes \rho_B]], \tag{3.4}$$

with ρ_B being the density operator of the environment. The Born-Markov approximation assumes weak system-environment coupling so that the time-scale τ_{SB} over which $\rho(t)$ evolves, known as the system's relaxation time, is the slowest time scale compared to the environment's relaxation time τ_B and the environment correlation time-scale τ_{corr}. The detailed steps from (3.3) to (3.4) can be found in other references such as Ref. [89, 90].

Next, we write the system-environment interaction Hamiltonian as

$$H_{SB} = \sum_{\alpha,\omega} A_\alpha(\omega) \otimes B_\alpha + \mathrm{h.c.} \tag{3.5}$$

where h.c. stands for Hermitian conjugate. The operator $A_\alpha(\omega)$ is a systems' operator that maps one eigenstate of H_S into another eigenstate with energy difference ω and B_α is the associated environment operator. By definition, the operator $A_\alpha(\omega)$ satisfies a commutation relation,

$$[H_S, A_\alpha(\omega)] = \omega A_\alpha(\omega) \tag{3.6}$$

In general, there can be multiple operators that map the same energy transitions. The label $\{\alpha\}$ distinguishes these different operators. For example, it can label the polarization degrees of freedom for B_α if the environment is treated as a continuum electromagnetic field.

The consequence of (3.6) is that H_{SB} has a simple form in the interaction picture

$$H_{SB}(t) = \sum_{\alpha,\omega} e^{i\omega t} A_\alpha(\omega) \otimes B_\alpha(t) + \mathrm{h.c.}, \tag{3.7}$$

where $B_\alpha(t) = e^{-iH_B t} B_\alpha e^{iH_B t}$. This simple form is obtained by substituting the commutation (3.6) to the famous Baker-Hausdorff formula [92]

$$e^X A e^{-X} = A + [X, A] + \frac{1}{2}[X, [X, A]] + ... + \frac{1}{n!}\underbrace{[X, [X, ..., [X, A]]...]}_{\text{n times}} + ... \quad (3.8)$$

We then proceed by substituting (3.7) into (3.4) and obtain

$$\frac{d\rho}{dt} = \sum_{\omega,\omega'}\sum_{\alpha,\beta} e^{i(\omega'-\omega)t}\Gamma_{\alpha\beta}(\omega)(A_\beta(\omega)\rho A_\alpha^\dagger(\omega') - A_\alpha^\dagger(\omega')A_B(\omega)\rho) + \text{h.c.} \quad (3.9)$$

The coefficients $\Gamma_{\alpha\beta}(\omega)$ are the Fourier transform of *environment correlation function* $\langle B_\alpha^\dagger(\tau)B_\beta(0)\rangle \equiv \text{Tr}_B\left(B_\alpha^\dagger(\tau)B_\beta(0)\rho_B\right)$,

$$\Gamma_{\alpha\beta}(\omega) \equiv \int_0^\infty d\tau\, e^{i\omega\tau}\,\langle B_\alpha^\dagger(\tau)B_\beta(0)\rangle \quad (3.10)$$

The environment correlation time-scale τ_{corr} mentioned in the discussion about Born-Markov approximation is associated with the time scale of the decay of the correlation function.

At this point, one usually takes the *secular approximation* whereby the summation terms over which $\omega' \neq \omega$ in (3.9) is ignored. This is justified if the timescale of systems' intrinsic unitary evolution $\tau_S = |\omega' - \omega|^{-1}$ for $\omega \neq \omega'$ is much faster than systems' relaxation time scale τ_{SB}. The secular approximation can be applied when the spectrum of H_S is either well-separated or exactly degenerate, but not in between [89, 93]. We will see in the next chapter that the secular approximation can be relaxed when one deals with a quasi-degenerate system. For now, we apply the secular approximation and obtain

$$\frac{d\rho}{dt} = \sum_{\omega}\sum_{\alpha,\beta}\Gamma_{\alpha\beta}(\omega)(A_\beta(\omega)\rho A_\alpha^\dagger(\omega) - A_\alpha^\dagger(\omega)A_B(\omega)\rho) + \text{h.c.} \quad (3.11)$$

We now summarize the approximations used to arrive at (3.11). There are four timescales in the problem: environment's relaxation time τ_B, environment's correlation time τ_{corr}, system's relaxation time τ_{SB}, and system's unitary evolution time τ_S. The assumptions we have made so far is that τ_{SB} is much slower than the other three $\tau_{SB} \gg \tau_B, \tau_{corr}, \tau_S$.

We can simplify (3.11) further by diagonalizing $\Gamma_{\alpha\beta}(\omega)$, known as the Kossakowski matrix. Finally, we will obtain the Lindblad (or Lindblad-Gorini-

Kossakowski-Sudarshan) Quantum Master Equation (QME) [94, 95]

$$\frac{d\rho}{dt} = -i[H,\rho] + \sum_{\mu} \gamma_{\mu}\Big(L_{\mu}\rho L_{\mu}^{\dagger} - \frac{1}{2}\{L_{\mu}^{\dagger}L_{\mu},\rho\}\Big) \equiv \mathcal{L}[\rho], \tag{3.12}$$

where $\{A,B\} = AB + BA$ is the anti-commutator. The operators L_{μ} are the so-called *jump operators* and $\gamma_{\mu} > 0$ are the decay rates.

The generator of the dynamics $\mathcal{L}[\rho]$ (also called as *Liouvillian*) is a *superoperator* - it maps an operator into another operator in Hilbert space. The map, when it has the form (3.12), is completely positive and trace-preserving (CPTP) - the two properties that are normally considered important for a valid quantum dynamical map [94, 95].

A steady-state ρ_{ss} is a state that satisfies $\mathcal{L}[\rho_{ss}] = 0$. In other words, it is a state that no longer evolves under the Liouvillian dynamics $d\rho_{ss}/dt = 0$. Evans' theorem [96] guarantees that for a map of the form (3.12), there is at least one such steady-state. When the system possesses certain symmetries, multiple steady-states may arise [97, 98]. But, in this thesis, we only consider the case of a unique steady-state.

To illustrate the usage of Eq. (3.12) as well as the concept of steady-state, we provide a simple example of a two-level system (qubit) in contact with a thermal reservoir. This example will also help clarify some of the concepts introduced in the next sections.

3.1.1 Example: Qubit in a thermal reservoir

Let us consider a qubit $\{|0\rangle, |1\rangle\}$ with energy gap ω in contact with a thermal reservoir of inverse temperature β. We will not derive the QME in detail [see Refs. [89, 90]], but we will only use the result

$$\frac{d\rho}{dt} = \mathcal{L}[\rho] = -i\frac{\omega}{2}[\sigma_z,\rho] + \gamma_h n_h \mathcal{D}[\sigma_+]\rho + \gamma_h(1+n_h)\mathcal{D}[\sigma_-]\rho, \tag{3.13}$$

where $\mathcal{D}[C]\rho = C\rho C^{\dagger} - \frac{1}{2}\{C^{\dagger}C,\rho\}$ is the Lindblad superoperator. The operators $\sigma_{\pm} = \sigma_x \pm i\sigma_y$ are the spin ladder operators and $\sigma_{x,y,z}$ are the Pauli matrices. The system-reservoir coupling strength is denoted by γ_h and $n_h = [\exp(\beta\omega) - 1]^{-1}$ is the bosonic mean occupation number of the reservoir.

Note that the dissipator consist of two parts: gain (σ_+) and loss (σ_-). In the next sections, the balance between dissipative gain and loss would become one of the keys to understand synchronization. For now, we will show the typical dynamics of qubit in a thermal reservoir.

Equation (3.13) can be expanded in terms of the components of density operator $\rho_{ij} = \langle i|\rho|j\rangle$,

$$\dot{\rho}_{00} = \gamma_h(1+n_h)\rho_{11} - \gamma_h n_h \rho_{00} \tag{3.14}$$

$$\dot{\rho}_{11} = \gamma_h n_h \rho_{00} - \gamma_h(1+n_h)\rho_{11} \tag{3.15}$$

$$\dot{\rho}_{01} = i\omega\rho_{01} - \frac{\gamma_h(1+2n_h)}{2}\rho_{01} \tag{3.16}$$

$$\dot{\rho}_{10} = -i\omega\rho_{10} - \frac{\gamma_h(1+2n_h)}{2}\rho_{10} \tag{3.17}$$

The resulting system of differential equations is simple enough to solve analytically

$$\rho_{11}(t) = Ce^{-\gamma_h(1+2n_h)t} + \frac{n_h}{(1+2n_h)} \qquad \rho_{00}(t) = 1 - \rho_{11}(t) \tag{3.18}$$

$$\rho_{01}(t) = De^{i\omega t}e^{-\gamma_h(1+2n_h)t/2} \qquad \rho_{10}(t) = \rho_{01}^*(t), \tag{3.19}$$

where C, D are constants that depend on the initial condition. In the long-time limit, the density operator goes into the steady-state

$$\rho_{ss} = \frac{1}{1+2n_h}\begin{pmatrix} 1+n_h & 0 \\ 0 & n_h \\ & . \end{pmatrix} \tag{3.20}$$

One can easily confirm that $\mathcal{L}[\rho_{ss}] = 0$. Furthermore, the population ratio is equal to the ratio between gain rate and loss rate, which in the case of thermal bath is exactly the Boltzmann factor

$$\frac{\rho_{11}}{\rho_{00}} = \frac{n_h}{1+n_h} = e^{-\beta\omega}. \tag{3.21}$$

The decay of coherence (off-diagonal element in the density matrix) such as in Eq. (3.19) is known as *decoherence*. Decoherence is a process whereby the phase of the system becomes random. It can be understood as a phase diffusion process due to noise from the environment [99–103]. In typical situations, the time in which the population stabilizes is faster than the decay of the coherence. In this example, it is faster by a factor of two as can be inferred from (3.18)-(3.19).

3.2 Quantization of Stuart-Landau Oscillator

In this section, we will use the Lindblad QME developed in the previous section to quantize the Stuart-Landau (SL) oscillator. Let's recall a classical Stuart-Landau limit cycle,

$$\dot{\alpha} = \left(\frac{\gamma_1}{2} - i\omega - \gamma_2|\alpha|^2\right)\alpha, \tag{3.22}$$

with $\gamma_{1,2}$ are constants and ω is the natural frequency. A limit cycle of radius $\gamma_1/2\gamma_2$ in phase-space can be obtained if we interpret the complex number α as a complex summation of position and momentum $\alpha = x + ip$.

In quantum mechanics, physical observables are represented by Hermitian operators. The procedure to promote a classical observable to a quantum observable is known as canonical quantization [104]. The idea of the quantum SL oscillator is to apply canonical quantization to Eq. (3.22) by promoting x and p into Hermitian operators and then impose the canonical commutation relation $[\hat{x}, \hat{p}] = i$. After x and p have been quantized, we can associate α with the annihilation operator $a = \hat{x} + i\hat{p}$. Finally, the goal is to look for a QME that can reproduce (3.22) when the system is in the eigenstate of a, i.e. a coherent state [105]

$$|\alpha\rangle = e^{-|\alpha|^2/2} \sum_{n=0}^{\infty} \frac{\alpha^n}{\sqrt{n!}} |n\rangle\,, \tag{3.23}$$

with α being a complex number and $|n\rangle$ is the Fock state of quantum harmonic oscillator. It turns out, the following Liouvillian can do the job [24–26]

$$\frac{d\rho}{dt} = \mathcal{L}[\rho] = -i\omega[a^\dagger a, \rho] + \gamma_1 \mathcal{D}[a^\dagger]\rho + \gamma_2 D[a^2]\rho, \tag{3.24}$$

where $\mathcal{D}[\hat{c}]\rho$ is defined below Eq. (3.13). The QME (3.24) is the main object of study in this section. First, we will show explicitly how this QME can reproduce the classical SL equation (3.22). Let us calculate the equation of motion for $\langle a\rangle = \mathrm{Tr}\,\rho a$ by first computing

$$-i\omega\,\mathrm{Tr}\,([a^\dagger a, \rho]a) = -i\omega\,\mathrm{Tr}\,(\rho a a^\dagger a - \rho a^\dagger a^2) = -i\omega\,\langle a\rangle \tag{3.25}$$

$$\gamma_1\,\mathrm{Tr}\left((\mathcal{D}[a^\dagger]\rho)a\right) = \frac{\gamma_1}{2}\,\mathrm{Tr}\,(\rho a^2 a^\dagger - \rho a a^\dagger a) = \frac{\gamma_1}{2}\,\langle a\rangle \tag{3.26}$$

$$\gamma_2\,\mathrm{Tr}\left((\mathcal{D}[a^2]\rho)a\right) = \frac{\gamma_2}{2}(\rho(a^\dagger)^2 a^3 - \rho a(a^\dagger)^2 a^2) = -\gamma_2\,\langle a^\dagger a^2\rangle\,. \tag{3.27}$$

In deriving (3.25)-(3.27), we have used the cyclic property of trace and the commutation relation $[a, a^\dagger] = 1$. With these, we can obtain the equation of motion for $\langle a \rangle$

$$\frac{d}{dt}\langle a \rangle = \frac{\gamma_1}{2}\langle a \rangle - i\omega \langle a \rangle - \gamma_2 \langle a^\dagger a^2 \rangle . \tag{3.28}$$

The last ingredient to recover the SL equation is by assuming the system is in coherent state $\rho(t) = |\alpha(t)\rangle \langle \alpha(t)|$ *at all times* t. Then, the non-linear term in the SL equation is obtained from the last term in Eq. (3.28)

$$\langle a^\dagger a^2 \rangle = \mathrm{Tr}\left(a^\dagger a^2 |\alpha\rangle \langle \alpha|\right) = |\alpha^2| \langle a \rangle = |\alpha|^2 \alpha. \tag{3.29}$$

After substituting (3.29) to (3.28) and using $\langle a \rangle = \alpha$, we can recover Eq. (3.22).

The assumption that the state of the system is always represented by $|\alpha(t)\rangle$ is a semi-classical approximation. In general, such an approximation does not hold. In other words, if one is to draw the snapshot of $\rho(t)$ as a function of α, it will not always correspond to a point. Instead, it will be represented by a distribution defined over α [106]. Recall that in the case of a noisy classical limit cycle oscillator (Sec. 2.5), one also talks about the phase distribution instead of the phase itself. In this view, the quantum SL oscillator is analogous to a classical SL oscillator in the presence of noise [25, 26].

The QME (3.24) has a straightforward interpretation. It is a harmonic oscillator with one-particle gain and two-particle loss. Moreover, the QME can probe the classical limit, characterized by $|\alpha| \gg 1$ and the quantum limit $|\alpha| \ll 1$. The quantum limit is equivalent to the limit $\gamma_2 \gg \gamma_1$ since the steady-state $|\alpha|$ is proportional to γ_1/γ_2 [see Eq. (3.22)]. Physically, this means that the quantum limit is reached when the Fock state occupation number is small in the steady state and it can occur via the domination of two-particle loss over one-particle gain. By virtue of its simplicity and richness, the QME (3.24) has been intensely investigated in the literature [24–26]. Note, however, that some literature calls Eq. (3.24) as the equation for quantum *van der Pol* oscillator. This is a misnomer as pointed out in Ref. [28].

In order to study the limit cycle of the quantum SL oscillator, it is convenient to adopt a phase space representation. Suppose we choose to adopt the Wigner function $W(\alpha, \alpha^*, t)$ [106, 107]. It can be shown that the steady-state Wigner function takes the form [24]

$$W_{ss}^{(c)}(|\alpha|) \propto \exp\Big(\frac{2(\gamma_1|\alpha|^2 - \gamma_2|\alpha|^4)}{3\gamma_1 + 2\gamma_2}\Big) \tag{3.30}$$

$$W_{ss}^{(q)}(|\alpha|) \propto (4|\alpha|^2 + 1) \exp(-2|\alpha|^2), \tag{3.31}$$

where the subscript ss denotes the steady-state and the superscipts c and q represents classical and quantum limit respectively. The Wigner distribution is plotted in Fig. 3.2(a)-3.2(b). Surprisingly, in both cases, the Wigner distribution peaked away from the origin, indicating a limit cycle behavior. However, instead of rotating along a circle of fixed radius, the steady-state forms a stationary uniform ring distribution due to phase diffusion from environmental noise. The distribution also has a finite width attributed to quantum noise (i.e. the uncertainty principle) [24–26]. As expected, the effect of quantum noise is much more pronounced in the quantum regime 3.2(b).

In addition, Ref. [27] showed that the quantum SL equation exhibits a *time-scale* separation between limit cycle and phase diffusion. Starting from an arbitrary initial condition, the Wigner distribution will be attracted to a finite radius with respect to the origin. Only after the system settles into a limit cycle, does phase diffusion dominate and the distribution spreads over the ring.

So far, we have established the QME (3.24) as the quantization of the Stuart-Landau limit cycle (with noise). Recall that the Stuart-Landau equation is a universal equation for weakly non-linear oscillator [68]. Thus, Eq. (3.24) can potentially be universal for any weakly non-linear quantum oscillator. We will not discuss the quantization of limit cycle oscillators with stronger non-linearity such as the van der Pol oscillator and Rayleigh oscillator here, but it has been discussed in Refs. [27, 28].

3.2.1 Driven Quantum Stuart-Landau Oscillator

In Chapter 2, we examined two ways to achieve synchronization after limit cycle has been established: entrainment and mutual coupling. Let us now consider entrainment of a quantum SL oscillator to an external driving of strength λ and frequency Ω described by the Hamiltonian

$$H = \omega a^\dagger a + \lambda a e^{i\Omega t} + \lambda a^\dagger e^{-i\Omega t}. \tag{3.32}$$

We can make this Hamiltonian time-independent by transforming to rotating frame $A \to e^{i\Omega a^\dagger a t} A e^{-i\Omega a^\dagger a t}$ for any operator A. The QME (3.24) is now trans-

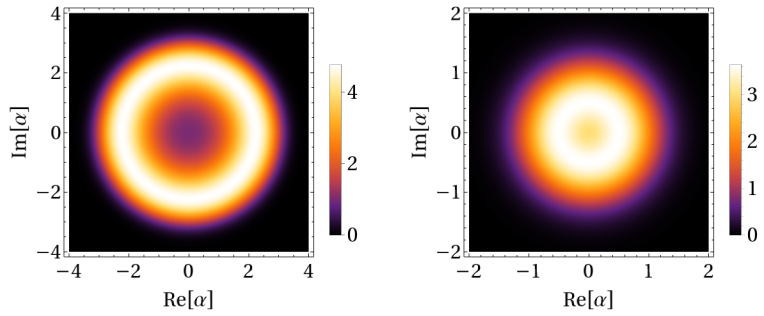

(a) $W_{ss}^{(c)}$ (b) $W_{ss}^{(q)}$

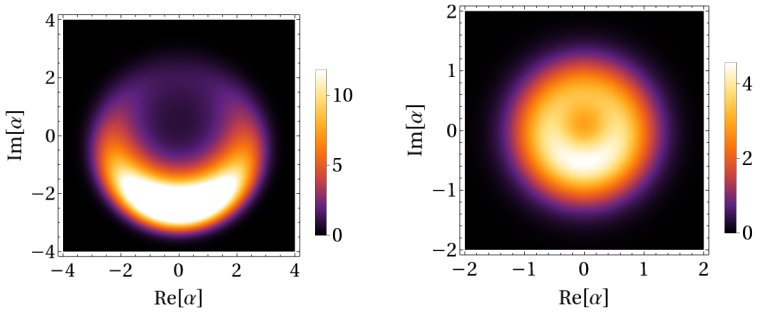

(c) $W_{ss}^{(c)\prime}$ (d) $W_{ss}^{(q)\prime}$

Figure 3.2: Steady-state Wigner function of (a,b) undriven quantum SL equation (3.24) in (a) classical limit $\gamma_1 = 1,\ \gamma_2 = 0.1$ (b) quantum limit $\gamma_2 \to \infty$. (c,d) Driven quantum SL equation (3.33) in (c) classical limit $\lambda = 0.5$ (d) quantum limit $\gamma_2 \to \infty,\ \gamma_1 = 1,\ \lambda = 0.5$.

formed into,

$$\frac{d\rho}{dt} = -i[(\omega - \Omega)a^\dagger a + \lambda a + \lambda a^\dagger, \rho] + \gamma_1 \mathcal{D}[a^\dagger]\rho + \gamma_2 \mathcal{D}[a^2]. \tag{3.33}$$

Entrainment refers to the phenomenon of phase-locking between the system and the drive. However, as demonstrated in Sec. 2.5, in particular Fig. 2.5(b), perfect phase locking is not possible in the presence of noise. Instead, the phase distribution will localize to a certain region over the ring. Consider the simplest case of $\Omega = \omega$. The corresponding steady-state Wigner function in the classical

and quantum limit are given by [24],

$$W_{ss}^{(c)\prime}(|\alpha|,\phi) \propto \exp\Big(\frac{2(\gamma_1|\alpha|^2-\gamma_2|\alpha|^4-2\lambda|\alpha|\sin\phi)}{3\gamma_1+2\gamma_2}\Big) \tag{3.34}$$

$$W_{ss}^{(q)\prime}(|\alpha|,\phi) \propto \Big[\frac{9}{4}\gamma_1^2+4\lambda^2|\alpha|^2-2\lambda|\alpha|\gamma_1\sin\phi\Big]\exp(-2|\alpha|^2), \tag{3.35}$$

where $\alpha = |\alpha|e^{i\phi}$. Clearly, we see that the radial symmetry has been lost due to λ. The phase localization behavior in the classical and quantum limit are shown in Fig. 3.2(c)-3.2(d). In particular, 3.2(d) clearly demonstrates the persistence of phase-locking in the quantum limit.

As a side note, phase localization is not the only way to observe quantum synchronization. An alternative way is to look at the power spectrum $S(\omega)$

$$S(\omega) = \int_{-\infty}^{\infty} dt\; e^{i\omega t}\,\langle a^\dagger(t)a(0)\rangle\,. \tag{3.36}$$

The peak of $S(\omega)$ can be regarded as the observed frequency of the oscillator. Thus, by calculating $S(\omega)$, one may study the shift of the observed frequency compared to the natural frequency of the oscillator. A detailed analysis of the power spectrum of the quantum SL oscillator can be found in Ref. [25].

Up to now, we have discussed the entrainment of a quantum SL oscillator to an external drive. As we know, synchronization can also arise from mutual coupling between multiple oscillators. We will not discuss in synchronization between multiple coupled quantum SL oscillators in detail, but it has been studied in Refs. [24,26]. Curiously, the entanglement between two quantum SL oscillators follows the Arnold tongue structure associated with their synchronization [26]. This connects synchronization, which was originally a classical phenomenon, with a purely quantum phenomenon, namely entanglement. To investigate this connection further, we will develop a framework to study synchronization in Hilbert space of finite dimension in the next section.

3.3 Quantum Synchronization in Finite Dimensional Systems

In the previous section, we learned that limit cycle oscillators can be mimicked in quantum systems by quantizing the classical equation of motion. In

particular, we have quantized the Stuart-Landau equation into the dissipative dynamics of quantum harmonic oscillators with gain and loss. It is shown that the (noisy) limit cycle persists in the quantum regime and that it can be entrained by an external drive.

The position and momentum of a quantum harmonic oscillator are continuous variables. Accordingly, the Hilbert space associated with a quantum harmonic oscillator is *infinite-dimensional*. In many cases, the state of a quantum system can be described by a state vector in a *finite-dimensional* Hilbert space. For instance, infinite-dimensional Hilbert space can be truncated if one has physical reasons to ignore states beyond the cut-off (e.g. energy cut-off in quantum harmonic oscillator). Moreover, many artificial quantum systems such as Josephson junction [108], Rydberg atoms [109], and quantum dots [110] can be effectively described by finite-dimensional quantum mechanics. But, far from being only an effective description, finite-dimensional quantum mechanics is also related to fundamental quantum properties, i.e. spin. Other than being a fundamental property, spin is also responsible for many atomic quantum phenomena such as hyperfine splitting, the Pauli exclusion principle, magnetism and many more. Quantum mechanics in finite-dimensional Hilbert space is therefore at least as important as that in infinite-dimension. With that being said, understanding quantum synchronization in finite-dimensional Hilbert space is thus in order.

Let us consider the standard quantum mechanics of an isolated system in the Hilbert space of dimension governed by the Schrödinger equation,

$$i\frac{d}{dt}\left|\psi\right\rangle = H\left|\psi\right\rangle, \tag{3.37}$$

with H as the Hamiltonian operator. The solution to (3.37) can be written in terms of the eigenstates of the Hamiltonian satisfying $H\left|n\right\rangle = \omega_n\left|n\right\rangle$ as

$$\left|\psi(t)\right\rangle = \sum_{n=1}^{N} c_n(0)e^{-i\omega_n t}\left|n\right\rangle. \tag{3.38}$$

The evolution can be understood as a superposition of linear oscillators with amplitude $|c_n(0)|$ and frequency ω_n in the complex plane. Thus, the state $\left|\psi\right\rangle$ already contains multiple amplitudes, frequencies, and phases simultaneously. Naturally, energy difference leads to phase drift between the eigenstates $\phi_n - \phi_m = (\omega_n - \omega_m)t$, which implies that the phase difference is unbounded (mod 2π).

Quantum synchronization in N-levels system is concerned with establishing stable phase relation $\phi_n - \phi_m = \Phi_{nm}$ where Φ_{nm} is a constant independent of the

initial condition. The independence from the initial condition implies that the system's evolution has to be non-unitary, which can be realized by considering an open quantum system as explained in Sec. 3.1. Note that in this framework, the phases we are trying to synchronize are inherently quantum. Therefore, unlike the quantum SL oscillator studied in the previous section, the synchronization discussed here does not have a classical limit.

Let ρ^{ss} be the steady-state density operator from a non-unitary evolution. If ρ_{ss} has a certain phase coherence ($\rho^{ss}_{nm} = \langle n|\rho^{ss}|m\rangle \neq 0$ for $n \neq m$), then the phase relation between $|n\rangle$ and $|m\rangle$ has been stabilized. We can then interpret steady-state coherences ρ^{ss}_{nm} as a multi-phase generalization to continuous Kuramoto order parameter (Eq. (2.50))

$$\rho^{ss}_{nm} \propto \int_0^{2\pi} e^{i(\phi_n - \phi_m)} \mathcal{Q}^{ss}(\phi_1, \phi_2, ..., \phi_{N-1}) \prod_{\mu=1}^{N} d\phi_\mu \tag{3.39}$$

where $\mathcal{Q}(\phi_1, \phi_2, ..., \phi_{N-1})$ is the joint quasi-probability distribution for the phase variables which will be discussed in more detail later. As a consequence, the magnitude $|\rho_{nm}|$ will be related to synchronization strength and $\arg(\rho_{nm})$ is interpreted as the average phase. In this way, quantum synchronization is analogous to classical synchronization in the presence of noise (Sec. 2.5). This analogy can be motivated by the fact that fluctuation due to interaction with the environment is unavoidable in open quantum systems, as we also see in the case of the quantum SL oscillator.

From the basic positivity property of the density operator, one can derive an upper bound to $|\rho^{ss}_{nm}|$ in terms of the steady-state population ρ^{ss}_{nn} and ρ^{ss}_{mm}

$$|\rho^{ss}_{nm}| \leq \sqrt{\rho^{ss}_{nn}\rho^{ss}_{mm}} \tag{3.40}$$

Thus, a prerequisite for having steady-state coherence is to have a non-zero steady-state population in the associated eigenstates. For this to occur, one must have both dissipative gain and loss in the $|n\rangle \leftrightarrow |m\rangle$ transition such as what happens in the two-level system in the presence of thermal bath (Subsec. 3.1.1). Recall that ρ_{nn} is the probability of the system to be in state $|n\rangle$, and thus it plays the role of amplitude. The stable preference of population ratio ρ_{nn}/ρ_{mm} can be interpreted as stabilization of amplitude (limit cycle). However, as we saw in Subsec. 3.1.1, the amplitude stabilization by dissipation inevitably also induces decoherence, which is analogous to what happens in a noisy classical limit cycle where the continuous order parameter decays to zero [Eq. (2.52)].

In general, for a given steady state ρ^{ss}, there could be multiple steady-state coherence ρ^{ss}_{nm} for different values of n and m. Furthermore, they are not necessarily independent from each other. A synchronized state is not only a state possessing a high degree of steady-state coherence, but it also constrains their phase relations to be compatible, e.g. denoting $\arg(\rho^{ss}_{nm}) = \varphi_{nm}$ we must have $\varphi_{nm} - \varphi_{mp} = \varphi_{np}$ for any triplets (n, m, p). Thus, one needs an overall synchronization measure possibly combining all the steady-state coherences to characterize the strength of synchronization of a general N-level state. This measure can be systematically derived by phase space representation as will be explained in detail below.

As demonstrated in Fig. 2.5(b) and Fig. 3.2, in the presence of noise, synchronization can be observed from localization in phase probability distribution [29, 37, 41, 48]. If we want to follow the same framework, we need a notion of phase space for N-dimensional system. In general, such phase space representation is not unique. In this thesis, we will define our phase space by the Husimi Q-function [106] associated with the $SU(N)$ coherent state [111–113]. The Husimi-Q representation is connected to the Wigner representation employed in Sec. 3.2 via Weierstrass transformation [106].

First, following the approach in Ref. [112], we define $SU(N)$ coherent state as

$$|\alpha_N\rangle = \sum_{n=0}^{N-1} \alpha_N^n |n\rangle \qquad \alpha_N^n = \begin{cases} \cos\theta_1 & n = 0 \\ e^{i\phi_n} \cos\theta_{n+1} \prod_{k=1}^{n} \sin\theta_k & 0 < n < N-1 \\ e^{i\phi_{n-1}} \prod_{k=1}^{N-1} \sin\theta_k & n = N-1. \end{cases} \tag{3.41}$$

The basis $\{|n\rangle\}$ are chosen to be the eigenstate of the Hamiltonian H. If the spectrum of H is non-degenerate, the basis $\{|n\rangle\}$ is unique. However, when there is degeneracy, a more careful treatment is needed. In general, a consistent treatment can still be applied if there exists a preferred basis in the degenerate system, e.g. local excitation basis in spin chain systems. The coherent state $|\alpha_N\rangle$ can be regarded as a unit vector in $N-1$ dimensional hypersphere, having $N-1$ polar angles θ_n encoding the amplitudes $|c_n|$ and $N-1$ azimuthal angles ϕ_n encoding coherences (phase relation between $|n\rangle$). In other words, Eq. (3.41) is a straightforward N-levels generalization of Bloch sphere representation for a qubit. The Husimi Q-function is defined by the overlap between the density

operator with the coherent state

$$Q_N[\rho] \equiv \frac{N!}{\pi^{N-1}} \langle \alpha_N|\rho|\alpha_N\rangle \,, \tag{3.42}$$

with the normalization factor arising from the resolution of unity

$$\frac{N!}{\pi^{N-1}} \int |\alpha_N\rangle \langle \alpha_N| \, d\Theta \, d\Phi = I. \tag{3.43}$$

We have denoted $d\Theta$ and $d\Phi$ as infinitesimal elements of all polar angles and all azimuthal angles. The $Q_N[\rho]$ defined above is a functional of ρ, i.e. it maps an input ρ to an output of Husimi Q-function $Q_N(\theta_1, ..., \theta_{N-1}, \phi_1, ..., \phi_{N-1})$. The Husimi Q-function is in general not a probability distribution, but a quasi-probability distribution, because different coherent states are not orthogonal [106].

A typical steady-states of dissipative dynamics has the form $\rho_{ss} = \sum_n \rho_{nn} |n\rangle \langle n|$. The associated Q-function for this steady-state is given by

$$Q_N[\rho_{ss}] = \frac{N!}{\pi^{N-1}} \sum_{n=0}^{N-1} \rho_{nn} |\alpha_N^n|^2 = Q_N(\theta_1, \theta_2, ..., \theta_{N-1}). \tag{3.44}$$

Thus, for a diagonal state, the Q-function is independent of $\{\phi_n\}$. This results in a distribution that is phase-symmetric, similar to Fig. 3.2(a) - 3.2(b). Such phase-symmetric distribution resembles a noisy limit cycle.

Phase localization, and thus synchronization, emerges if there is non-vanishing steady-state coherence $\rho_{nm}^{ss} \neq 0$ for $n \neq m$. To see this, we integrate out the polar angles in $Q_N[\rho]$, i.e.,

$$\int Q_N[\rho] \, d\Theta_N = \frac{N!}{\pi^{N-1}} \sum_{n,m=0}^{N-1} \rho_{nm} \int_0^{\pi/2} \alpha_N^{n*} \alpha_N^m \prod_{l=1}^{N-1} \cos\theta_l \, (\sin\theta_l)^{2N-2l-1} \, d\theta_l \tag{3.45}$$

The diagonal contribution ($n = m$) gives,

$$\int_0^{\pi/2} |\alpha_N^j|^2 \prod_{l=1}^{N-1} \cos\theta_k (\sin\theta_k)^{2n-2k-1} \, d\theta_l = \frac{1}{2^{N-1}N!} \qquad \forall n, \tag{3.46}$$

while the off-diagonal ($n < m$) contribution yields,

$$e^{i(\phi_m - \phi_n)} \int_0^{\pi/2} \cos\theta_{n+1} \cos\theta_{m+1} \prod_{k=1}^{n} \sin^2\theta_k \prod_{j=n+1}^{k} \sin\theta_j \prod_{l=1}^{N-1} \cos\theta_l (\sin\theta_l)^{2n-2l-1} \, d\theta_l$$
$$= \frac{\pi}{2^{N+1}N!} e^{i(\phi_m - \phi_n)}. \tag{3.47}$$

Substituting (3.46) & (3.47) to (3.45) yields a phase distribution function over $N-1$ torus,

$$\begin{aligned}\mathcal{Q}(\phi_1,\phi_2,...,\phi_{N-1}) &\equiv \int Q_N[\rho]\, d\Theta_N \\ &= \frac{1}{2^{N+1}\pi^{N-2}} \sum_{\substack{n,m=0 \\ n\neq m}}^{N-1} \rho_{nm} e^{i(\phi_m-\phi_n)} + \frac{1}{(2\pi)^{N-1}}, \end{aligned} \tag{3.48}$$

where by convention we set $\phi_0 = 0$. Clearly, the case $\rho_{nm} = 0\ \forall n \neq m$, corresponds to a uniform distribution over the torus. Therefore, as soon as $\rho_{nm} \neq 0$ *in the steady-state*, phase preference is developed and the system is said to possess a certain degree of synchronization. This can be more clearly illustrated if one inverts Eq. (3.48) to express ρ_{nm} as a function of $\mathcal{Q}$. To this aim, we multiply both sides of (3.48) with $e^{i(\phi_k-\phi_l)}$ and integrate over all phases. Then, use the identity

$$\int_0^{2\pi} e^{i(\phi_m-\phi_n+\phi_k-\phi_l)} \prod_{\mu=1}^{N-1} d\phi_\mu = (2\pi)^{N-1}\delta_{ml}\delta_{nk} \tag{3.49}$$

to obtain

$$\rho_{nm} = \frac{4}{\pi}\int_0^{2\pi} e^{i(\phi_n-\phi_m)}\mathcal{Q}(\phi_1,\phi_2,...,\phi_{N-1}) \prod_{\mu=1}^{N} d\phi_\mu. \tag{3.50}$$

Thus, we have proven Eq. (3.39), demonstrating that steady-state coherence can be viewed as a synchronization order parameter. Here, we would like to emphasize the difference between coherence and *steady-state* coherence. It is well-known that coherence is a signature of quantum property not present in any classical systems. However, in standard quantum mechanics, the presence of coherence always depends on the initial condition. Steady-state coherence, on the other hand, is independent of the initial condition. In other words, one could start from a totally incoherent initial condition (e.g. a diagonal initial state), and as time evolves, coherence will be built up and maintained as long as the system is kept out of equilibrium. This distinction is crucial for understanding the relationship between quantum synchronization and coherence. As we have seen from Ch. 2, the robustness from perturbation in the initial condition is one of the hallmarks of synchronization.

One way to quantify synchronization is by associating synchronization measure with the peak of $\mathcal{Q}$

$$S_{\max} = \max_{\phi_1,\phi_2,...,\phi_N} \mathcal{Q}(\phi_1,\phi_2,...,\phi_N). \tag{3.51}$$

In this thesis, we will use S_{max} to quantify quantum synchronization. This quantity is always zero for any diagonal state (limit cycle). We note that S_{max} is different from the purity of the steady state $tr(\rho_{ss}^2)$ because in general different diagonal states would have different purity. In particular, the energy eigenstate is maximally pure, but its S_{max} is zero.

Moreover, we remark that there exist other synchronization measures in the literature. Equation (3.51) belongs to the category of phase-space synchronization measure. A different phase-space measure using $SO(3)$ projection instead of $SU(N)$ has been studied in Refs. [29, 41]. One may also imagine choosing the Wigner representation [114] or other representations instead of the Husimi-Q representation. Information-theoretic measures such as mutual information [115], coherence [39] and entanglement measures [49] to quantify quantum synchronization have also been explored. It is expected that all these various measures to differ only quantitatively with converging qualitative behavior.

It is worth noting that using SO(3) phase projection, it has been claimed that the smallest Hilbert space dimension over which synchronization can occur is three [29–31,41]. In other words, it has been argued that synchronization is not possible for a qubit due to its inability to host a limit cycle. On the other hand, earlier research has shown that synchronization can occur in a driven-dissipative qubit system [36,42], albeit without explicit reference toward the associated limit cycle. The discussion on the existence of a limit cycle for qubit can be found in Refs. [37, 48]

In this section, we have established a diagonal steady-state in the eigenbasis of the Hamiltonian as an analogue to a noisy classical limit cycle [37, 48]. Phase localization, and thus synchronization, occurs as the system starts to possess steady-state coherence. Lastly, we have derived a measure of synchronization $S_{\max}$ based on the localization of Husimi-Q representation and $SU(N)$ coherent state. This generic framework can be applied to various systems possessing steady-state coherence. One such system is an atomic maser, a system that we will explore in detail in the next chapter.

Chapter 4

Quantum Synchronization in Thermal Maser

4.1 Synchronization in Three-Level Thermal Maser

In this chapter, we will start building a connection between synchronization and thermodynamics. We do this by investigating synchronization in a quantum heat engine model. Several prior studies indicate that synchronization can be used to enhance the performance of classical thermodynamic machines [50, 52]. In the same spirit, we aim to investigate whether quantum synchronization can enhance the performance of quantum thermodynamic devices. Specifically, we consider the synchronization of quantum maser (Microwave Amplification by Stimulated Emission of Radiation) heat engines, first proposed by Scovil and Schulz-Dubois [116] in the 1960s. Recently, it has been shown that synchronization measure bounds the steady-state power of this engine [40]. The connection between synchronization and the thermodynamic performance of this engine will be explored in more detail in the next chapter. Here, we will focus on explaining the basic setup as well as deriving its synchronization properties following the approach of Ref. [40].

Let us consider a three-level-system (3LS) labelled by $\{|0\rangle, |1\rangle, |2\rangle\}$ continu-

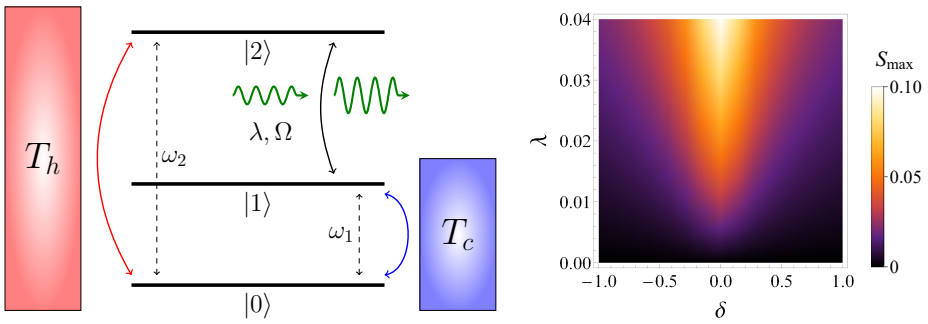

Figure 4.1: (a) Schematic diagram of three-level maser heat engine with $T_{h,c} = \beta_{h,c}^{-1}$ (b) Arnold tongue for $S_{\max}$ with the values of the parameters given by $\gamma_h = 10^{-2}$, $\gamma_c = 0.1$, $n_h = 5$, $n_c = 0.1$.

ously in contact with two thermal baths of inverse temperatures β_h and β_c where the subscripts refer to 'hot' and 'cold' respectively ($\beta_c > \beta_h$). The hot (cold) bath induces incoherent transition $|0\rangle \leftrightarrow |2\rangle$ ($|0\rangle \leftrightarrow |1\rangle$) with energy gap ω_2 (ω_1). The role of the baths is to establish population inversion between $|2\rangle$ and $|1\rangle$ (i.e. $\rho_{22} > \rho_{11}$). After population inversion has been established, the maser is emitted by introducing a weak drive with frequency Ω resonant with $\omega_2 - \omega_1$. The schematic diagram of the system is shown in Fig. 4.1(a).

The QME governing the density operator of the 3LS is written as

$$\dot{\rho} = -i[H(t), \rho] + \mathcal{D}_h[\rho] + \mathcal{D}_c[\rho], \tag{4.1}$$

where the Hamiltonian $H(t)$ can be divided into two parts: the bare Hamiltonian H_0 and the drive $V(t)$,

$$H_0 = \omega_1 |1\rangle\langle 1| + \omega_2 |2\rangle\langle 2| \qquad V(t) = \lambda e^{i\Omega t} |1\rangle\langle 2| + \lambda e^{-i\Omega t} |2\rangle\langle 1|. \tag{4.2}$$

Meanwhile, the hot and cold baths' dissipators are of the Lindblad form,

$$D_h[\rho] = \sum_{\mu=1}^{2} \Gamma_{h_\mu} (2h_\mu \rho h_\mu^\dagger - \{h_\mu^\dagger h_\mu, \rho\}) \tag{4.3}$$

$$D_c[\rho] = \sum_{\mu=1}^{2} \Gamma_{c_\mu} (2c_\mu \rho c_\mu^\dagger - \{c_\mu^\dagger c_\mu, \rho\}), \tag{4.4}$$

with thermal decay rates $\Gamma_{h_1} = \gamma_h(1+n_h)$, $\Gamma_{h_2} = \gamma_h n_h$, $\Gamma_{c_1} = \gamma_c(1+n_c)$, $\Gamma_{c_2} = \gamma_c n_c$ and jump operators $h_1 = h_2^\dagger = |0\rangle\langle 2|$, $c_1 = c_2^\dagger = |0\rangle\langle 1|$. Here, $\gamma_h(\gamma_c)$ is the coupling strength between the system and the hot (cold) bath and $n_h = [\exp(\beta_h\omega_2) - 1]^{-1}$ ($n_c = [\exp(\beta_c\omega_1) - 1]^{-1}$) is the bosonic mean occupation number of the hot (cold) bath.

In the absence of driving $\lambda = 0$, the steady-state of QME (4.1)-(4.4) is diagonal in the basis of H_0

$$\rho_{22} = \frac{n_h(1+n_c)}{1+2n_h+n_c(3n_h+2)} \qquad \rho_{11} = \frac{n_c(1+n_h)}{1+2n_h+n_c(3n_h+2)}, \tag{4.5}$$

and by normalization $\rho_{00} = 1 - \rho_{11} - \rho_{22}$. As discussed in Sec. 3.3, a diagonal steady-state is analogous to a noisy limit cycle whose phases are free to synchronize.

Population inversion $\rho_{22} > \rho_{11}$ is achieved if and only if $n_h > n_c$. Suppose we turn on a weak-driving $\lambda \neq 0$. For $n_h > n_c$, the 3LS continuously transforms thermal energy into work (lasing), i.e. the TLS operates as an engine. On the other hand, if $n_h < n_c$, the TLS would absorb work accompanied by heat flow from the cold bath to the hot bath, i.e. the TLS operates as a refrigerator [117].

Due to driving, the equation of motion (EOM) for the coherence ρ_{12} is coupled to the population,

$$\dot{\rho}_{12} = i[(\omega_2 - \omega_1)\rho_{12} - \lambda e^{i\Omega t}(\rho_{22} - \rho_{11})] - [\gamma_h(1+n_h) + \gamma_c(1+n_c)]\rho_{12} \tag{4.6}$$

which leads to non-vanishing value of ρ_{12} in the steady-state. To observe the connection between entrainment and steady-state coherence, let us perform polar decomposition $\rho_{12} = |\rho_{12}|e^{i\phi_{12}}$. The EOM for $|\rho_{12}|$ and ϕ_{12} are given by

$$\frac{d|\rho_{12}|}{dt} = \lambda(\rho_{22} - \rho_{11})\sin(\Omega t - \phi_{12}) - [\gamma_c(1+n_c) + \gamma_h(1+n_h)]|\rho_{12}| \tag{4.7}$$

$$\frac{d\phi_{12}}{dt} = \frac{1}{|\rho_{12}|}\Big(\omega_2 - \omega_1 - \lambda(\rho_{22} - \rho_{11})\cos(\Omega t - \phi_{12})\Big). \tag{4.8}$$

In particular, the EOM (4.8) resembles that of the Adler equation with cosine forcing.

The steady-state of QME (4.1)-(4.4) can be more easily solved if one transforms to a frame rotating with frequency Ω. We then define a rotating Hamiltonian

$$H_r = \frac{\Omega}{2}|2\rangle\langle 2| - \frac{\Omega}{2}|1\rangle\langle 1|, \tag{4.9}$$

by which we transform any operator $A \to e^{iH_r t} A e^{-iH_r t}$. One may check that due to its Lindblad form, the dissipators are invariant to this transformation. Meanwhile, the Hamiltonian becomes time-independent

$$H(t) \to H = H_0 - H_r + V_r \qquad V_r = \lambda(|1\rangle\langle 2| + |2\rangle\langle 1|). \tag{4.10}$$

Solving for the steady-state in this frame, we obtain a non-vanishing steady-state coherence ρ_{12}

$$\rho_{12} = \frac{(n_c - n_h)\gamma_h\gamma_c\Gamma_{12}}{F(\lambda, \gamma_h, \gamma_c, n_h, n_c)}, \tag{4.11}$$

where

$$\Gamma_{12} = \gamma_h(1 + n_h) + \gamma_c(1 + n_c) + i\delta \tag{4.12}$$

$$\begin{aligned} F(\lambda, \gamma_h, \gamma_c, n_h, n_c) =& \lambda^2[\gamma_c(1 + 3n_c) + \gamma_h(1 + 3n_h)][\gamma_h(1 + n_h) + \gamma_c(1 + n_c)] \\ &+ |\Gamma_{12}|^2\gamma_c\gamma_h(n_c(3n_h + 2) + 1 + 2n_h) \end{aligned} \tag{4.13}$$

and $\delta = \Omega - \omega_2 - \omega_1$. Other coherences vanish in the steady state. For completeness, we also write down the solution for the steady-state populations,

$$\rho_{11} = \frac{\lambda^2(\gamma_h(1 + n_h) + \gamma_c(1 + n_c))(\gamma_h n_h + \gamma_c n_c) + |\Gamma_{12}|^2\gamma_c\gamma_h n_c(1 + n_h)}{F(\lambda, \gamma_h, \gamma_c, n_h, n_c)} \tag{4.14}$$

$$\rho_{22} = \frac{\lambda^2(\gamma_h(1 + n_h) + \gamma_c(1 + n_c))(\gamma_h n_h + \gamma_c n_c) + |\Gamma_{12}|^2\gamma_c\gamma_h n_h(1 + n_c)}{F(\lambda, \gamma_h, \gamma_c, n_h, n_c)} \tag{4.15}$$

and $\rho_{00} = 1 - \rho_{11} - \rho_{22}$. We focus on the case where $\lambda \ll \max(\gamma_h, \gamma_c)$ so that the populations only slightly deviate from their equilibrium values (4.5). In terms of the limit cycle, this means that the radius of the limit cycle stays approximately constant.

As soon as there is a non-vanishing steady-state coherence, the phase distribution localizes. Note that the localization occurs in the rotating frame. In the original frame, the localized phase distribution rotates with frequency Ω. The phase distribution function $\mathcal{Q}(\phi_1, \phi_2)$ can be obtained by adopting the Husimi-Q distribution with respect to the SU(3) coherent states and integrating out the polar angles

$$\mathcal{Q}(\phi_1, \phi_2) = \frac{1}{8\pi}\mathrm{Re}(\rho_{12}e^{i(\phi_2 - \phi_1)}), \tag{4.16}$$

where we have ignored the constant $1/(2\pi)^2$ term. Synchronization measure can then be calculated from the strength of localization in $\mathcal{Q}(\phi_1, \phi_2)$

$$S_{\max} \equiv \max_{\phi_1, \phi_2} \mathcal{Q}(\phi_1, \phi_2) = \frac{1}{8\pi}|\rho_{12}|, \tag{4.17}$$

with an optimum phase configuration $\phi_2 - \phi_1 = \arg(\rho_{12})$. Notably, for $\delta = 0$, we have $\phi_2 - \phi_1 = \pm\pi/2$. Remarkably, the synchronization measure $S_{\max}$ follows the Arnold tongue behavior (see Sec. 2.2) with respect to the forcing strength λ and detuning δ as shown in Fig. 4.1(b). The Arnold tongue has been recognized as one of the characteristics of synchronization for limit cycle oscillators in classical systems. Figure 4.1(b) serves as an example that Arnold tongue behavior can also be observed in quantum synchronization.

4.2 Injection Locking: Classical and Quantum

In the discussion of entrainment thus far, we only consider the entrainment of a single self-sustained oscillator. What would happen if we have multiple self-sustained oscillators with possibly differing natural frequencies influenced by a common drive? Entrainment of multiple self-sustained oscillators to a common drive, otherwise known as injection locking [1], has been used to standardize radio-controlled watch, amplifying laser [71, 118], and reducing phase noise in LC circuits [119].

Injection locking can be modelled by a series of Adler equations (see Eqn. (2.6)). Here, we consider the Adler equation with cosine forcing and in the presence of noise,

$$\dot{\phi}_i = \omega_i + F\cos(\Omega t - \phi_i) + \sqrt{2}D\xi_i(t) \tag{4.18}$$

where the subscript $i = 1, 2, ..., N$ label different oscillators having distinct but close natural frequencies ω_i. The choice of cosine forcing is motivated by Eq. (4.8).

Let us consider the long-time behavior of Eq. (4.18) for various limiting values of diffusion coefficients D and forcing strength F. First, consider the deterministic limit $D \to 0$. Without forcing ($F = 0$), the phase difference between the oscillators will drift over time $\phi_i - \phi_j = (\omega_i - \omega_j)t$, giving a largely incoherent motion. However, by applying a force $F > 0$ one finds that in the long-time limit, the phases can be locked to $\arccos(|\delta_i|/F)$ provided that $|\delta_i|/F < 1$ where $\delta_i = \omega_i - \Omega$. In contrast, oscillators whose $|\delta_i|/F > 1$ will continue to drift away from the drive.

In the presence of noise $D > 0$, the dynamics become stochastic and so we can only talk about phase distribution $P(\phi_1, ..., \phi_N) = \prod_{i=1}^{N} P(\phi_i)$ rather than

the phases themselves. For $F = 0$, the distribution will drift while simultaneously diffusing such that in the long-time limit, it approaches a uniform distribution (see Sec 2.5). On the other hand, if $F > 0$ the phase distribution in the long-time limit would localize to a finite region in the reference frame rotating with Ω provided that $|\delta_i|/F < 1\ \forall i$. The stronger the forcing F, the more localized its phase distribution (see Fig. 2.5).

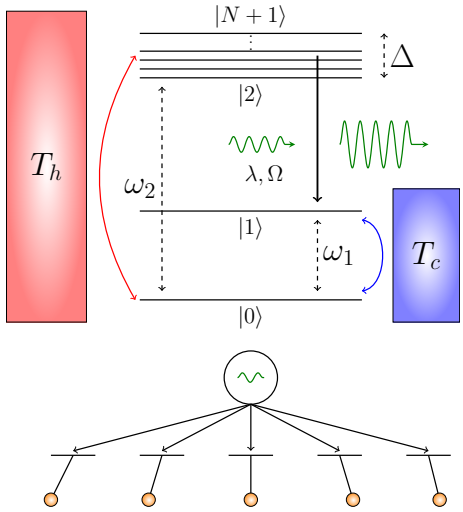

Figure 4.2: (Top) Schematic diagram of quantum model for injection locking, with auxiliary ground state $|0\rangle$ and two thermal baths to control population inversion between $|1\rangle$ and the near-degenerate subspace $|m\rangle$ for $m = 2, 3, .., N+1$. (Bottom) Schematic diagram of classical injection locking, where multiple phase oscillators are entrained to a common drive. In the quantum model, the drive couples to the collective modes of the system, causing the phases of the oscillators to be correlated.

Our aim here is to study the quantum model for injection locking and connect it to the synchronization of maser heat engine. To this end, we consider a driven-dissipative system satisfying a QME,

$$\dot{\rho} = -i[H_0 + V(t), \rho] + \mathcal{D}[\rho] \tag{4.19}$$

where in the absence of driving $V(t) = 0$, the steady-state of the QME is diagonal in the basis of H_0, which is the preferred basis used here.

The system we are considering consists of a state $|1\rangle$ with energy ω_1 and a set of near-degenerate states $|m\rangle$ for $m = 2, 3, ..., N+1$ having energy between ω_2 and $\omega_2 + \Delta$ with $\omega_2 > \omega_1$ and $\Delta \ll \omega_2 - \omega_1$. This system represents N "quantum clocks" [120, 121] with close frequencies distributed between $\omega_2 - \omega_1$ and $\omega_2 - \omega_1 + \Delta$. For simplicity, we assume the states belonging to the near-degenerate subspace are equispace in energy. The bare Hamiltonian is then,

$$H_0 = \omega_1 |1\rangle \langle 1| + \sum_{m=0}^{N-1} \left(\omega_2 + \frac{m\Delta}{N-1}\right) |m+2\rangle \langle m+2| \tag{4.20}$$

Furthermore, all the transitions $|1\rangle \leftrightarrow |j\rangle$ for $j = 2, 3, ..., N+1$ are simultaneously driven by $V(t)$

$$V(t) = \lambda \sum_{j=1}^{N} e^{-i\Omega t} |1\rangle \langle j| + \text{h.c.} = \lambda\sqrt{N} e^{-i\Omega t} |1\rangle \langle W| + \text{h.c.} \tag{4.21}$$

with $|W\rangle = \frac{1}{\sqrt{N}} \sum_{j=2}^{N+1} |j\rangle$ is the symmetric superposition of the near-degenerate subspace. By writing $V(t)$ in this way, we have assumed $\Omega \gg \Delta$ since the drive does not resolve the phases of the states within the near-degenerate suspace. Note that unlike in the classical model, the drive couples to the collective mode of the system, which in turns enhance the driving strength by a factor of $\sqrt{N}$. The near-degenerate subspace is spanned by symmetric and non-symmetric states $\{|W\rangle, |A_1\rangle, ..., |A_{N-1}\rangle\}$ where $|A_i\rangle$ represents the other superposition states orthogonal to $|W\rangle$, which can be explicitly found from Gram-Schmidt procedure. The states $|A_i\rangle$ are not directly coupled to the drive, but they are still indirectly coupled to the drive by influencing the population of $|W\rangle$ since these states are not eigenstates of H_0 for $\Delta \neq 0$. For example, in the simplest case of $N = 2$, bare Hamiltonian is given by,

$$H_0 = \omega_1 |1\rangle \langle 1| + \left(\omega_2 + \frac{\Delta}{2}\right)(|W\rangle \langle W| + |A\rangle \langle A|) + \frac{\Delta}{2}(|W\rangle \langle A| + |A\rangle \langle W|) \tag{4.22}$$

where $|W\rangle = (|2\rangle + |3\rangle)/\sqrt{2}$ and $|A\rangle = (|2\rangle - |3\rangle)/\sqrt{2}$.

The system-drive collective coupling in Eq. (4.21) marks the main difference between the classical and the quantum model. In the classical model of Eq. (2.48), the individual phases of the oscillators are decoupled. By contrast, in the quantum model their phases are automatically correlated in the presence of driving. In other words, the drive not only attracts the phases of each oscillator, but it also induces mutual coupling between them. The interplay between

entrainment and mutual coupling for synchronization has been studied in several classical models as elaborated in Sec. 2.4. However, to the best of our knowledge, such interplay has not been studied in the context of quantum synchronization.

We focus here on two cases: when the dissipator $\mathcal{D}[\rho]$ can sustain population inversion ($\rho_{mm} > \rho_{11}$ for $m = 2, 3, ..., N+1$), and when it can not. As a specific example, we consider again maser heat engine setup. We add an auxiliary ground-state $|0\rangle$ by which the system continuously couples to hot and cold baths such that $\mathcal{D}[\rho] = \mathcal{D}_c[\rho] + \mathcal{D}_h[\rho]$. The cold bath induces incoherent transition $|0\rangle \leftrightarrow |1\rangle$ while the hot-bath simultaneously induces coherent transition between multiple levels $|0\rangle \leftrightarrow |m\rangle$ for $m = 2, 3, ..., N+1$ (see Fig. 4.2). Note that for $N = 1$, this model is reduced to the three-level maser heat engine studied in the previous section. Knowing the entrainment result for the three-level case, one might naively expects all the phases $\varphi_{m1} \equiv \phi_m - \phi_1$ to localize near $\pm\pi/2$. Indeed, this is true if only entrainment is present. But, in the presence of mutual coupling, it is no longer guaranteed.

The mutual coupling effect manifests as a preference on the near-degenerate collective modes. For example, in the engine regime, the population of asymmetric modes $\{|A_i\rangle\}$ will be preferred in the steady-states due to continuous net stimulated emission from $|W\rangle \to |1\rangle$. The asymmetric modes in general will prefer each individual mode to be out-of-phase from each other. This results in the phase preferences due to entrainment and due to mutual coupling to be incompatible. On the one hand, entrainment attracts the phases of all the near-degenerate states to be in-phase while mutual coupling prefer them to be out of phase. This incompatibility leads to a competition between the two mechanisms in the engine regime. By contrast, $|W\rangle$ prefers each individual mode to be in-phase. Therefore, we expect a cooperation between entrainment and mutual coupling in the refrigerator regime, since the symmetric mode $|W\rangle$ will be preferred owing to net absorption in the steady-state.

Let us concretize our discussion by writing down the form of $\mathcal{D}[\rho]$. The cold-bath dissipator $\mathcal{D}_c[\rho]$ has the same form as Eq. (4.4) while the formula for $D_h[\rho]$ is no longer guaranteed to have a Lindblad form due to the presence of near-degeneracy. Recall from Sec. 3.1 that one of the assumptions to derive a Lindblad equation is the *secular* approximation which breaks down in the presence of near-degeneracy. We then resort to the Bloch-Redfield (B-R) QME [91, 93, 122–125], a non-secular QME which still assumes the validity of Born-Markov approximation. Using the B-R master equation, the hot-bath contribution to the dissipator can

be written as,

$$\mathcal{D}_h[\rho] = \sum_{\mu=1}^{2} \sum_{i,j=2}^{N+1} (\Gamma_\mu^{ij} + \Gamma_\mu^{ji}) h_\mu^i \rho h_\mu^{j\dagger} - \Gamma_\mu^{ij} \rho h_\mu^{j\dagger} h_\mu^i - \Gamma_\mu^{ji} h_\mu^{j\dagger} h_\mu^i \rho \tag{4.23}$$

with pairwise rates $\Gamma_1^{ij} = p_{ij}\sqrt{\gamma_h^i \gamma_h^j}(1 + n_h^j)$, $\Gamma_2^{ij} = p_{ij}\sqrt{\gamma_h^i \gamma_h^j} n_h^j$ and jump operators $h_1^j = h_2^{j\dagger} = |0\rangle\langle j|$. Here, γ_h^j and n_h^j are the system-hot bath coupling strength and the hot bath's mean occupation number associated with the transition $|0\rangle \leftrightarrow |j\rangle$. The coefficients p_{ij} are the *dipole-alignment factor* $p_{ij} = \mathbf{d_i}.\mathbf{d_j}/|\mathbf{d_i}||\mathbf{d_j}|$ with $\mathbf{d}_i = \langle i|\mathbf{d}|i\rangle$ and $\mathbf{d}$ is the dipole-transition operator [126–129]. They can also be understood as the strength of correlation between jump operators associated with the transition $|0\rangle \leftrightarrow |i\rangle$ and $|0\rangle \leftrightarrow |j\rangle$ due to quantum interference effect [126]. Equation (4.23) is reduced to a Lindblad form in two cases: if all the dipole moments are perpendicular $p_{ij} = 0\ \forall i, j$ or if the system is exactly degenerate $n_h^i = n_h^j\ \forall i, j$.

Recall from Sec. 3.3, we need to have a diagonal steady-state for the purely dissipative dynamics (without driving) to study synchronization. This diagonal steady-state will serve as a (noisy) limit cycle whose phases are free to synchronize. We will show that, in the absence of driving $\lambda = 0$, the dissipator $\mathcal{D}[\rho] = \mathcal{D}_h[\rho] + \mathcal{D}_c[\rho]$ still takes the system to a diagonal steady-state [126, 129] despite $\mathcal{D}_h[\rho]$ coupling the dynamics of coherence and population. This is because the the EOM of coherence specifically couples to the rate of change of population, which vanishes in the steady-state limit. To see this, let us divide the density operator elements into three groups: population ρ_{ll} for $l = 0, 1, .., N+1$, non-degenerate coherence ρ_{1j}, and degenerate coherence ρ_{jk} for $j, k = 2, 3, .., N+1$ and $j \neq k$.

Below, we will write down the EOM for each group. But before that, we employ the same trick as Eq. (4.9). We define a rotating Hamiltonian

$$H_r = \frac{\Omega}{2} \sum_{j=2}^{N+1} |j\rangle\langle j| - \frac{\Omega}{2} |1\rangle\langle 1| \tag{4.24}$$

by which we transform the Hamiltonian into a time-independent form while leaving the dissipator invariant. The EOM of each density operator element written below is expressed in this rotating frame. We begin with the population EOM

$$\dot{\rho}_{00} = 2\gamma_c(1+n_c)\rho_{11} - (2\gamma_c n_c + 2\gamma_h \sum_{j=2}^{N+1} n_h^j)\rho_{00} + \gamma_h \sum_{k,l=2}^{N+1} p_{kl}(2 + n_h^k + n_h^l)\rho_{kl} \tag{4.25}$$

$$\dot{\rho}_{11} = i\lambda \sum_{k=2}^{N+1} (\rho_{1k} - \rho_{k1}) - 2\gamma_c(1+n_c)\rho_{11} + 2\gamma_c n_c \rho_{00} \tag{4.26}$$

$$\dot{\rho}_{jj} = -i\lambda(\rho_{1j} - \rho_{j1}) - \gamma_h \sum_{k=2}^{N+1} p_{jk}(1+n_h^k)(\rho_{jk} + \rho_{kj}) + 2\gamma_h n_h^j \rho_{00}. \tag{4.27}$$

Now, the EOM for non-degenerate coherences

$$\dot{\rho}_{01} = i\Big(\omega_1 + \frac{\Omega}{2}\Big)\rho_{01} - \gamma_c(1+2n_c)\rho_{01} \tag{4.28}$$

$$\dot{\rho}_{0j} = i\Big(\omega_2 - \frac{\Omega}{2} + \frac{j-2}{N-1}\Delta\Big)\rho_{0j} - \gamma_h \sum_{k=2}^{N+1} p_{jk}(1+n_h^k)\rho_{0k} \tag{4.29}$$

$$\begin{aligned}\dot{\rho}_{1j} =& \Big[i\Big(\omega_2 - \omega_1 - \Omega + \frac{j-2}{N-1}\Delta\Big) - \gamma_c(1+n_c)\Big]\rho_{1j} - \gamma_h \sum_{k=2}^{N+1}(1+n_h^k)p_{jk}\rho_{1k} \\ &+ i\lambda\Big(\rho_{11} - \sum_{k=2}^{N+1}\rho_{kj}\Big).\end{aligned} \tag{4.30}$$

Lastly, the EOM for degenerate coherence $j \neq k$ and $j,k \geq 2$

$$\dot{\rho}_{jk} = i\frac{(j-k)\Delta}{N-1}\rho_{jk} - i\lambda(\rho_{1k} - \rho_{j1}) + \gamma_h(n_h^j + n_h^k)p_{jk}\rho_{00} - \gamma_h \sum_{l=2}^{N+1}(1+n_h^l)(p_{kl}\rho_{jl} + p_{jl}\rho_{lk}). \tag{4.31}$$

Thus, even when $\lambda = 0$, there is a coupling between coherence ρ_{jk} and the population (consider $l = j$ or $l = k$). But, we will show that this coupling vanishes in the steady-states since ρ_{jk} only depends on the rate of population change $\dot{\rho}_{jj}$ and $\dot{\rho}_{kk}$. To start, we rewrite equation (4.31) as

$$\begin{aligned}\dot{\rho}_{jk} =& i\frac{(j-k)\Delta}{N-1}\rho_{jk} - \gamma_h(2 + n_h^j + n_h^k)\rho_{jk} - i\lambda(\rho_{1k} - \rho_{j1}) - \gamma_h \sum_{\substack{l=2 \\ l\neq j,k}}^{N+1}(1+n_h^l)(p_{kl}\rho_{jl} + p_{jl}\rho_{lk}) \\ &+ \gamma_h p_{jk}[\rho_{00}(n_h^j + n_h^k) - (1+n_h^k)\rho_{kk} - (1+n_h^j)\rho_{jj}].\end{aligned} \tag{4.32}$$

Only the terms on the second line are population-dependent. From Eq. (4.27) one may write (assuming $\lambda = 0$)

$$2\gamma_h[(n_h^j + n_h^k)\rho_{00} - (1+n_h^j)\rho_{jj} - (1+n_h^k)\rho_{kk}] = \dot{\rho}_{jj} + \dot{\rho}_{kk} + \gamma_h \sum_{k=2}^{N+1}(1+n_h^k)(p_{jk}\rho_{jk} + p_{ik}\rho_{ik}). \tag{4.33}$$

Notice that the left-hand side of Eq. (4.33) can be substituted to the right-hand side of Eq. (4.32). Therefore, the dynamics of degenerate coherence $\dot{\rho}_{jk}$ only depends on the rate of population change $\dot{\rho}_{jj}$ and $\dot{\rho}_{kk}$. In other words, as the system reaches its steady-state population, the coherence and population gets decoupled and the coherence continues to decay to zero in the steady-state.

The diagonal steady-state in the undriven dynamics provides a stable limit cycle whose phases are free to synchronize. In the next section, we will study analytical and numerical solutions for the steady-state of EOM (4.25)-(4.31) for $\lambda \neq 0$. We will then analyze the synchronization measure induced by driving and compare it to the classical injection locking.

4.3 Entrainment Stability and Thermodynamics

We first consider the simplest non-trivial case of $N = 2$ where we have a four-level system $\{|0\rangle, |1\rangle, |2\rangle, |3\rangle\}$ with $|2\rangle$ and $|3\rangle$ are near-degenerate. We numerically solve the steady-state and draw the phase distribution $\mathcal{Q}(\varphi_{31}, \varphi_{32})$ with varying dipole-alignment factor $p = \mathbf{d_2}.\mathbf{d_3}/|\mathbf{d_2}||\mathbf{d_3}|$. We find that depending on p and whether the system is operating as an engine ($n_h^j > n_c \ \forall j$) or refrigerator ($n_h^j < n_c \ \forall j$), the phase distribution can have distinct qualitative behavior as shown in Fig. 4.3.

Particularly, in the engine case, we observe a bifurcation from a single global maximum to two global maxima in the phase distribution. For $p = 0.5$ [Fig. 4.3(a)], both phases φ_{21} and φ_{31} are localized around $\pi/2$, which implies the state $|2\rangle$ and $|3\rangle$ are generally in-phase and entrained to the drives oscillation. However, the maximum point splits into two when $p = -0.5$ [Fig. 4.3(b)]. As $p \to -1$, the phase distribution forms a stripe [Fig. 4.3(c)], indicating that entrainment with respect to the drive is lost, but relative out-of-phase synchronization persists $\varphi_{23} \approx \pm\pi$.

We can explain this behavior by calculating the steady state analytically in the limit $\Delta \to 0$. In this limit, we have $n_h^j = n_h \ \forall j$ which leads to symmetric pairwise rates $\Gamma_\mu^{ij} = \Gamma_\mu^{ji}$. For simplicity, we also assume $\gamma_h^j = \gamma_h \ \forall j$. In this limit, the hot-bath dissipator becomes a Lindblad form with a non-diagonal Kossakowski matrix [89],

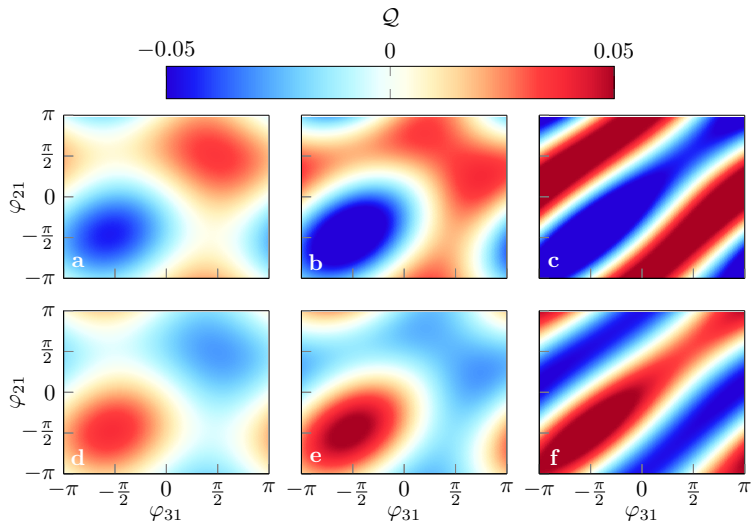

Figure 4.3: Phase quasiprobability distribution function $\mathcal{Q}(\varphi_{21}, \varphi_{31})$ in the engine (a-c) and refrigerator (d-f) regime. The values for p are 0.5 (a,d), -0.5 (b,e) and -0.95(c,f). The parameters used are $\omega_1 = 1$, $\omega_2 = 3$, $\Delta = 0.05$, $\Omega = \omega_2 - \omega_1 + \Delta/2$, $\gamma_c = \gamma_h = 0.1$, $\lambda = 0.05$, $n_h = 0.287$, $n_c = 0.0068$ (a-c) and $n_c = 1.055$ (d-f).

$$\mathcal{D}_h[\rho] = \sum_{\mu=1}^{2} \sum_{i,j=2}^{3} \Gamma_\mu p_{ij} (2h_\mu^i \rho h_\mu^{j\dagger} - \rho h_\mu^{j\dagger} h_\mu^i - h_\mu^{j\dagger} h_\mu^i \rho) \tag{4.34}$$

where $\Gamma_1 = \gamma_h(1 + n_h)$ and $\Gamma_2 = \gamma_h n_h$. Clearly, the Kossakowski matrix is proportional to the matrix form of the dipole-alignment factors p_{ij} which we refer to as *correlation matrix* [130]. For $\mathcal{D}[\rho]$ to be a completely positive map, the Kossakowski matrix has to be positive definite. That implies the correlation matrix also has to be positive definite. For $N = 2$ the correlation matrix is only a 2×2 matrix

$$P_{2\times 2} = \begin{bmatrix} 1 & p \\ p & 1 \end{bmatrix}. \tag{4.35}$$

The eigenvalues of this matrix can be easily calculated as $1 \pm p$ with eigenvectors $(1, \pm 1)^T$. This matrix is positive definite for $-1 < p < 1$. On the boundaries $p = \pm 1$, one of the eigenvalues is zero, which implies the existence of a *dark state*. A dark state is not affected by dissipation $\mathcal{D}_h[\rho_{\text{dark}}] = 0$ and so it evolves unitarily under the QME. The existence of a dark state means that the steady

state will depend on the overlap between the initial condition and the dark state. We avoid the parameter values where dark state is present because a stable limit cycle requires a unique diagonal steady-state.

Beside the existence of dark state, the correlation matrix is also useful to calculate the collective mode participating in the dissipation. For example, from the correlation matrix given by Eq. (4.35), we can deduce that the hot bath induces incoherent transition $|0\rangle \leftrightarrow |\pm\rangle$ with effective system-bath coupling strength $\gamma_h(1 \pm p)$ where $|\pm\rangle = (|2\rangle \pm |3\rangle)/\sqrt{2}$.

With all of these in mind, we can analytically solve for the steady state. Especially to study synchronization, it is important to obtain the expressions for steady-state coherences

$$\rho_{12} = \rho_{13} = i\frac{\lambda\gamma_c\gamma_h(1+p)(n_c - n_h)(1+n_h)}{F(n_h, n_c, \gamma_c, \gamma_h, \lambda, p)} \tag{4.36}$$

$$\rho_{23} = \frac{\lambda^2\gamma_c(n_c - n_h)}{F(n_h, n_c, \gamma_h, \gamma_c, \lambda, p)} \tag{4.37}$$

with

$$\begin{aligned} F = {} & 2\lambda^2\Big[\gamma_c(1 + 3n_c + 2n_h + 4n_h n_c) + \gamma_h(1+p)(1+n_h)(1+4n_h)\Big] \\ & + \gamma_c\gamma_h(1+p)(1+n_h)(1+3n_h+2n_c+4n_h n_c)(\gamma_c(1+n_c) + \gamma_h(1+p)(1+n_h)). \end{aligned} \tag{4.38}$$

For the sake of completeness, we also write down the steady-state populations,

$$\rho_{11} = \frac{E(n_h, n_c, \gamma_h, \gamma_c, \lambda, p)}{F(n_h, n_c, \gamma_h, \gamma_c, \lambda, p)} \tag{4.39}$$

$$\rho_{22} = \rho_{33} = \frac{G(n_h, n_c, \gamma_h, \gamma_c, \lambda, p)}{F(n_h, n_c, \gamma_h, \gamma_c, \lambda, p)} \tag{4.40}$$

$$\rho_{00} = 1 - \rho_{11} - \rho_{22} - \rho_{33} \tag{4.41}$$

where,

$$E = (1+n_h)\Big\{2\lambda^2\big[n_c\gamma_c + \gamma_h(1+p)n_h\big] + \gamma_c\gamma_h(1+p)(1+n_h)n_c\big[\gamma_c(1+n_c) + \gamma_h(1+p)(1+n_h)\big]\Big\} \tag{4.42}$$

and

$$\begin{aligned} G = {} & \lambda^2\big[\gamma_c(n_h + 2n_h n_c + n_c) + 2\gamma_h n_h(1+n_h)(1+p)\big] \\ & + \gamma_c\gamma_h(1+p)n_h(1+n_h)(1+n_c)\big[\gamma_c(1+n_c) + \gamma_h(1+p)(1+n_h)\big] \end{aligned} \tag{4.43}$$

Let us calculate $S_{\max}$ when the system operates as an engine. We have $n_h > n_c$ so $\rho_{1j} = |\rho_{1j}|e^{-i\pi/2}$ and $\rho_{23} = |\rho_{23}|e^{i\pi}$. The phase distribution function $\mathcal{Q}(\phi_1, \phi_2, \phi_3)$ can then be written as

$$\mathcal{Q}(\phi_1, \phi_2, \phi_3) = |\rho_{12}| \sin(\phi_2 - \phi_1) + |\rho_{13}| \sin(\phi_3 - \phi_1) - |\rho_{23}| \cos(\phi_3 - \phi_2) \quad (4.44)$$

Next, we define *dissipation-to-driving* ratio

$$k \equiv \frac{\gamma_h(1+p)(1+n_h)}{\lambda} = \frac{|\rho_{12}|}{|\rho_{23}|} = \frac{|\rho_{13}|}{|\rho_{23}|} \quad (4.45)$$

which is the ratio between dissipative loss rate $|+\rangle \to |0\rangle$ and the driving strength. Crucially, this ratio is also the ratio between non-degenerate coherence to degenerate coherence. As we will see, this ratio is the key parameter governing entrainment stability. The phase distribution function can be rewritten in terms of k as

$$\mathcal{Q}(\varphi_{21}, \varphi_{31}) = |\rho_{23}|(k \sin \varphi_{21} + k \sin \varphi_{31} - \cos(\varphi_{31} - \varphi_{21})). \quad (4.46)$$

In this way, calculating $S_{\max} = \max_{\varphi_{21}, \varphi_{31}} \mathcal{Q}(\varphi_{21}, \varphi_{31})$ can be recast into finding the global maximum of a function $f(x, y)$ where

$$f(x, y) \equiv k \sin x + k \sin y - \cos(y - x). \quad (4.47)$$

One can easily show that for $k > 2$, this function has four critical points $(\pm\pi/2, \pm\pi/2)$. For $k < 2$, the number of critical points becomes six with the addition of $(\chi, \pi - \chi)$ and $(\pi - \chi, \chi)$ where $\chi = \arcsin(k/2)$. By comparing the values of $f(x, y)$ at each of these points, one obtains a bifurcating global maximum behavior

$$\max_{x,y} f(x, y) = \begin{cases} 2k - 1 & \text{if } k > 2 \text{ with } (x, y) = (\pi/2, \pi/2) \\ 1 + k^2/2 & \text{if } 0 < k \leq 2 \text{ with } (x, y) = \{(\chi, \pi - \chi), (\pi - \chi, \chi)\}. \end{cases} \quad (4.48)$$

As we recall that $k = |\rho_{12}|/|\rho_{23}| = |\rho_{13}|/|\rho_{23}|$, we finally obtain an expression for the synchronization measure $S_{\max}$

$$S_{\max}(n_h > n_c) = \begin{cases} |\rho_{12}| + |\rho_{13}| - |\rho_{23}| & \text{if } k > 2 \\ (1 + \frac{k^2}{2})|\rho_{23}| & \text{if } 0 < k \leq 2 \end{cases} \quad (4.49)$$

The above analytical expression obtained for $\Delta = 0$ is compared to numerical data for $\Delta = 0.05$ in Fig. 4.4(a), where a quantitative deviation is observed for

$0 < k < 2$, but without a significant qualitative difference except for a slight discontinuity at $k = 2$.

Equation (4.49) provides valuable insight into the underlying mechanism for entrainment instability in Fig. 4.3. For example, we see that the bifurcation from a unique global maximum to a pair of global maxima is determined by the dissipation-to-driving ratio k. We also find that entrainment instability arises as a consequence of the competition between non-degenerate coherences $|\rho_{1j}|$ for $j = 2, 3$ and degenerate coherence $|\rho_{23}|$. The competition between coherences can be seen clearly in the expression of $S_{\max}$ for $k > 2$. It can also be interpreted as competition between entrainment and coupling as follows.

Recall from Eq. (4.21) the drive only directly couples to the symmetric mode $|+\rangle$. As the system undergoes continuous stimulated emission $|+\rangle \to |1\rangle$ in the steady-state, the steady-state maintains coherence $\rho_{1+} = (\rho_{12} + \rho_{13})/\sqrt{2}$. Both coherences ρ_{12} and ρ_{13} collectively oscillate with frequency Ω in the original frame ($\rho_{1+} \to \rho_{1+}e^{i\Omega t}$). This implies that the non-degenerate coherences are exactly the coherences associated with entrainment. Since we know that entrainment tends to make both phases φ_{21} and φ_{31} to localize near $\pm\pi/2$, it attracts the near-degenerate states $|2\rangle$ and $|3\rangle$ to be in-phase $\varphi_{23} \to 0$.

But this is not the end of the story. Coherence is also generated from the asymmetry between $|+\rangle$ and $|-\rangle$. When $\lambda = 0$, the coherent population are balanced $\rho_{++} = \rho_{--} = (\rho_{22} + \rho_{33})/2$. This balance is disturbed by $\lambda \neq 0$ since a fraction ρ_{++} will be depopulated to ρ_{11} through net stimulated emission. The imbalance induces coherence ρ_{23} that is invariant to the drive's rotating coordinate transformation. We then associate ρ_{23} with a coherence generated by mutual coupling. In the engine case, ρ_{--} is more preferred in the steady-state $\rho_{++} - \rho_{--} = \mathrm{Re}(\rho_{23}) < 0$. This implies the asymmetry between symmetric and non-symmetric modes lead to a tendency for $\varphi_{23} \to \pm\pi$.

Clearly, the two synchronization mechanisms - entrainment and mutual coupling - prefer incompatible phase configurations, leading to competition between them. Depending on k, one of the mechanisms is dominant. For $k > 2$, $|\rho_{12}|$ and $|\rho_{13}|$ are dominant over $|\rho_{23}|$. We call this regime as *entrainment-dominated regime*. In this regime, the rate $\gamma_h(1+p)n_h$ at which $|+\rangle$ is pumped by the bath is enough to suppress the asymmetry between $|+\rangle$ and $|-\rangle$. Although the coherence is dominated by ρ_{1+}, a net stimulated emission still favors ρ_{--} over ρ_{++}, leading to effective synchronization blockade by $|\rho_{23}|$ [30, 47]. Meanwhile, for $k < 2$, $|\rho_{23}|$

dominates over $|\rho_{12}|$ and $|\rho_{13}|$. We call this regime as *coupling-dominant regime*. In this regime, the hot bath excitation $|0\rangle \to |+\rangle$ rate is too slow compared to λ.

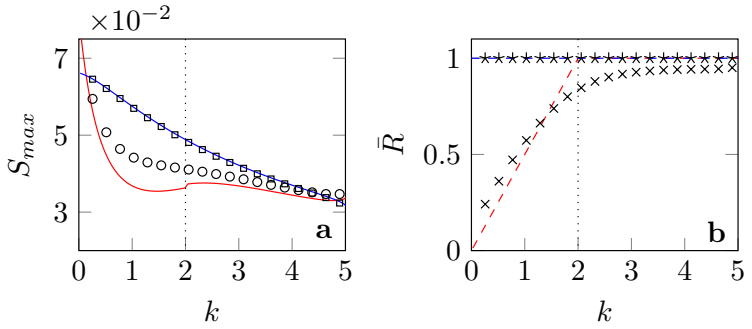

Figure 4.4: Synchronization parameters $S_{\max}$ and $\bar{R}$ as a function of dissipation-to-driving ratio $k = \gamma_h(1+n_h)(1+p)/2$ for $N = 2$ (a) $S_{\max}$ in the engine ($\circ$, solid red line) and refrigerator ($\square$, solid blue line) regime. The markers represent numerical data and solid lines represent the analytical prediction of (4.49) & (4.54) (b) $\bar{R}$ in the engine ($\times$, dashed red line) and refrigerator ($\star$, dashed blue line) regime. The markers are again numerical data and the dashed lines are analytical predictions of (4.50) & (4.55). The parameters used are $\omega_1 = 1, \omega_2 = 3$, $\Delta = 0.05$, $\Omega = \omega_2 - \omega_1 + \Delta/2$, $\gamma_c = \gamma_h = 0.1$, $\lambda = 0.05$, $n_h = 0.287$, $n_c = 0.0068$ in the engine regime and $n_c = 1.055$ in the refrigerator regime.

To distinguish between entrainment-dominant and coupling-dominant regimes, we define an order parameter $\bar{R}$

$$\bar{R} = \frac{1}{N}\Big|\sum_{j=1}^{N-1} e^{i\phi_j}\Big|_{\mathcal{Q}=S_{\max}} \tag{4.50}$$

which determines whether the optimum phases ϕ_j tend to cluster at the same point. Although the formula for $\bar{R}$ looks similar to the Kuramoto order parameter (Eq. (2.20)), one has to be careful interpreting $\bar{R}$ as a synchronization measure since it only uses the phases that maximize $\mathcal{Q}$ without considering the localization strength, i.e. $\bar{R}$ can be close to one even if $S_{\max}$ is close to zero. Nevertheless, we will see that $\bar{R}$ is a useful quantity to distinguish entrainment-dominant and mutual-coupling dominant regimes. From Eq. (4.48) one can easily calculate

$$\bar{R}(n_h > n_c) = \begin{cases} 1 & \text{if } k > 2 \\ \frac{k}{2} & \text{if } 0 < k \leq 2 \end{cases} \tag{4.51}$$

The order parameter is always maximum (unity) in the entrainment-dominant regime ($k > 2$) while it is linearly increasing with k in the coupling-dominant regime ($0 < k < 2$). The transition between the entrainment-dominant and the coupling-dominant regime is not as sharp when we consider finite gap $\Delta \neq 0$ as shown in Fig. 4.4(b). But one can still observe a qualitative change in the behavior of $\bar{R}$ around $k = 2$.

Up to this point, we have explicitly seen that entrainment in a near-degenerate four-level maser heat engine can be destabilized. The destabilization is observed from the splitting of the global maximum into a pair of global maxima in the phase distribution function. It can be understood as a consequence of competition between coherence induced by entrainment and coherence induced by mutual coupling. Finally, the transition between the entrainment-dominant and the coupling-dominant regime is determined by dissipation-to-driving ratio $k = \gamma_h(1+p)(1+n_h)/\lambda$.

Let us now discuss synchronization in the refrigerator regime ($n_c > n_h$). From Eqs. (4.36) - (4.37) we have $\rho_{1j} = |\rho_{1j}|e^{i\pi/2}$ for $j = 2, 3$ and $\rho_{23} = |\rho_{23}|$. Then, the phase distribution function is written as

$$\mathcal{Q}(\varphi_{21}, \varphi_{31}) = |\rho_{23}|(-k\sin\varphi_{21} - k\sin\varphi_{31} + \cos(\varphi_{31} - \varphi_{21})) = -|\rho_{23}|f(\varphi_{21}, \varphi_{31}). \tag{4.52}$$

Equation (4.52) is plotted for different values of dipole-alignment p in Fig. 4.3(d)-(f). Interestingly, the phase distribution in the engine and refrigerator regime has a mirror symmetry. A maxima in the engine phase distribution corresponds to a minima in the refrigerator phase distribution and vice versa. This is simply due to $\mathcal{Q}$ having the same functional form in both cases but with opposite signs. Thus, finding $S_{\max}$ in the refrigerator regime is equivalent to finding the global minimum of $f(x, y)$. Unlike the global maximum, the extremum phases associated with the global minimum of $f(x, y)$ are stable (independent of the system's parameter)

$$\min_{x,y} f(x, y) = -2k - 1 \qquad \text{with} \qquad (x, y) = (-\pi/2, -\pi/2) \tag{4.53}$$

Finally, we obtain $S_{\max}$ in the refrigerator regime

$$S_{\max}(n_c > n_h) = |\rho_{12}| + |\rho_{13}| + |\rho_{23}| = C_{l1} \tag{4.54}$$

where $C_{l_1} = \sum_{j<k} |\rho_{jk}|$ is the l_1-norm of coherence [131]. This analytical formula is reliable for a small non-zero Δ as shown in Fig. 4.4(a). Moreover, the

corresponding optimum phases are $(\varphi_{21},\varphi_{31})|_{\mathcal{Q}=S_{\max}}=(-\pi/2,-\pi/2)$, giving

$$\bar{R}(n_c>n_h)=\frac{1}{N}\Big|\sum_{j=1}^{N-1}e^{i\phi_j}\Big|_{\mathcal{Q}=S_{\max}}=1 \tag{4.55}$$

in agreement with numerical data in Fig. 4.4(b).

We see that the coherence $|\rho_{1j}|$ and $|\rho_{23}|$ no longer compete in the refrigerator regime. To the contrary, they are now in synergy to enhance synchronization measure $S_{\max}$. This synergy is due to the fact that the symmetric mode $|+\rangle$ continues to be generated by absorption $|1\rangle\rightarrow|+\rangle$ (and consecutively decays via the hot bath and generates heat flow to the hot bath). Contrary to the engine case where mutual coupling tend to destabilize entrainment, in the refrigerator regime mutual coupling helps enhancing and stabilizing entrainment.

So far, we have analyzed the synchronization properties of a four-level engine/refrigerator with a pair of near-degenerate states ($N=2$). How will the result generalize if we increase N? We first focus on the simplest case of $p_{ij}=0\ \forall i,j$. We write down the analytical solution for $\Delta=0$ and compare it with the numerical data for $\Delta\neq 0$. The analytical solution for the steady-state coherences in the limit $\Delta\rightarrow 0$ are given by,

$$\rho_{1j}=\frac{i\lambda(n_c-n_h)\gamma_c\gamma_h(1+n_h)}{F_N(N,\lambda,\gamma_c,\gamma_h,n_h,n_c)}\qquad\forall j\geq 2 \tag{4.56}$$

$$\rho_{j\ell}=\frac{\lambda^2\gamma_c(n_c-n_h)}{F_N(N,\lambda,\gamma_c,\gamma_h,n_h,n_c)}\qquad\forall j,\ell\geq 2\ \&\ j\neq\ell \tag{4.57}$$

with,

$$F_N=AN^2+BN+C \tag{4.58}$$

$$A=\lambda^2 n_h(\gamma_c(1+n_c)+\gamma_h(1+n_h)) \tag{4.59}$$

$$\begin{aligned}B=&\lambda\gamma_c(1+3n_c+2n_hn_c)+\lambda\gamma_h(1+n_h)(1+2n_h)\\&+n_h\gamma_h\gamma_c(1+n_h)(n_h+n_c)(\gamma_h(1+n_h)+\gamma_c(1+n_c))\end{aligned} \tag{4.60}$$

$$C=\gamma_h\gamma_c(1+n_h)^2(1+2n_c)(\gamma_h(1+n_h)+\gamma_c(1+n_c)) \tag{4.61}$$

One may notice that a similar structure arises for the calculation of $S_{\max}$. In particular, we have the same ratio between degenerate and non-degenerate

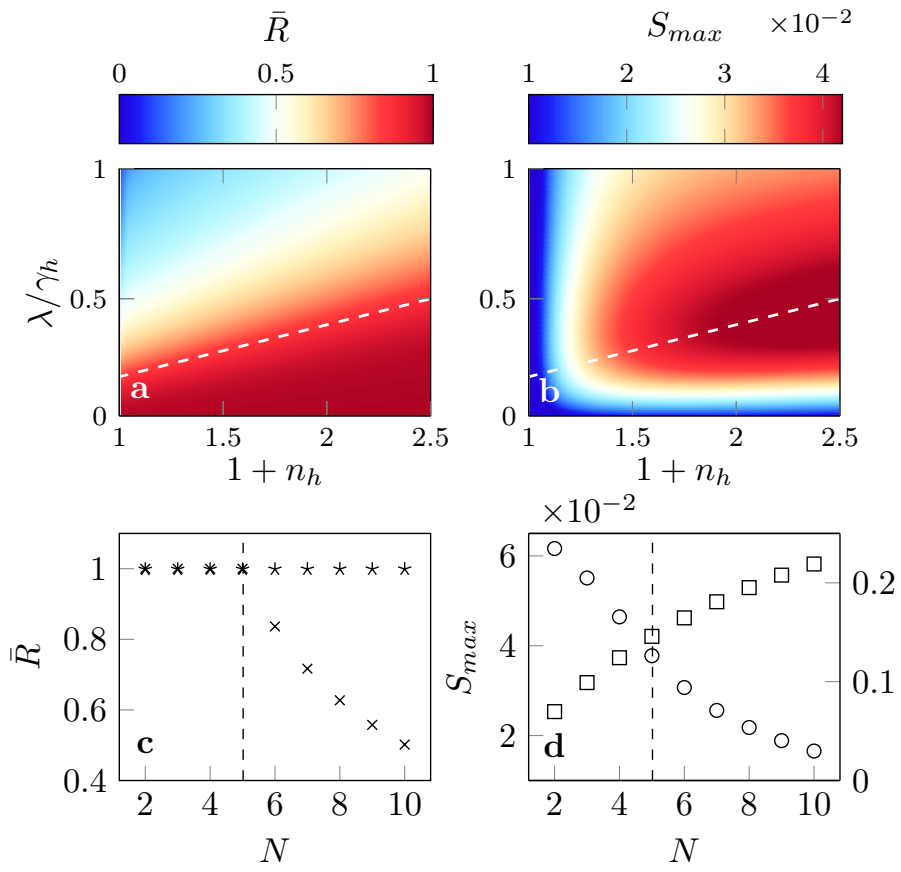

Figure 4.5: Phase diagram for $\bar{R}$ (a) and $S_{\max}$ (b) for $N = 5$ and $\Delta = 0.05$ in the engine regime. Scaling with N for (c) $\bar{R}$ in the engine regime ($\times$) and refrigerator regime ($\star$) (d) $S_{\max}$ in the engine regime ($\circ$, left axis) and refrigerator regime ($\square$, right axis). The parameter chosen for engines are $n_h = 4.0185,\ n_c = 0.0068,\ \Delta = 0,\ \lambda = 0.1$ and for refrigerators $n_h = 0.287,\ n_c = 1.055,\ \Delta = 0.05, \lambda = 0.05$. The dashed lines are the line $k = k_c = N$. The common parameters for (a)-(d) are $\omega_1 = 1$, $\omega_2 = 3$, $\Omega = \omega_2 - \omega_1 + \Delta/2$,$\gamma_h = \gamma_c = 0.1$ and $p_{ij} = 0\ \forall i, j$.

coherence $|\rho_{1j}|/|\rho_{jl}| = \gamma_h(1 + n_h)/\lambda = k$ for all j and l. In the engine regime ($n_h > n_c$), we again have $\rho_{1j} = |\rho_{1j}|e^{-i\pi/2}$ and $\rho_{jl} = |\rho_{jl}|e^{i\pi}$. Therefore, the

phase distribution function can be written as

$$\mathcal{Q}(\varphi_{21},...,\varphi_{N+1,1}) = |\rho_{jl}|\Big\{\sum_{\substack{i,j=2\\ i\neq j}}^{N+1} k\sin\varphi_{j1} - \cos(\varphi_{j1} - \cos\varphi_{i1})\Big\}. \tag{4.62}$$

Similarly, in the refrigerator regime

$$\mathcal{Q}(\varphi_{21},...,\varphi_{N+1,1}) = -|\rho_{jl}|\Big\{\sum_{\substack{i,j=2\\ i\neq j}}^{N+1} k\sin\varphi_{j1} - \cos(\varphi_{j1} - \cos\varphi_{i1})\Big\}. \tag{4.63}$$

Thus, calculating $S_{\max}$ is equivalent to finding the global maximum (minimum) of the following multi-variable function

$$g(x_1,..,x_N) = \sum_{\substack{i,j=1\\ j\neq i}}^{N-1} k\sin x_i - \cos(x_i - x_j), \tag{4.64}$$

with $k = \gamma_h(1+n_h)/\lambda$. Consider the first and second derivative of g with respect to x_i

$$\frac{\partial g}{\partial x_i} = k\cos x_i + \sum_{\substack{j=1\\ j\neq i}}^{N} \sin(x_i - x_j) \tag{4.65}$$

$$\frac{\partial^2 g}{\partial x_i^2} = -k\sin x_i + \sum_{\substack{j=1\\ j\neq i}}^{N} \cos(x_i - x_j). \tag{4.66}$$

Clearly, $x_i = \pi/2$ and $x_i = -\pi/2$ are critical points satisfying $\partial g/\partial x_i = 0\ \forall i$. In order for $x_i = \pi/2$ to be a (local) maximum point, we must have $\partial^2 g/\partial x_i^2 > 0\ \forall i$, which from Eq. (4.66) is the same as $k > N-1$. Note that this does not guarantee $x_i = \pi/2\ \forall i$ to be a *global* maximum. On the other hand $x_i = -\pi/2\ \forall i$ is always a (local) minimum since $\partial^2 g/\partial x_i^2 > 0$.

Second derivative test revealed that entrainment to the drive in the engine regime requires $k > N-1$. However, numerically, we find that the critical dissipation-to-driving ratio k_c for the transition between entrainment-dominant and coupling-dominant regime is given by $k_c = N$. The numerical evidence for this result is given in Fig. 4.5(a)-(c). For $N < k$, the order parameter $\bar{R}$ is always close to unity, indicating stable entrainment. However, when $N > k$ the mutual coupling take over and $\bar{R}$ linearly declines. By contrast, in the refrigerator regime

$\bar{R} = 1$ for any N. This indicates that the destabilization of entrainment in the engine regime and its stability in the refrigerator regime is also true for larger values of N.

Another numerical observation one can make is that in the engine case, stronger driving does not necessarily lead to stronger phase localization [see Fig. 4.5(b)]. This is in contrast to classical injection locking where entrainment is always enhanced with stronger driving [see Fig. 2.5]. The difference lies in the fact that in quantum injection locking, entrainment is not the only mechanism by which the system synchronizes. Instead, one has to take into account both entrainment and mutual coupling. As discussed before, in the engine regime, entrainment and mutual coupling compete. Since stronger driving can strengthen the influence of mutual coupling, it can reduce synchronization measures. Indeed, stronger driving still enhances phase localization in the entrainment-dominated regime. However, as the mutual coupling becomes more dominant, stronger driving would instead destabilize entrainment and reduce overall synchronization.

Furthermore, the scaling behavior of $S_{\max}$ in the engine regime is found to be the opposite of that in the refrigerator regime as shown in Fig. 4.5(d). In the engine case, $S_{\max}$ drops with N while it increases with N in the refrigerator regime. The drop of $S_{\max}$ in the engine regime is caused by two factors: stronger driving strength $\lambda\sqrt{N}$ and the increase in the number of accessible non-symmetric modes $\{|A_i\rangle\}$. In other words, as we increase N, the steady-state becomes closer to a mixture of $\{|A_i\rangle\}$ without favoring any specific phase configuration in the engine regime. Meanwhile, the rise of $S_{\max}$ with N in the refrigerator regime can be explained by cooperation between entrainment and mutual coupling which grows stronger as we add more near-degenerate states.

The analysis for a general N-level near-degenerate states can be extended to various scenarios not explicitly treated here. For example, one may ask what would be the influence of sampling p_{ij} from a certain distribution instead of setting all of them to zero as we did here? We also choose an equispace distribution for energy gap Δ between the near-degenerate states. Would the result change if we choose other distributions such as a Poisson distribution or Wigner distribution [132]? Is the analytical solution in the continuum limit $N \to \infty$ possible? We hope to be able to answer these questions in future work (see. Ch. 6).

To sum up, we have seen how the framework of quantum synchronization is applied to quantum injection locking in a near-degenerate quantum thermal

maser. We argue that in such models entrainment and mutual coupling co-exist. We also show that the interplay between entrainment and mutual coupling can be either competitive or cooperative. Interestingly, their interplay is tied to the thermodynamic function of the maser. They are competitive when the system operates as an engine and cooperative when the system operates as a refrigerator. In the next chapter, we will see how synchronization affects the thermodynamic performance of such near-degenerate quantum maser heat engines.

Chapter 5

Quantum Synchronization and the Performance of Thermal Maser

5.1 Thermodynamics of Maser

In Chapter 4, we extensively discussed the synchronization properties of a three-level thermal maser as well as its multilevel near-degenerate generalization. It was briefly mentioned that synchronization is connected to their thermodynamic performance. In this section, we will derive the formula for thermodynamic quantities such as steady-state power, steady-state heat current, and efficiency of a maser. These thermodynamic quantities will be related to synchronization in the later sections of this chapter.

Recall that the dynamics of thermal maser is governed by a QME

$$\dot{\rho} = -i[H_0 + V(t), \rho] + \mathcal{D}_h[\rho] + \mathcal{D}_c[\rho] \tag{5.1}$$

where the detailed explanation for each term can be found in the previous chapter. Here, we only focus on the thermodynamics of the QME (5.1). To do so, we follow the weak-coupling thermodynamics formulation pioneered by Alicki [133], which

is then generalized by Tannor and Boukobza [117, 134]. We define the system's internal energy as

$$U = \mathrm{Tr}\,(\rho H_0) = \sum_{j=1}^{N+1} \omega_j \rho_{jj}. \tag{5.2}$$

Note that only the bare Hamiltonian H_0 appears in the definition for U. The driving Hamiltonian $V(t)$ acts as a piston by which energy is exchanged as work. This definition is only valid in the weak system-bath coupling regime. For a finite coupling strength, the definition of internal energy (and consequently work & heat) might change [135–137].

The first law of thermodynamics is concerned with the partition of energy exchange between the system and its surroundings into work and heat. For a system undergoing a continuous energy exchange with the environment, the first law can be recast in terms of power and heat current. We first calculate the energy current $\dot{U}$

$$\dot{U} = \mathrm{Tr}\,(\dot{\rho} H_0) = -i\,\mathrm{Tr}\,([V(t), \rho] H_0) + \mathrm{Tr}\,(\mathcal{D}_h[\rho] H_0) + \mathrm{Tr}\,(\mathcal{D}_c[\rho] H_0). \tag{5.3}$$

We now define the partition of energy current into power P and heat current $\dot{Q}$ as

$$P \equiv -i\,\mathrm{Tr}\,([V(t), \rho] H_0) \qquad \dot{Q}_{h,c} \equiv \mathrm{Tr}\,(\mathcal{D}_{h,c}[\rho] H_0). \tag{5.4}$$

On top of being intuitive, this partition has also been shown to be frame-independent and satisfy the second law of thermodynamics [134]. It can also be derived by considering energy flow between a bipartite system with a time-independent total Hamiltonian [134]. Using this partition, the first law of thermodynamics can be written as

$$\dot{U} = P + \dot{Q}_h + \dot{Q}_c. \tag{5.5}$$

Here, we use the convention $P < 0$ ($P > 0$) as the system (surrounding) performing work to the surrounding (system). Similarly, $\dot{Q} > 0$ ($\dot{Q} < 0$) implies a heat flow from (to) the bath.

Using explicit expressions for each term of the QME (5.1), one can obtain formulas for power and heat current as a function of density operator matrix elements

$$P = 2\lambda \sum_{j=2}^{N+1} (\omega_j - \omega_1)\,\mathrm{Im}(\rho_{1j} e^{i\Omega t}) \tag{5.6}$$

$$\dot{Q}_c = 2\omega_1 \gamma_c (n_c \rho_{00} - (1 + n_c)\rho_{11}) \tag{5.7}$$

$$\dot{Q}_h = 2\gamma_h \sum_{i=2}^{N+1} \omega_i [n_i \rho_{00} - (1+n_h^i)\rho_{ii}] - \gamma_h \sum_{i\neq j}^{N+1} [(1+n_h^i)\omega_j + (1+n_h^j)\omega_i] p_{ij}\rho_{ij}. \quad (5.8)$$

The crucial point to be noted here is that coherences appear in the formula for thermodynamic currents, especially power and hot bath's heat current. The fact that $\dot{Q}_h$ is affected by coherences ρ_{ij} for $i \neq j$, is a non-trivial fact arising from the near-degeneracy. One can then split $\dot{Q}_h$ into coherent and incoherent heat currents, the notions that will be explored in more detail in the Sec. 5.3.

Let us calculate the steady-state thermodynamic currents explicitly for the four-level engine ($N = 2$) with exactly degenerate excited states $\Delta = 0$ and resonant drive ($\Omega = \omega_2 - \omega_1$). The steady-state density matrix elements are already provided in Eqs. (4.36)-(4.43). Substituting them to (5.6)-(5.10) gives

$$P^{ss} = -\frac{2\lambda^2(\omega_2 - \omega_1)\gamma_c\gamma_h(1+n_h)(1+p)(n_h - n_c)}{F(\gamma_h, \gamma_c, n_h, n_c\lambda, p)} \quad (5.9)$$

$$\dot{Q}_h^{ss} = \frac{2\lambda^2\omega_2\gamma_c\gamma_h(1+n_h)(1+p)(n_h - n_c)}{F(\gamma_h, \gamma_c, n_h, n_c, \lambda, p)} \quad (5.10)$$

$$\dot{Q}_c^{ss} = -\frac{2\lambda^2\omega_1\gamma_c\gamma_h(1+n_h)(1+p)(n_h - n_c)}{F(\gamma_h, \gamma_c, n_h, n_c, \lambda, p)}. \quad (5.11)$$

It was claimed without proof in Ch. 4, that the system operates as an engine if $n_h > n_c$ and as a refrigerator if $n_h < n_c$. This assertion can be proven using (5.9)-(5.11) by simply noticing that for $n_h > n_c$ ($n_h < n_c$), we have $P < 0$ ($P > 0$), $\dot{Q}_h > 0$ ($\dot{Q}_h < 0$), and $\dot{Q}_c < 0$ ($\dot{Q}_c > 0$), implying that the system operates as an engine (refrigerator).

If one takes into account the denominator function F as defined in Eq. (4.38), the steady-state power P^{ss} is not a monotonic function of dipole-alignment factor p as shown in Fig. 5.1(a). The physical explanation for this non-monotonicity will be explained in Sec. 5.3. Here, we simply point out that there exists an optimum value p_{opt} for which steady-state power $|P^{ss}|$ is maximum. The analytical formula for p_{opt} is easily calculated as,

$$p_{opt} = \frac{\lambda\sqrt{2}}{\gamma_h(1+n_h)}\sqrt{\frac{1+3n_c+2n_h+4n_hn_c}{1+3n_h+2n_c+4n_hn_c}} - 1 \quad (5.12)$$

in agreement with numerical result in Fig. 5.1(a).

So far, we have formulated and applied the first law of thermodynamics to calculate the steady-state power and heat current of a four-level degenerate thermal maser. The remaining question is whether the second law of thermodynamics

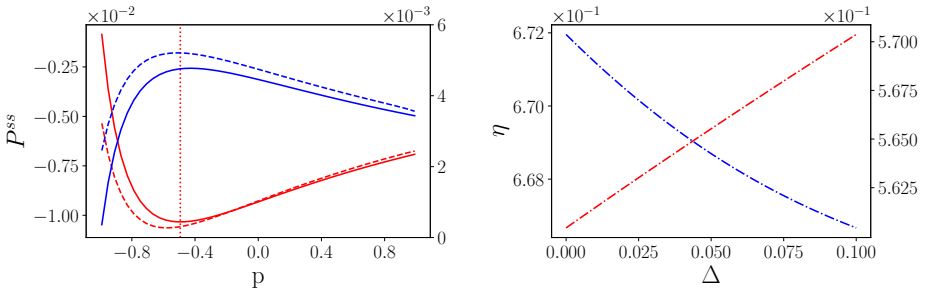

(a) P^{ss} (b) η

Figure 5.1: (a) Steady-state power P^{ss} as a function of dipole-alignment factor p for $\Delta = 0$ (solid line) and $\Delta = 0.1$ (dashed) in the engine (red, left axis) and refrigerator (blue, right axis) regime. The dashed line denotes p_{opt} for the engine's maximum steady-state power. (b) Efficiency η as a function of near-degenerate gap Δ of the engine (red, left axis) and refrigerator (blue, right axis). The (common) parameters used are $\omega_1 = 1$, $\omega_2 = 3$, $\Omega = \omega_2 - \omega_1 + \Delta/2$, $\gamma_h = \gamma_c = 0.1$, $n_h = 0.287$, $n_c = 0.0068$, and $\lambda = 0.05$.

is also satisfied in this setup. We will use Carnot's formulation of the second law of thermodynamics, which states that the efficiency of a heat engine operating between two temperatures $T_h > T_c$ can not be higher than Carnot's efficiency $\eta = 1 - T_c/T_h$. To check this, we first write down an expression for the engine's efficiency

$$\eta_{eng} \equiv -\frac{P}{\dot{Q}_h} = 1 - \frac{\omega_1}{\omega_2}, \tag{5.13}$$

where we have used Eqs. (5.9)-(5.10) to obtain the second equality. This is the same efficiency as the standard three-level maser heat engine [117]. Note that this efficiency only depends on the natural energy scale of the system without any dependence on other specific parameters. Due to its simple form, we can easily show that this efficiency formula abides by Carnot's bound by writing $\omega_{1,2}$ in terms of $n_{h,c}$ and $T_{h,c}$

$$\eta_{eng} = 1 - \frac{T_c}{T_h}\frac{\ln((1+n_h)/n_h)}{\ln((1+n_c)/n_c)} \leq 1 - \frac{T_c}{T_h}. \tag{5.14}$$

Thus, our system satisfies both the first and second law of thermodynamics.

When the system operates as a refrigerator, it is of interest to minimize the

power consumed for a given amount of heat absorbed from the cold bath. The refrigerator efficiency is then given by

$$\eta_{ref} = \frac{\dot{Q}_c}{P} = \frac{\omega_1}{\omega_2 - \omega_1}. \tag{5.15}$$

Equations (5.13) & (5.15) show efficiency formulas of a four-level maser heat engine and refrigerator in the $\Delta = 0$ case. It could be of interest how these efficiencies change as we lift the degeneracy. Figure 5.1(b) shows that increasing Δ can improve the engine's efficiency while reducing the refrigerator's efficiency up to $\sim 1\%$ for $\Delta \leq 0.1$.

5.2 Power-Synchronization Bound

In this section, we will connect synchronization with the thermodynamic performance of the thermal maser. Specifically, we will use steady-state power as a metric of performance. Jaseem and collaborators have pointed out that synchronization measure bounds the steady-state power of the three-level Schovil-Schulz Dubois thermal maser [40]. We can immediately see this once we write down the formula for steady-state power of a thermal three-level maser

$$P^{ss} = 2\lambda(\omega_2 - \omega_1)\mathrm{Im}(\rho_{12}^{ss}). \tag{5.16}$$

To connect P^{ss} with synchronization, we need to recall from Eq. (4.17), the formula for synchronization measure of this maser (up to normalization factor)

$$S_{\max} = |\rho_{12}^{ss}|. \tag{5.17}$$

It is crucial to note that both steady-state power and synchronization measures depend on the same steady-state coherence. It is now clear why the synchronization measure bounds the steady-state power (up to a unit-conversion factor)

$$|P^{ss}| \leq 2\lambda(\omega_2 - \omega_1)S_{\max}, \tag{5.18}$$

where we have used the fact $\mathrm{Im}(\rho_{12}^{ss}) \leq \rho_{12}^{ss}$. We will refer to (5.18) as the *power-synchronization bound*. In the three-level case, the bound is saturated when the drive frequency is resonant ($\Omega = \omega_2 - \omega_1$) because ρ_{12} becomes purely imaginary.

We will now check whether the bound is still satisfied if we add another near-degenerate excited state. Consider again the four-level engine $N = 2$ with

$\Delta = 0$. The formula for steady-state power is

$$\begin{aligned} |P^{ss}| &= 2\lambda(\omega_2 - \omega_1)|\mathrm{Im}(\rho_{12}^{ss}) + \mathrm{Im}(\rho_{13}^{ss})| \\ &\leq 2\lambda(\omega_2 - \omega_1)(|\rho_{12}^{ss}| + |\rho_{13}^{ss}|), \end{aligned} \tag{5.19}$$

where the inequality is saturated for a resonant drive ($\Omega = \omega_2 - \omega_1$), a case we will focus on, unless explicitly stated.

Recall from Eq. (4.49) that the formula for $S_{\max}$ in four-level degenerate thermal maser depends on whether the system operates as an engine or as a refrigerator and also on the value of *dissipation-to-driving* ratio k

$$S_{\max} = \begin{cases} |\rho_{12}^{ss}| + |\rho_{13}^{ss}| - |\rho_{23}^{ss}| & \text{if } n_h > n_c \;\&\; k > 2 \\ (1 + \frac{k^2}{2})|\rho_{23}^{ss}| & \text{if } n_h > n_c \;\&\; 0 < k \leq 2 \\ |\rho_{12}^{ss}| + |\rho_{13}^{ss}| + |\rho_{23}^{ss}| & \text{if } n_h \leq n_c, \end{cases} \tag{5.20}$$

where $k \equiv \gamma_h(1+p)(1+n_h)/\lambda$. It is immediately obvious that P^{ss} and $S_{\max}$ no longer depend on the same coherences. Specifically, P^{ss} only depends on *non-degenerate coherences* while $S_{\max}$ depend on both *non-degenerate* and *degenerate coherences*. From the previous chapter, we learned that the non-degenerate coherence is said to be induced by entrainment while the degenerate coherence is induced by mutual coupling. By comparing (5.20) and (5.19), we find that steady-state power is only related to entrainment and is oblivious to synchronization by mutual coupling.

From the previous chapter, we argue that entrainment and mutual coupling are competitive in the engine regime. Even when entrainment dominates over mutual coupling, the coupling still suppresses synchronization measure, the effect we call coupling-induced synchronization blockade [30, 47]. We thus observe power-synchronization bound violation due to $|\rho_{23}^{ss}|$ in the entrainment-dominated engine regime ($n_h > n_c,\ k > 2$)

$$|P^{ss}| > 2\lambda(\omega_2 - \omega_1)S_{\max} \qquad n_h > n_c \;\&\; k > 2. \tag{5.21}$$

However, deep in the entrainment regime $k \gg 2$ the suppression can be negligible $|\rho_{23}^{ss}|/|\rho_{12}^{ss}| = |\rho_{23}^{ss}|/|\rho_{13}^{ss}| \to 0$, and therefore restoring the validity of the bound.

In contrast, entrainment and mutual coupling are cooperative in the refrigerator regime. Rather than suppressed, entrainment is enhanced by mutual

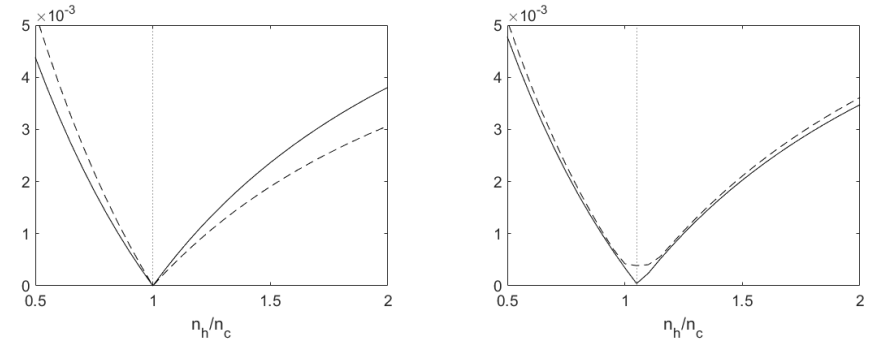

(a) $\Delta = 0$ (b) $\Delta = 0.17$

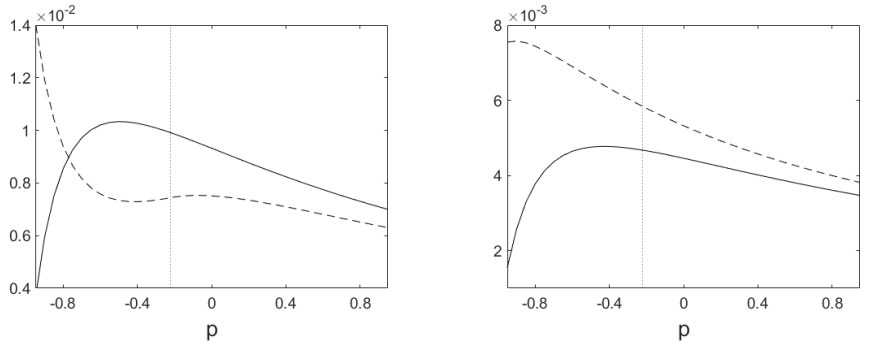

(c) $n_h > n_c$ (d) $n_h < n_c$

Figure 5.2: (a,b) $|P^{ss}|$ (solid lines) and $2\lambda(\omega_2-\omega_1)S_{\max}$ (dashed lines) as a function of n_h/n_c where in (a) $\Delta = 0$ and in (b) $\Delta = 0.17$ with $p = 0$. The dotted line represents the borderline between the engine and refrigerator regime. (c,d) The same quantities as a function of p where in (c) $n_c = 0.0068$ and in (d) $n_c = 1.055$ with $\Delta = 0$. The dotted line represents represents $k = 2$ line. The (common) parameters used are $\omega_1 = 1$, $\omega_2 = 3$, $\Omega = \omega_2 - \omega_1 + \Delta/2$, $\gamma_h = \gamma_c = 0.1$, $n_h = 0.287$, and $\lambda = 0.05$.

coupling. Consequently, the power-synchronization bound is always satisfied in this regime

$$|P^{ss}| < 2\lambda(\omega_2 - \omega_1)S_{\max} \qquad n_h < n_c. \tag{5.22}$$

The numerical simulation for power-synchronization bound is presented in Fig. 5.2. For $\Delta = 0$, the bound's violation in the engine regime and its restoration

in the refrigerator regime is shown in Fig. 5.2(a). Interestingly, from numerical simulation, we find that the violation disappears when the degeneracy is lifted far enough as indicated by Fig. 5.2(b). In other words, for a large enough Δ, the validity of power-synchronization bound (5.18) is restored. A theoretical explanation for this restoration is still unknown.

The above discussion has not included the mutual-coupling dominant ($k < 2$) regime, where the synchronization measure is dominated by ρ_{23}^{ss}. Since power is oblivious to this coherence, it is expected that synchronization and power decouple from each other. This decoupling is numerically found to be true for both the engine and refrigerator regimes, even though $k = 2$ is not a special point for the calculation of $S_{\max}$ in the refrigerator regime. From Figs. 5.2(c)-5.2(d), one can see that the qualitative behavior of $S_{\max}$ and $|P^{ss}|$ deviate from each other for $k < 2$.

Let us summarize this section. We consider the relationship between synchronization measure and steady-state power in the four-level (near-)degenerate maser engine/refrigerator. We deduce that it is not as straightforward as its three-level counterpart. The main reason behind it is that they no longer depend on the same steady-state coherence. Specifically, we have investigated the validity of power-synchronization bound (5.18) in the engine and refrigerator regime. We find that the bound can be violated in the engine regime while it is always satisfied in the refrigerator regime. We also numerically find that as we lift the degeneracy far enough, the validity of the bound is restored. Lastly, we have identified the regime where power and synchronization decouple as the regime in which synchronization is dominated by mutual coupling as opposed to entrainment.

5.3 Heat & Entropy Production due to Synchronization

We have seen that the relationship between synchronization and steady-state power in the four-level near-degenerate thermal maser is not as straightforward as that of its three-level counterpart. The complication arises due to the two quantities no longer depend on the same steady-state coherence. Essentially, the power is independent of the degenerate coherence induced by mutual coupling

synchronization. In this section, we will show that instead of affecting steady-state power, mutual coupling synchronization crucially affects the heat flow and entropy production of the thermal maser.

By Eq. (5.10), we have shown that the hot bath's heat flow depends on both population and degenerate coherence. We can then define *coherent* and *incoherent* heat flow as follows

$$\dot{Q}_h^{coh} \equiv -\gamma_h \sum_{i\neq j}^{N+1} [(1+n_h^i)\omega_j + (1+n_h^j)\omega_i] p_{ij}\rho_{ij} \tag{5.23}$$

$$\dot{Q}_h^{inc} \equiv 2\gamma_h \sum_{i=2}^{N+1} \omega_i [n_i\rho_{00} - (1+n_h^i)\rho_{ii}], \tag{5.24}$$

where $\dot{Q}_h = \dot{Q}_h^{coh} + \dot{Q}_h^{inc}$. The incoherent heat current contribution $\dot{Q}_h^{inc}$ is proportional to the deviation of the populations from their equilibrium values. Meanwhile, the coherent contribution $\dot{Q}_h^{coh}$ represents the heat current associated with synchronization, specifically synchronization by mutual coupling which gives rise to steady-state degenerate coherence ρ_{ij}^{ss}. As a result, $\dot{Q}_h^{coh} \neq 0$ even in the steady-state, provided that there is at least one non-vanishing p_{ij}.

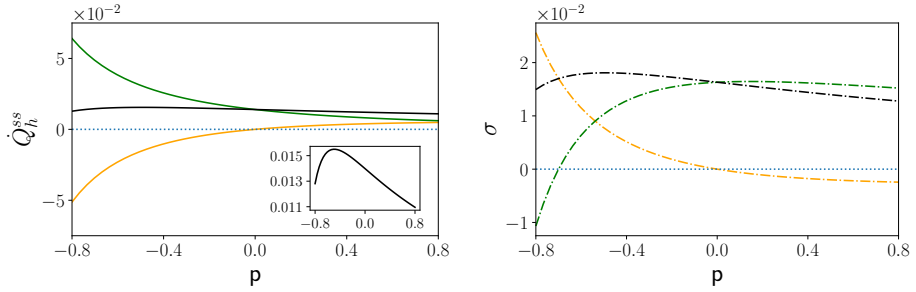

(a) $\dot{Q}_h^{ss}$ (b) σ

Figure 5.3: Components of (a) steady-state heat current $\dot{Q}_h^{ss}$ (solid lines) (b) and entropy production σ (dotted-dashed lines) as a function of dipole-alignment factor p. The yellow line represents the coherent part $(\dot{Q}_h^{coh}(t\to\infty), \sigma_{coh})$, the red lines represent the incoherent part $(\dot{Q}_h^{inc}(t\to\infty), \sigma_{inc})$, and the black lines represent their sum $(\dot{Q}_h^{ss}, \sigma)$. The parameters used are $\omega_1 = 1$, $\omega_2 = 3$, $\Omega = \omega_2 - \omega_1$, $\Delta = 0$, $\gamma_h = \gamma_c = 0.1$, $n_h = 0.287$, $n_c = 0.0068$, and $\lambda = 0.05$

Let us now explicitly connect the steady-state coherent heat current $\dot{Q}_h^{coh}(t \to \infty)$ with synchronization measure $S_{\max}$. We focus on specific case $N = 2$, $\Delta = 0$, and $\Omega = \omega_2 - \omega_1$ where $|\dot{Q}_h^{coh}(t \to \infty)|$ can be simply written as

$$|\dot{Q}_h^{coh}(t \to \infty)| = |p|\gamma_h(1 + n_h)\omega_2|\mathrm{Re}(\rho_{23}^{ss})|. \tag{5.25}$$

From Eq. (5.20), we see that in general $S_{\max}$ depends on both degenerate and non-degenerate steady-state coherences and so a relation with $\dot{Q}_h^{coh}(t \to \infty)$ is not straightforward. But, in a coupling-dominant regime ($k < 2$), $S_{\max}$ only predominantly depends on degenerate coherence. Let us assume that we are deep in coupling dominant regime where k is very small, which can correspond to $p \to -1$, weak dissipation rate $\gamma_h(1 + n_h)$ or strong coupling λ. In this case, we have $S_{\max} \approx |\rho_{23}| > |\mathrm{Re}(\rho_{23})|$. Finally, we obtain *coherent heat-synchronization bound*

$$|\dot{Q}_h^{coh}(t \to \infty)| \leq \gamma_h(1 + n_h)\omega_2|p|S_{\max}. \tag{5.26}$$

This bound has not been discussed in the literature before. It shows that deep in the coupling regime, the coherent heat current is bounded by synchronization measure, emphasizing a deep connection between synchronization and thermodynamics. Thus, not only does synchronization is connected to power by entrainment, but it is also connected to heat current by mutual coupling. Finally, it underscores the thermodynamic importance of the dipole-alignment factor p, without which the coherent heat current would vanish.

Next, we calculate explicit expressions for $\dot{Q}_h^{coh}$ and $\dot{Q}_h^{inc}$ in the steady-state with density matrix elements provided in (4.36)-(4.43),

$$\dot{Q}_h^{coh}(t \to \infty) = \frac{2p\lambda^2\omega_2\gamma_c\gamma_h(1 + n_h)(n_h - n_c)}{F(\gamma_h, \gamma_c, n_h, n_c, \lambda, p)} \tag{5.27}$$

$$\dot{Q}_h^{inc}(t \to \infty) = \frac{2\lambda^2\omega_2\gamma_c\gamma_h(1 + n_h)(n_h - n_c)}{F(\gamma_h, \gamma_c, n_h, n_c, \lambda, p)}, \tag{5.28}$$

which implies $\lim_{t\to\infty} \dot{Q}_h^{coh}/\dot{Q}_h^{inc} = p$. This relation gives a thermodynamic meaning to p as the ratio between steady-state coherent and incoherent heat current. If the dipole orientation tends to be parallel ($p > 0$), one obtains a heat boost due to coherence. On the flip side, if the dipole orientation tends to be anti-parallel ($p < 0$), a heat leak occurs. However, this does not necessarily imply that the total steady-state heat current is larger for $p > 0$ compared to $p < 0$, since one also has to take into account the deviation of steady-state population from their equilibrium values as one varies p. The steady-state coherent and incoherent heat current and their sum are plotted as a function of p in Fig. 5.3(a).

From this plot, we can see that although for $p < 0$ heat leak occurs, the population is pushed further from equilibrium giving larger $\dot{Q}_h^{inc}$. The two effects: heat boost/leak and population deviation from equilibrium compete with each other. This trade-off is the main reason behind the non-monotonicity of thermodynamic currents with respect to p as mentioned in Sec. 5.1. The optimum value of p_{opt} optimizing the heat current (and consequently power) has been derived in Eq. (5.12).

Let us compute the entropy production associated with the engine's operation. We start from the Spohn entropy production [138],

$$\sigma = \frac{dS}{dt} - \frac{\dot{Q}_h}{T_h} - \frac{\dot{Q}_c}{T_c}, \tag{5.29}$$

where $S = -\operatorname{Tr}(\rho \ln \rho)$ is the von Neumann entropy of the system representing the system's contribution to the entropy production. The second and third terms are the environment's contribution to entropy production. In the steady state, $dS/dt = 0$, and so we only need to calculate the environment's entropy production. In the same spirit as (5.23) & (5.24), we define coherent and incoherent entropy production

$$\sigma_{coh} = -\frac{\dot{Q}_h^{coh}}{T_h} \qquad \sigma_{inc} = -\frac{\dot{Q}_h^{inc}}{T_h} - \frac{\dot{Q}_c}{T_c}. \tag{5.30}$$

Equation (5.30) separates entropy production due to out-of-equilibrium population and entropy production due to quantum synchronization. In other words, we have provided strong evidence to the assertion made in the introduction (Ch. 1), where we claim that the maintenance of synchronization requires a continuous production of entropy in the environment. Intriguingly, we also find that synchronization can reduce overall entropy production, which is associated with the heat boost from the hot bath for $p > 0$ as shown in Fig. 5.3(b).

Clearly, when the system operates as an engine, the total entropy production satisfies the second law of thermodynamics $\sigma = \sigma_{coh} + \sigma_{inc} > 0$, which is equivalent to Carnot's second law in (5.14). However, as one can see from Fig. 5.3(b), the incoherent entropy production alone can be negative for some values of p. For such values of p, the environment's entropy production has to be dominated by its coherent component so that the total entropy production remains positive. In other words, without taking into account entropy production due to synchronization, one would observe a violation of the second law.

Concluding this chapter, we have shown an intimate relationship between quantum synchronization and quantum thermodynamics. Earlier work connects synchronization and the steady-state power of quantum thermal maser [40] as demonstrated by power-synchronization bound (5.18). However, in the presence of (near-)degeneracy, we find that the bound can be violated due to *blockade* by mutual coupling. We further demonstrate that deep in the coupling regime, synchronization measure bounds the coherent heat current. Thus, it relates synchronization, not only to steady-state power but also to the steady-state heat current and the entropy production of thermal maser engine/refrigerator, signifying a deep connection between quantum synchronization and thermodynamics.

Chapter 6

Summary & Outlook

We began this thesis by reviewing the notion of synchronization in classical physics. Then, we generalized some of the concepts we learned in classical synchronization to quantum synchronization. Especially, we have seen that quantum synchronization in N-level systems has a lot of similarities with classical synchronization in the presence of noise, but is applied to quantum phases which have no classical counterpart. We also argued that steady-state coherence can be viewed as a synchronization order parameter [Eq. (3.39)]. Moreover, we showed a specific quantum model where the two main varieties of synchronization, entrainment and mutual coupling, co-exist. The model we studied is a specific quantum heat engine model operating out-of-equilibrium. As a result, beyond exploring the interplay between entrainment and coupling, the study of synchronization in this system also opens up a possibility to relate synchronization and thermodynamics, in particular, the thermodynamics performance of quantum heat engines.

Conventionally, synchronization is treated from the perspective of non-linear dynamics. In this thesis, we explored a different viewpoint where synchronization is viewed as a non-equilibrium thermodynamics phenomenon. We focused particularly on studying synchronization in a quantum maser heat engine. We chose this engine because it is a type of quantum heat engine that continuously operates in out-of-equilibrium, thus allowing for synchronization in the steady-state. Earlier work has shown that the steady-state power of a three-level maser heat engine is bounded by synchronization measure [40]. Here, we investigate

the relationship between synchronization and the thermodynamics of a multi-level near-degenerate extension of such engines. We showed that near-degeneracy and quantum interference gives rise to two distinct synchronization mechanisms influencing the system: *entrainment* and *mutual coupling*. We found that their interplay is determined by the thermodynamics functionality of the system. Entrainment and mutual coupling are competitive when the system operates as an engine, and cooperative when the system operates as a refrigerator. As a result, in the engine regime, the synchronization properties depend on which synchronization mechanism is dominant. When entrainment is dominant, the engine's quantum phases get entrained to the drive but with a reduction in localization strength due to suppression by mutual coupling. On the other hand, when mutual coupling is dominant the engine's quantum phases no longer follow the drives oscillation but still manage to keep their relative phases to be constant.

Moreover, we proved that the transition between the two regimes is governed by *dissipation-to-driving ratio* [Eq. (4.45)], which as the name suggests, is the ratio between the effective thermal dissipation rate and the driving strength. We also found that the interplay between entrainment and mutual coupling affects the relationship between synchronization and steady-state power. Notably, the power-synchronization bound (5.18) can be violated when the system operates as an engine. The main reason for this violation is the fact that steady-state power is only sensitive to entrainment while being oblivious to synchronization by mutual coupling. As a result, when the synchronization measure is dominated by mutual coupling, power and synchronization decouple from each other. Yet, even in this regime, synchronization is still deeply connected to thermodynamics as demonstrated by the *coherent heat-synchronization bound* (5.26). Finally, we calculated the entropy production and showed that one needs to take into account the entropy production associated with synchronization to not violate the second law of thermodynamics in some parameter regimes.

When presenting the results of this thesis, it is often the case that we focus on specific cases where analytical solutions are accessible. The generality of the result needs to be further investigated in future work, both through analytical calculation and numerical simulations. For example, only a few results are presented for the case of more than two-level degeneracy ($N > 2$). There is still a lack of encompassing theory that can explain the relationship between synchronization and thermodynamics in the N-fold degenerate case. One of the reasons why this is the case is due to the limitation in obtaining analytical solutions. In this thesis, the analytical solution for the steady-state of the N-fold degeneracy model

is presented only in a very limited case of exact degeneracy and no correlation between the degenerate levels. It remains to be seen whether a general analytical solution is possible at least in the continuum limit $N \to \infty$. If such a solution is possible, it will give insight into the influence of the energy gap distribution and the correlation matrix to the results presented here. In this thesis, the energy gap distribution is taken to be either equispaced or exactly degenerate. However, one need not restrict themselves to such a choice. It could be interesting to explore other types of energy gap distribution with or without level repulsion such as that of Poisson and Wigner distribution, which are well-known distributions in the field of random matrix theory and quantum chaos [132]. One could also consider the influence of randomly sampling dipole-alignment factors from a distribution of possible correlation matrices, e.g. the LKJ distribution [139]. Physically, we expect that it would affect the collective re-pumping rate as well as modify the steady-state heat current. How exactly would those quantities depend on the correlation matrix and whether it would fundamentally change the results presented here are currently unknown. Moreover, a precise connection between synchronization and the performance of the near-degenerate thermal maser is yet to be made. For example, one may ask, does synchronization ultimately enhance or reduce the performance of the engine/refrigerator? What are the appropriate metrics that need to be evaluated to answer such questions? We hope to be able to answer all these questions in future work.

Throughout this thesis, we have witnessed synchronization as a fascinating phenomenon that appears in a variety of contexts with many facets to explore. There are many unanswered questions on the thermodynamics of quantum synchronization both within the model studied here and also in general. Nevertheless, we hope that this research can contribute to advancing the thermodynamics understanding of quantum synchronization as a non-equilibrium collective phenomenon in quantum systems. Synchronization is not only an enticing natural phenomenon by itself, but it is also useful for various applications. In line with the five grand challenges for basic energy science in the 21^{st} century [59], we envisage that quantum synchronization will be an essential control tool for the development of quantum devices. Thus, ultimately we hope our research paves a way for the application of quantum synchronization in future quantum technology.

Bibliography

[1] Arkady Pikovsky, Michael Rosenblum, Jürgen Kurths, and A Synchronization. A universal concept in nonlinear sciences. *Self*, 2:3, 2001.

[2] Alexander Balanov, Natalia Janson, Dmitry Postnov, and Olga Sosnovtseva. *Synchronization: from simple to complex*. Springer Science & Business Media, 2008.

[3] Christiaan Huygens. *Œuvres complètes de Christiaan Huygens: Correspondance 1664-1665*, volume 5. Martinus Nijhoff, 1893.

[4] J Pena Ramirez, Rob HB Fey, and H Nijmeijer. Synchronization of weakly nonlinear oscillators with Huygens' coupling. *Chaos: An Interdisciplinary Journal of Nonlinear Science*, 23(3):033118, 2013.

[5] Jonatan Pena Ramirez, Luis Alberto Olvera, Henk Nijmeijer, and Joaquin Alvarez. The sympathy of two pendulum clocks: beyond Huygens' observations. *Scientific reports*, 6(1):1–16, 2016.

[6] J Peña Ramirez, RHB Fey, K Aihara, and H Nijmeijer. An improved model for the classical Huygens experiment on synchronization of pendulum clocks. *Journal of Sound and Vibration*, 333(26):7248–7266, 2014.

[7] J Pena Ramirez, K Aihara, RHB Fey, and H Nijmeijer. Further understanding of Huygens' coupled clocks: The effect of stiffness. *Physica D: Nonlinear Phenomena*, 270:11–19, 2014.

[8] Eugene M Izhikevich. *Dynamical systems in neuroscience*. MIT press, 2007.

[9] Donald C Michaels, Edward P Matyas, and Jose Jalife. Dynamic interactions and mutual synchronization of sinoatrial node pacemaker cells. a mathematical model. *Circulation research*, 58(5):706–720, 1986.

[10] Vincent Torre. A theory of synchronization of heart pace-maker cells. *Journal of Theoretical Biology*, 61(1):55–71, 1976.

[11] John Bonner Buck. Synchronous rhythmic flashing of fireflies. *The Quarterly Review of Biology*, 13(3):301–314, 1938.

[12] John Buck and Elisabeth Buck. Mechanism of rhythmic synchronous flashing of fireflies: Fireflies of southeast asia may use anticipatory time-measuring in synchronizing their flashing. *Science*, 159(3821):1319–1327, 1968.

[13] Rory Barnes. Tidal locking of habitable exoplanets. *Celestial Mechanics and Dynamical Astronomy*, 129(4):509–536, 2017.

[14] Sara J Aton and Erik D Herzog. Synchronization of rhythms in a mammalian circadian clock. *Neuron*, 48(4):531–534, 2005.

[15] Christoph Lenzen, Philipp Sommer, and Roger Wattenhofer. Pulsesync: An efficient and scalable clock synchronization protocol. *IEEE/ACM Transactions on Networking*, 23(3):717–727, 2014.

[16] Adilson E Motter, Seth A Myers, Marian Anghel, and Takashi Nishikawa. Spontaneous synchrony in power-grid networks. *Nature Physics*, 9(3):191–197, 2013.

[17] Takashi Nishikawa and Adilson E Motter. Comparative analysis of existing models for power-grid synchronization. *New Journal of Physics*, 17(1):015012, 2015.

[18] Dirk Witthaut, Frank Hellmann, Jürgen Kurths, Stefan Kettemann, Hildegard Meyer-Ortmanns, and Marc Timme. Collective nonlinear dynamics and self-organization in decentralized power grids. *Reviews of Modern Physics*, 94(1):015005, 2022.

[19] Peter J Uhlhaas and Wolf Singer. Neural synchrony in brain disorders: relevance for cognitive dysfunctions and pathophysiology. *Neuron*, 52(1):155–168, 2006.

[20] Louis M. Pecora and Thomas L. Carroll. Synchronization in chaotic systems. *Phys. Rev. Lett.*, 64:821–824, 1990.

[21] Denis S. Goldobin and Arkady Pikovsky. Synchronization and desynchronization of self-sustained oscillators by common noise. *Phys. Rev. E*, 71:045201, 2005.

[22] Kevin M Cuomo, Alan V Oppenheim, and Steven H Strogatz. Synchronization of lorenz-based chaotic circuits with applications to communications. *IEEE Transactions on circuits and systems II: Analog and digital signal processing*, 40(10):626–633, 1993.

[23] Changsong Zhou and Jürgen Kurths. Noise-induced synchronization and coherence resonance of a hodgkin–huxley model of thermally sensitive neurons. *Chaos: An Interdisciplinary Journal of Nonlinear Science*, 13(1):401–409, 2003.

[24] Tony E. Lee and H. R. Sadeghpour. Quantum synchronization of quantum van der pol oscillators with trapped ions. *Phys. Rev. Lett.*, 111:234101, 2013.

[25] Stefan Walter, Andreas Nunnenkamp, and Christoph Bruder. Quantum synchronization of a driven self-sustained oscillator. *Phys. Rev. Lett.*, 112:094102, 2014.

[26] Tony E. Lee, Ching-Kit Chan, and Shenshen Wang. Entanglement tongue and quantum synchronization of disordered oscillators. *Phys. Rev. E*, 89:022913, 2014.

[27] Lior Ben Arosh, M. C. Cross, and Ron Lifshitz. Quantum limit cycles and the rayleigh and van der pol oscillators. *Phys. Rev. Research*, 3:013130, 2021.

[28] A. Chia, L. C. Kwek, and C. Noh. Relaxation oscillations and frequency entrainment in quantum mechanics. *Phys. Rev. E*, 102:042213, 2020.

[29] Alexandre Roulet and Christoph Bruder. Synchronizing the smallest possible system. *Phys. Rev. Lett.*, 121:053601, Jul 2018.

[30] Martin Koppenhöfer and Alexandre Roulet. Optimal synchronization deep in the quantum regime: Resource and fundamental limit. *Phys. Rev. A*, 99:043804, Apr 2019.

[31] Martin Koppenhöfer, Christoph Bruder, and Alexandre Roulet. Quantum synchronization on the IBM Q system. *Phys. Rev. Research*, 2:023026, 2020.

[32] Joshua M. Weiner, Kevin C. Cox, Justin G. Bohnet, and James K. Thompson. Phase synchronization inside a superradiant laser. *Phys. Rev. A*, 95:033808, 2017.

[33] M. A. Galin, E. A. Borodianskyi, V. V. Kurin, I. A. Shereshevskiy, N. K. Vdovicheva, V. M. Krasnov, and A. M. Klushin. Synchronization of large josephson-junction arrays by traveling electromagnetic waves. *Phys. Rev. Applied*, 9:054032, 2018.

[34] Bihui Zhu, Johannes Schachenmayer, Minghui Xu, F Herrera, Juan G Restrepo, Murray J Holland, and Ana Maria Rey. Synchronization of interacting quantum dipoles. *New Journal of Physics*, 17(8):083063, 2015.

[35] Aniket Patra, Boris L. Altshuler, and Emil A. Yuzbashyan. Chaotic synchronization between atomic clocks. *Phys. Rev. A*, 100:023418, 2019.

[36] Igor Goychuk, Jesús Casado-Pascual, Manuel Morillo, Jörg Lehmann, and Peter Hänggi. Quantum stochastic synchronization. *Phys. Rev. Lett.*, 97:210601, 2006.

[37] Álvaro Parra-López and Joakim Bergli. Synchronization in two-level quantum systems. *Phys. Rev. A*, 101:062104, 2020.

[38] Arif Warsi Laskar, Pratik Adhikary, Suprodip Mondal, Parag Katiyar, Sai Vinjanampathy, and Saikat Ghosh. Observation of quantum phase synchronization in spin-1 atoms. *Phys. Rev. Lett.*, 125:013601, 2020.

[39] Noufal Jaseem, Michal Hajdušek, Parvinder Solanki, Leong-Chuan Kwek, Rosario Fazio, and Sai Vinjanampathy. Generalized measure of quantum synchronization. *Phys. Rev. Research*, 2:043287, 2020.

[40] Noufal Jaseem, Michal Hajdušek, Vlatko Vedral, Rosario Fazio, Leong-Chuan Kwek, and Sai Vinjanampathy. Quantum synchronization in nanoscale heat engines. *Phys. Rev. E*, 101:020201, 2020.

[41] Alexandre Roulet and Christoph Bruder. Quantum synchronization and entanglement generation. *Phys. Rev. Lett.*, 121:063601, 2018.

[42] O. V. Zhirov and D. L. Shepelyansky. Synchronization and bistability of a qubit coupled to a driven dissipative oscillator. *Phys. Rev. Lett.*, 100:014101, 2008.

[43] Lei Ying, Ying-Cheng Lai, and Celso Grebogi. Quantum manifestation of a synchronization transition in optomechanical systems. *Phys. Rev. A*, 90:053810, Nov 2014.

[44] A. Mari, A. Farace, N. Didier, V. Giovannetti, and R. Fazio. Measures of quantum synchronization in continuous variable systems. *Phys. Rev. Lett.*, 111:103605, Sep 2013.

[45] Simon E. Nigg. Observing quantum synchronization blockade in circuit quantum electrodynamics. *Phys. Rev. A*, 97:013811, Jan 2018.

[46] Mahmood Bagheri, Menno Poot, Linran Fan, Florian Marquardt, and Hong X. Tang. Photonic cavity synchronization of nanomechanical oscillators. *Phys. Rev. Lett.*, 111:213902, Nov 2013.

[47] Niels Lörch, Simon E. Nigg, Andreas Nunnenkamp, Rakesh P. Tiwari, and Christoph Bruder. Quantum synchronization blockade: Energy quantization hinders synchronization of identical oscillators. *Phys. Rev. Lett.*, 118:243602, 2017.

[48] H Eneriz, DZ Rossatto, Francisco A Cárdenas-López, E Solano, and M Sanz. Degree of quantumness in quantum synchronization. *Scientific Reports*, 9(1):1–9, 2019.

[49] Tian-tian Huan, Ri-gui Zhou, and Hou Ian. Synchronization of two cavity-coupled qubits measured by entanglement. *Scientific Reports*, 10(1):1–11, 2020.

[50] Yuki Izumida, Hiroshi Kori, and Udo Seifert. Energetics of synchronization in coupled oscillators rotating on circular trajectories. *Phys. Rev. E*, 94:052221, 2016.

[51] Sangwon Lee, Changbong Hyeon, and Junghyo Jo. Thermodynamic uncertainty relation of interacting oscillators in synchrony. *Phys. Rev. E*, 98:032119, 2018.

[52] Jung-Wan Ryu, Alexandre Lazarescu, Rahul Marathe, and Juzar Thingna. Stochastic thermodynamics of inertial-like stuart–landau dimer. *New Journal of Physics*, 23(10):105005, 2021.

[53] Tim Herpich, Juzar Thingna, and Massimiliano Esposito. Collective power: Minimal model for thermodynamics of nonequilibrium phase transitions. *Phys. Rev. X*, 8:031056, 2018.

[54] Sourav Bhattacharjee and Amit Dutta. Quantum thermal machines and batteries. *The European Physical Journal B*, 94(12):1–42, 2021.

[55] C. Jarzynski. Nonequilibrium equality for free energy differences. *Phys. Rev. Lett.*, 78:2690–2693, 1997.

[56] Udo Seifert. Stochastic thermodynamics, fluctuation theorems and molecular machines. *Reports on Progress in Physics*, 75(12):126001, 2012.

[57] Shamik Gupta, Alessandro Campa, and Stefano Ruffo. *Statistical physics of synchronization*, volume 48. Springer, 2018.

[58] John Goold, Marcus Huber, Arnau Riera, Lídia Del Rio, and Paul Skrzypczyk. The role of quantum information in thermodynamics—a topical review. *Journal of Physics A: Mathematical and Theoretical*, 49(14):143001, 2016.

[59] John Hemminger, Graham Fleming, and M Ratner. Directing matter and energy: Five challenges for science and the imagination. Technical report, DOESC (USDOE Office of Science (SC)), 2007.

[60] SH Strogatz. *Non-linear Dynamics and Chaos*. Perseus, New York, 1994.

[61] Balthasar Van der Pol. Theory of the amplitude of free and forced triode vibrations. *Radio Review*, 1:701–710, 1920.

[62] Mark Denny. The pendulum clock: a venerable dynamical system. *European Journal of Physics*, 23(4):449, 2002.

[63] Balth Van Der Pol and Jan Van Der Mark. Lxxii. the heartbeat considered as a relaxation oscillation, and an electrical model of the heart. *The London, Edinburgh, and Dublin Philosophical Magazine and Journal of Science*, 6(38):763–775, 1928.

[64] Klaus M Stiefel and G Bard Ermentrout. Neurons as oscillators. *Journal of Neurophysiology*, 116(6):2950–2960, 2016.

[65] A.A. Andronov, A.A. Vitt, and SE Khaikin. *Theory of oscillations*. International Series of Monographs in Physics, 1966.

[66] John Trevor Stuart. On the non-linear mechanics of hydrodynamic stability. *Journal of Fluid Mechanics*, 4(1):1–21, 1958.

[67] Anatol M Zhabotinsky. Belousov-Zhabotinsky reaction. *Scholarpedia*, 2(9):1435, 2007.

[68] Yoshiki Kuramoto. *Chemical oscillations, waves, and turbulence*. Courier Corporation, 2003.

[69] Takashi Kanamaru. Van der Pol oscillator. *Scholarpedia*, 2(1):2202, 2007.

[70] Julyan HE Cartwright, Víctor M Eguíluz, Emilio Hernández-García, and Oreste Piro. Dynamics of elastic excitable media. *International Journal of Bifurcation and Chaos*, 9(11):2197–2202, 1999.

[71] Carl J Buczek, Robert J Freiberg, and ML Skolnick. Laser injection locking. *Proceedings of the IEEE*, 61(10):1411–1431, 1973.

[72] R. Adler. A study of locking phenomena in oscillators. *Proceedings of the IRE*, 34(6):351–357, 1946.

[73] Wei Zou, D. V. Senthilkumar, Jinqiao Duan, and Jürgen Kurths. Emergence of amplitude and oscillation death in identical coupled oscillators. *Phys. Rev. E*, 90:032906, Sep 2014.

[74] Jung-Wan Ryu, Woo-Sik Son, Dong-Uk Hwang, Soo-Young Lee, and Sang Wook Kim. Exceptional points in coupled dissipative dynamical systems. *Phys. Rev. E*, 91:052910, 2015.

[75] K Premalatha, VK Chandrasekar, M Senthilvelan, and M Lakshmanan. Stable amplitude chimera states in a network of locally coupled stuart-landau oscillators. *Chaos: An Interdisciplinary Journal of Nonlinear Science*, 28(3):033110, 2018.

[76] Felix P Kemeth, Sindre W Haugland, and Katharina Krischer. Cluster singularity: The unfolding of clustering behavior in globally coupled stuart-landau oscillators. *Chaos: An Interdisciplinary Journal of Nonlinear Science*, 29(2):023107, 2019.

[77] Arthur T. Winfree. Biological rhythms and the behavior of populations of coupled oscillators. *Journal of Theoretical Biology*, 16(1):15–42, 1967.

[78] Yoshiki Kuramoto. Self-entrainment of a population of coupled non-linear oscillators. In Huzihiro Araki, editor, *International Symposium on Mathematical Problems in Theoretical Physics*, pages 420–422, Berlin, Heidelberg, 1975. Springer Berlin Heidelberg.

[79] Steven H. Strogatz. From Kuramoto to Crawford: exploring the onset of synchronization in populations of coupled oscillators. *Physica D: Nonlinear Phenomena*, 143(1):1–20, 2000.

[80] Hidetsugu Sakaguchi and Yoshiki Kuramoto. A Soluble Active Rotater Model Showing Phase Transitions via Mutual Entertainment. *Progress of Theoretical Physics*, 76(3):576–581, 09 1986.

[81] Hidetsugu Sakaguchi. Cooperative phenomena in coupled oscillator systems under external fields. *Progress of Theoretical Physics*, 79(1):39–46, 1988.

[82] Lauren M Childs and Steven H Strogatz. Stability diagram for the forced Kuramoto model. *Chaos: An Interdisciplinary Journal of Nonlinear Science*, 18(4):043128, 2008.

[83] Edward Ott and Thomas M Antonsen. Low dimensional behavior of large systems of globally coupled oscillators. *Chaos: An Interdisciplinary Journal of Nonlinear Science*, 18(3):037113, 2008.

[84] Jordan Snyder, Anatoly Zlotnik, and Aric Hagberg. Stability of entrainment of a continuum of coupled oscillators. *Chaos: An Interdisciplinary Journal of Nonlinear Science*, 27(10):103108, 2017.

[85] Bertrand Ottino-Löffler and Steven H. Strogatz. Kuramoto model with uniformly spaced frequencies: Finite-n asymptotics of the locking threshold. *Phys. Rev. E*, 93:062220, 2016.

[86] Crispin Gardiner. *Stochastic methods*, volume 4. Springer Berlin, 2009.

[87] Hannes Risken. *Fokker-Planck equation*. Springer, 1996.

[88] John Crank. *The mathematics of diffusion*. Oxford university press, 1979.

[89] Heinz-Peter Breuer, Francesco Petruccione, et al. *The Theory of Open Quantum Systems*. Oxford University Press on Demand, 2002.

[90] Daniel Manzano. A short introduction to the Lindblad master equation. *AIP Advances*, 10(2):025106, 2020.

[91] Alfred G Redfield. On the theory of relaxation processes. *IBM Journal of Research and Development*, 1(1):19–31, 1957.

[92] Jun John Sakurai and Eugene D Commins. *Modern quantum mechanics, Revised Edition*. American Association of Physics Teachers, 1995.

[93] Gavin McCauley, Benjamin Cruikshank, Denys I Bondar, and Kurt Jacobs. Accurate Lindblad-form master equation for weakly damped quantum systems across all regimes. *npj Quantum Information*, 6(1):1–14, 2020.

[94] Goran Lindblad. On the generators of quantum dynamical semigroups. *Communications in Mathematical Physics*, 48(2):119–130, 1976.

[95] Vittorio Gorini, Andrzej Kossakowski, and Ennackal Chandy George Sudarshan. Completely positive dynamical semigroups of N-level systems. *Journal of Mathematical Physics*, 17(5):821–825, 1976.

[96] David E Evans. Irreducible quantum dynamical semigroups. *Communications in Mathematical Physics*, 54(3):293–297, 1977.

[97] D Manzano and PI Hurtado. Harnessing symmetry to control quantum transport. *Advances in Physics*, 67(1):1–67, 2018.

[98] Juzar Thingna and Daniel Manzano. Degenerated Liouvillians and steady-state reduced density matrices. *Chaos: An Interdisciplinary Journal of Nonlinear Science*, 31(7):073114, 2021.

[99] Ady Stern, Yakir Aharonov, and Yoseph Imry. Phase uncertainty and loss of interference: A general picture. *Phys. Rev. A*, 41:3436–3448, 1990.

[100] Adrián A. Budini. Quantum systems subject to the action of classical stochastic fields. *Phys. Rev. A*, 64:052110, 2001.

[101] A. Chenu, M. Beau, J. Cao, and A. del Campo. Quantum simulation of generic many-body open system dynamics using classical noise. *Phys. Rev. Lett.*, 118:140403, Apr 2017.

[102] Wen Yang, Wen-Long Ma, and Ren-Bao Liu. Quantum many-body theory for electron spin decoherence in nanoscale nuclear spin baths. *Reports on Progress in Physics*, 80(1):016001, 2016.

[103] Bing Gu and Ignacio Franco. When can quantum decoherence be mimicked by classical noise? *The Journal of Chemical Physics*, 151(1):014109, 2019.

[104] Kurt Gottfried. *Quantum mechanics: fundamentals*. CRC Press, 2018.

[105] Roy J Glauber. Coherent and incoherent states of the radiation field. *Physical Review*, 131(6):2766, 1963.

[106] Wolfgang P Schleich. *Quantum optics in phase space*. John Wiley & Sons, 2011.

[107] William B Case. Wigner functions and Weyl transforms for pedestrians. *American Journal of Physics*, 76(10):937–946, 2008.

[108] Göran Wendin and VS Shumeiko. Quantum bits with Josephson junctions. *Low Temperature Physics*, 33(9):724–744, 2007.

[109] Mark Saffman, Thad G Walker, and Klaus Mølmer. Quantum information with rydberg atoms. *Reviews of Modern Physics*, 82(3):2313, 2010.

[110] Shu-Shen Li, Jian-Bai Xia, Jin-Long Liu, Fu-Hua Yang, Zhi-Chuan Niu, Song-Lin Feng, and Hou-Zhi Zheng. Inas/gaas single-electron quantum dot qubit. *Journal of Applied Physics*, 90(12):6151–6155, 2001.

[111] DM Gitman and AL Shelepin. Coherent states of SU (N) groups. *Journal of Physics A: Mathematical and General*, 26(2):313, 1993.

[112] Kae Nemoto. Generalized coherent states for SU(n) systems. *Journal of Physics A: Mathematical and General*, 33(17):3493, 2000.

[113] D. W. Barry and P. D. Drummond. Qubit phase space: SU(n) coherent-state p representations. *Phys. Rev. A*, 78:052108, Nov 2008.

[114] William K Wootters. A Wigner-function formulation of finite-state quantum mechanics. *Annals of Physics*, 176(1):1–21, 1987.

[115] V. Ameri, M. Eghbali-Arani, A. Mari, A. Farace, F. Kheirandish, V. Giovannetti, and R. Fazio. Mutual information as an order parameter for quantum synchronization. *Phys. Rev. A*, 91:012301, 2015.

[116] H. E. D. Scovil and E. O. Schulz-DuBois. Three-level masers as heat engines. *Phys. Rev. Lett.*, 2:262–263, Mar 1959.

[117] E. Boukobza and D. J. Tannor. Three-level systems as amplifiers and attenuators: A thermodynamic analysis. *Phys. Rev. Lett.*, 98:240601, 2007.

[118] J Wang, MK Haldar, L Li, and FVC Mendis. Enhancement of modulation bandwidth of laser diodes by injection locking. *IEEE Photonics Technology Letters*, 8(1):34–36, 1996.

[119] Behzad Razavi. A study of injection locking and pulling in oscillators. *IEEE Journal of Solid-state Circuits*, 39(9):1415–1424, 2004.

[120] Iman Marvian. Coherence distillation machines are impossible in quantum thermodynamics. *Nature communications*, 11(1):1–9, 2020.

[121] Hyukjoon Kwon, Hyunseok Jeong, David Jennings, Benjamin Yadin, and M. S. Kim. Clock–work trade-off relation for coherence in quantum thermodynamics. *Phys. Rev. Lett.*, 120:150602, 2018.

[122] Felix Bloch. Generalized theory of relaxation. *Physical Review*, 105(4):1206, 1957.

[123] Robert S Whitney. Staying positive: going beyond Lindblad with perturbative master equations. *Journal of Physics A: Mathematical and Theoretical*, 41(17):175304, 2008.

[124] Timur V Tscherbul and Paul Brumer. Partial secular Bloch-Redfield master equation for incoherent excitation of multilevel quantum systems. *The Journal of chemical physics*, 142(10):104107, 2015.

[125] P. R. Eastham, P. Kirton, H. M. Cammack, B. W. Lovett, and J. Keeling. Bath-induced coherence and the secular approximation. *Phys. Rev. A*, 94:012110, 2016.

[126] G. S. Agarwal and Sunish Menon. Quantum interferences and the question of thermodynamic equilibrium. *Phys. Rev. A*, 63:023818, 2001.

[127] Amro Dodin, Timur V Tscherbul, and Paul Brumer. Quantum dynamics of incoherently driven V-type systems: Analytic solutions beyond the secular approximation. *The Journal of Chemical Physics*, 144(24):244108, 2016.

[128] Amro Dodin and Paul Brumer. Noise-induced coherence in molecular processes. *Journal of Physics B: Atomic, Molecular and Optical Physics*, 2021.

[129] Suyesh Koyu, Amro Dodin, Paul Brumer, and Timur V. Tscherbul. Steady-state Fano coherences in a V-type system driven by polarized incoherent light. *Phys. Rev. Research*, 3:013295, Mar 2021.

[130] Alexandria Hadd and Joseph Lee Rodgers. *Understanding Correlation Matrices*. SAGE Publications, 2020.

[131] T. Baumgratz, M. Cramer, and M. B. Plenio. Quantifying coherence. *Phys. Rev. Lett.*, 113:140401, 2014.

[132] T. A. Brody, J. Flores, J. B. French, P. A. Mello, A. Pandey, and S. S. M. Wong. Random-matrix physics: spectrum and strength fluctuations. *Rev. Mod. Phys.*, 53:385–479, 1981.

[133] Robert Alicki. The quantum open system as a model of the heat engine. *Journal of Physics A: Mathematical and General*, 12(5):L103, 1979.

[134] E. Boukobza and D. J. Tannor. Thermodynamics of bipartite systems: Application to light-matter interactions. *Phys. Rev. A*, 74:063823, 2006.

[135] Massimiliano Esposito, Katja Lindenberg, and Christian Van den Broeck. Entropy production as correlation between system and reservoir. *New Journal of Physics*, 12(1):013013, 2010.

[136] M. Perarnau-Llobet, H. Wilming, A. Riera, R. Gallego, and J. Eisert. Strong coupling corrections in quantum thermodynamics. *Phys. Rev. Lett.*, 120:120602, 2018.

[137] Ángel Rivas. Strong coupling thermodynamics of open quantum systems. *Phys. Rev. Lett.*, 124:160601, 2020.

[138] Herbert Spohn. Entropy production for quantum dynamical semigroups. *Journal of Mathematical Physics*, 19(5):1227–1230, 1978.

[139] Daniel Lewandowski, Dorota Kurowicka, and Harry Joe. Generating random correlation matrices based on vines and extended onion method. *Journal of Multivariate Analysis*, 100(9):1989–2001, 2009.